This is to certify that the
dissertation entitled

INDEPENDENTLY GENERATED MAGMA BATCHES IN THE COMPOSITIONALLY ZONED ASH-FLOW SHEETS FROM THE SOUTHWEST NEVADA VOLCANIC FIELD

presented by

KAREN SUE TEFEND

has been accepted towards fulfillment
of the requirements for the

Ph.D. in
Geological
Sciences

Thomas A. Vogel

Major Professor's Signature

6-28-05

Date

INDEPENDENTLY GENERATED MAGMA BATCHES IN THE COMPOSITIONALLY ZONED ASH-FLOW SHEETS FROM THE SOUTHWEST NEVADA VOLCANIC FIELD

By

Karen Sue Tefend

A DISSERTATION

Submitted to
Michigan State University
in partial fulfillment of the requirements
for the degree of

DOCTOR OF PHILOSOPHY

Department of Geological Sciences

2005

ABSTRACT

INDEPENDENTLY GENERATED MAGMA BATCHES IN THE COMPOSITIONALLY ZONED ASH-FLOW SHEETS FROM THE SOUTHWEST NEVADA VOLCANIC FIELD

By

Karen Sue Tefend

Compositionally zoned ignimbrites have been inferred to represent the eruptive product of zoned magma chambers. Topopah Spring (12.8 Ma), Tiva Canyon (12.7 Ma), Rainier Mesa (11.6 Ma), and Ammonia Tanks (11.45 Ma) are four compositionally zoned ash-flow sheets within the southwest Nevada volcanic field, SW Nevada. These large volume ash-flow sheets have been extensively studied with the goal of understanding the formation of large volumes of high silica magmas that are, in this case, rapidly generated and erupted within short time intervals (150,000 years between the youngest of these ash flows). Previous studies have concluded, based on major and trace element geochemistry and isotopic analyses, that the lower silica magmas and high-silica rhyolite magmas within and among each ash-flow sheet cannot be related by assimilation/fractional crystallization processes occurring within a single magma chamber.

The purpose of this current study is to evaluate this conclusion using Polytopic Vector Analysis (PVA). Based on these analyses we conclude that not only can unrelated magma types be identified, but that magmas related by mixing processes can also be determined. Using PVA, it can be shown that the coevally erupted lower silica ($\leq$ 73 wt% SiO_2) and high-silica rhyolite magmas ($\geq$ 74 wt% SiO_2) within Topopah Spring, Tiva Canyon, Rainier Mesa, and Ammonia Tanks are unrelated, and must represent independent magma batches. An intermediate magma type identified in Tiva Canyon

was found not to be the result of mixing between the lower silica and high-silica rhyolites of Tiva Canyon; however, a similar intermediate magma type of Ammonia Tanks *can* be explained as the result of mixing between more evolved portions of the lower silica magma and the coevally erupted high-silica rhyolite. Rainier Mesa is unique among these ash-flow sheets in that three high-silica rhyolite magmas (HSR-1, HSR-2, and HSR-3) can be identified based on trace element geochemistry (in particular Th/Nb, and La). PVA results show that the HSR-1 magma type is unrelated to the coevally erupted lower silica magma and the other two high-silica rhyolites. However, HSR-2 and HSR-3 are related and may be considered as one magma type.

End members determined by PVA for each of the high-silica rhyolite magmas of Rainier Mesa overlap in composition, which may be interpreted as the result of mixing. Indeed, sanidine and melt inclusion, and glass matrix trace-element compositions support mixing among these high-silica magmas and also with a less evolved magma type. However, mixing is limited, such that standard geochemical modeling fails. PVA is more sensitive than typical major and trace element least squares linear regression models in recognizing mixing systems.

In loving memory of Sylvia B. Tefend

ACKNOWLEDGEMENT

I would like to thank Tom Vogel for his support and guidance throughout this project, as well as Lina Patino. I also thank the rest of my committee members, Duncan Sibley and William Cambray, for their efforts in making this dissertation possible. A special thanks goes out to Robert Ehrlich for his patience and assistance in explaining PVA. Thanks, Tom, for suggesting I try PVA in the first place. I would also like to thank the petrology group (Chad, Ela, Dave, Carmen, Melissa, Ryan and Sara), for some great discussions and very memorable times. A special thanks goes out to all of my office mates; I will miss the coffee runs and the group effort crossword puzzles. Also, thank you, Jason Price and Sumi Koh, for helping me get through some tough times; your friendship means a lot to me. I would also like to acknowledge my former Buckeye graduates, Cristina Millan and Jessica Albrecht (now Mrs. Olney!), for their continuing support; great friends like these are invaluable.

As always, my family have been very supportive and have been an inspiration to me throughout the years; I am more proud of my family, especially my father, Clifford Tefend, then words can describe. I would like to write about each and every member of my family, but as I have eight wonderful brothers and sisters, two step brothers, fantastic brother- and sister-in-laws (including Cindy Ayers and Doug Everhart), a step sister-in-law, and an awe-inspiring, absolutely fantastic group of *twenty* nephews and nieces, and of course my mom, step-dad Lee, aunts, uncles, cousins, and grandmother, I would run out of paper and ink toner. This work is dedicated to all of them, but most of all, this is for my stepmom. Sylvia, we will miss you forever.

TABLE OF CONTENTS

LIST OF TABLES

LIST OF FIGURES

CHAPTER 1

INTRODUCTION

Chemically and mineralogically zoned ash-flow sheets have been used to infer the existence of a compositionally zoned preeruptive magma body. Major- and trace-element variations within these ash-flow sheets have been attributed by earlier researchers as *in situ* differentiation processes within the magma chamber prior to eruption, where high-silica magma has formed by crystal fractionation processes from lower silica magma. However, recent studies have shown that compositionally zoned ash-flow sheets can result from open system processes where chemical variations are due to emplacement of different magma batches into the magma chamber prior to eruption. The Timber Mountain/Oasis Valley magmatic group of the southwest Nevada volcanic field (SWNVF) is a well-studied example where such processes have been inferred.

The southwest Nevada volcanic field (SWNVF) contains four large ash-flow sheets, the Topopah Spring (TS), Tiva Canyon (TC), Rainier Mesa (RM), and Ammonia Tanks (AT) tuffs that are some of the best studied series of ash-flow sheets in the world (Figure 1) (Lipman et al., 1966; Christiansen et al., 1977; Byers et al., 1989; Flood et al., 1989a; Flood et al., 1989b; Schuraytz et al., 1989; Warren et al., 1989; Farmer et al., 1991; Cambray et al., 1995; Vogel and Aines, 1996; Mills et al., 1997; Bindeman and Valley, 2003). These ash-flow sheets are interpreted as being compositionally zoned due to the emplacement of discrete, independently generated magma batches into a high-level magma chamber below Timber Mountain prior to eruption (Cambray et al., 1995; Mills

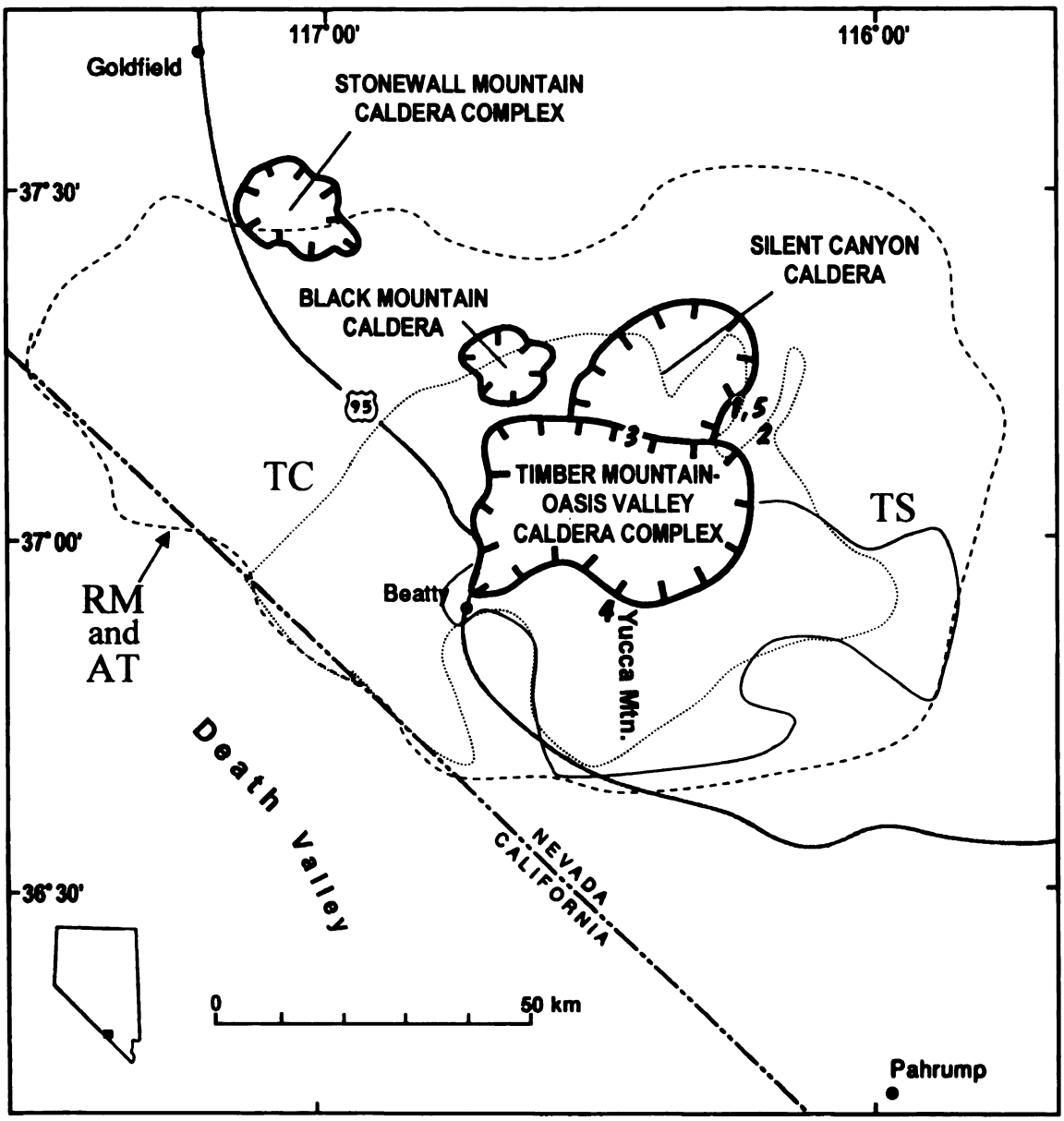

Figure 1. Location of the southwest Nevada volcanic field, Nevada, showing aerial extents of the Topopah Spring (TS), Tiva Canyon (TC), Rainier Mesa (RM) and Ammonia Tanks (AT) tuffs. (modified from Huysken et al, 2001).

et al., 1997). Each of the four ash flows have a lower, volumetrically dominant rhyolitic portion containing high-silica rhyolite pumice fragments, and a smaller volume, less evolved upper portion containing high-silica rhyolite and more mafic pumice fragments that represent the entire compositional range of the ash flow. These lower and upper portions of each ash flow have distinct Sr- and Nd- isotopic compositions (Farmer et al., 1991). Furthermore, $\delta^{18}O$ compositions show that the lower and upper portions of each ash-flow sheet cannot be related to one another by fractional crystallization, nor can the compositions from one ash-flow sheet be related to another ash-flow sheet by fractional crystallization (Bindeman and Valley, 2003).

The origin of silicic magmas in chemically zoned magma systems has long been an enigma; trace element studies and isotope analyses have been used to constrain the origin of silicic magmas and to infer the existence of compositionally zoned pre-eruptive magma bodies (Farmer et al., 1989; Cambray et al., 1995; Mills et al., 1997; Bindeman and Valley, 2003). However, in systems that have diverse silicic magma batches, the question still arises 'what is the relationship of these silicic magmas among the ash-flow sheets, and/or the relationship between the silicic magmas and the coeval mafic magmas within each ash-flow sheet?'. In this study, two types of analyses are used to answer these questions: 1) Polytopic Vector Analysis (PVA), a multivariate statistical method of determining end member compositions in a sample dataset, and 2) trace element compositions of melt inclusions and sanidine phenocrysts.

Polytopic Vector Analysis

Polytopic Vector Analysis (PVA) is explicitly designed to analyze samples that are mixtures; basically, each sample in a dataset is described in terms of some proportion of each end member generated by the program. Therefore, three parameters are needed to define a mixing system: 1) the number of end members, 2) the composition of each end member, and 3) the relative proportion of each end member in each sample within the dataset. Given knowledge of 1) and 2) the mixing proportions can be derived using many procedures. PVA is designed to estimate all three parameters from ambient data (e.g. chemical analyses of rock samples). The only assumptions are that every end member be present in low proportions in at least one sample and that the proportions of each end member within each sample sums to a constant (such as 1.00).

All mixing systems require plotting the data onto a geometric figure termed a simplex. A simplex may occur as a line with end members defined at the two ends (two end member, like the plagioclase series), an equilateral triangle (3 end members), a symmetric tetrahedron (4 end members) or a higher dimensional equivalent. For instance a five end member system requires a four dimensional simplex. Unfortunately the term "simplex" has been used as a label for the Simplex Method of Linear programming. To avoid confusion, the PVA procedure was named Polytopic Vector Analysis. All simplexes are polytopes but not all polytopes are simplexes; only "equilateral" polytopes are simplexes.

PVA was developed by and for geologists, and has evolved over a period of about 40 years; the procedure is now used in many other fields. The initial impetus came from John Imbrie who at the time was interested in grain size distributions and

micropaleontological data sets (Imbrie, 1963; Imbrie and Kipp, 1971). Imbrie, and his graduate student Ed Klovan, coded up a version of "Qmode" factor analysis where the data is placed in a covariance matrix that defines relationships between samples. This program was ultimately named "CABFAC" (Klovan, 1968; Klovan and Imbrie, 1971) and is now widely used to analyze faunal assemblages associated with climate analysis.

The next major development was made at the suggestion of Al Miesch, an igneous petrologist / geochemist at the USGS. Miesch and Klovan converted CABFAC into EXTENDED QMODEL and added the QMODEL procedure (Miesch, 1976a; Miesch, 1976b; Klovan and Miesch, 1976). Miesch wanted an analytical tool to test hypotheses. His concept was that petrologists had developed models of end member systems for a variety of igneous rock types and that a better way to evaluate sample data must exist in order to determine whether one or another model was feasible. Most petrologic data sets contain many more variables than the number of expected end members. If the variables (or analytes) were truly independent, then the data must be plotted using one reference axis for each analyte, in which case the data would plot as a multi-dimensional hypersphere. However, there are many correlations that exist between analytes such that fewer than k dimensions (where "k" is the number of variables) are necessary to enclose the data. Miesch and Klovan developed a superior way to determine the number of dimensions necessary for each variable: the now widely used "Coefficients of Determination" table. Once the dimensionality of the data is known, then the number of end members required is simple: one more than the true dimensionality. So, if this analysis determined that the system required 5 end members, for instance, and theory predicted three end members, then the theoretical system was incapable of defining the

variability among samples. QMODEL permits the analyst to input compositions of theoretical end members to define a simplex, and if all sample data fits within the simplex, then the imposed end member system is feasible. If some samples fall outside the simplex, negative mixing proportions occur and either the model end members are incorrect, or there are problems with data accuracy.

Finally, in 1982 the version that has evolved into the present version of PVA was developed in the context of a particular problem. The research group under Robert Ehrlich had developed a way to quantify grain shape, and it soon became clear that grain shape frequency distributions were polymodal: the sand samples were mixtures of grains of various provenance or transport history. With the help of Klovan, PVA was developed; the principle developer was William Full (Full, et al., 1981, 1982; Ehrlich and Full, 1987). Full's hyper-dimensional insight resulted in the creation of the DENEG procedure (Full, et al., 1981); when a simplex based on extreme samples in the dataset proved to be insufficient or was mis-oriented, the DENEG procedure allowed an iterative systematic enlargement and rotation of the simplex such that, at convergence, a simplex is defined where the compositions of each end member (located at the vertices) had non-negative components and all of the samples could contain non negative mixing proportions. At this stage the procedure was named EXTENDED QMODEL, which was then refined over the next 20 years, and the procedure was renamed PVA. The evolution in PVA continued with major improvements by Glenn Johnson, including the idea of the CD plot as well as the art and practice of PVA implementation with different data set (Johnson, 1997; Johnson, et al., 2000; Johnson, et al., 2002).

The VSPACE Module

PVA consists of 2 modules; the first module (VSPACE) is a variant of Q mode factor analysis that decomposes the covariance matrix into eigenvectors. Eigenvectors represent a rotation of the reference axes that were previously defined by the analytes. As with the original axes, the eigenvectors are mutually orthogonal. The orientation of each eigenvector is controlled by the orientation of the cloud of multivariate variance. By design, the first eigenvector is oriented in the direction of highest variance; the second is oriented in the direction of the highest variance residual to the first, and so on. The amount of variance each eigenvector absorbs is measured by the eigenvalue associated with each eigenvector. Because eigenvectors represent progressively less variance, a common assumption is that at some level variance is so low that it mostly consists of random noise, so that if the higher numbered eigenvectors are disregarded, only noise rather than information is lost. This is the equivalent of projecting the data from the original number of dimensions defined by the number of analytes to a lower dimension defined by the reduced set of eigenvectors.

A chronic problem has been to decide how many eigenvectors to discard. VSPACE utilizes criteria first described by Klovan and Miesch (1976) and later, extended by Johnson et al. (2002). In general these criteria are based on the agreement, variable by variable, between the values in the original data and the values of each variable obtained by back calculation using progressively fewer retained eigenvectors. If, for instance, all of the variables are well approximated by two eigenvectors, then all of the relationships between samples can be displayed on a two dimensional graph. As

discussed above, the number of end members is one higher than the number of necessary dimensions.

Often it is unclear whether there are k or (k+1) dimensions; commonly both solutions are run. The difference between the two solutions often hangs on the "importance" of the agreement between raw data and the back-calculated values for one or two variables.

The PVA Module

The second module is PVA proper. The task of the PVA module is to fit a simplex that encloses the data cloud once the number of end members is determined in the first module, VSPACE. Two criteria are needed to run PVA: 1) an initial guess for the initial simplex and 2) the DENEG procedure (Full et al.,1982).

PVA is an iterative procedure; that is, it starts with an initial simplex and then enlarges and reorients it so as to leave no samples outside the final simplex such that all of the vertices (end member compositions) have elements in the negative orthant. There are several ways to define the location of the initial simplex; the preferred procedure is to choose the most mutually distant samples. The EXRAWC procedure attempts this by initializing on the k samples (where k is the number of end members), each having maximum varimax loadings on an eigenvector; next, a simplex defined by those points is constructed, and then tested, to determine whether any sample is located outside of the simplex (e.g. has negative mixing proportions). The Achilles heel of this option is its' sensitivity to outliers that actually represent data analytical error or entry errors.

However, proper use of information from VSPACE can largely mitigate this problem; hence, this is the default option in PVA.

It is a simple matter to determine which samples fall outside the polytope, as well as determine the composition of any vertex (the candidate end member); the DENEG procedure is an iterative procedure aimed at defining a simplex that encloses all samples and determines the compositions of the vertices. The procedure is designed to operate incrementally by moving any "side" of the simplex outwards a given distance (the DNEG value) parallel to itself or until the DENEG distance contains no samples; at this point, the procedure signals convergence. Thus, each iteration has two parts: 1) the movement of the simplex edges outwards, thus defining new vertices, and 2) changing any negative elements in the end member compositions to zero, thus rotating the simplex.

Sometimes PVA does not converge, or it converges so slowly that the number of iterations is very large. If so, this can be ameliorated by either changing the DENEG value or accepting an iteration that has low negative values in either mixing proportions or end member compositions. Sometimes a lack of convergence reflects the fact that the data cloud is hyper-spherical and thus unmixing is not applicable.

PVA was used to evaluate the relationship of the co-erupted magmas within each of the major ash-flow sheets of SWNVF. Pumice fragment geochemistry and melt inclusion compositions were analyzed by PVA; furthermore, the end members recognized by PVA were used to identify disequilibrium compositions in sanidine phenocrysts.

Statement of the Problem

As stated earlier, the low silica and high silica magmas of each ash flow represent independently generated magmas; this hypothesis, as well as the question of the relationship between the high-silica rhyolites among the ash flows, will be tested by PVA. Furthermore, previous workers had identified the presence of more than one high-silica rhyolite magma represented by the pumice fragments within the Rainier Mesa tuff; these high-silica rhyolite magmas are distinguished from one another by their trace element compositions (Figure 2). PVA will be used to address the relationship of these coevally erupted magma batches of Rainer Mesa. In addition, sanidine and trace element compositions of melt inclusions were obtained in order to further evaluate the relationship among the magmas involved in the generation of these large ash-flow sheets.

Trace elements are sensitive indicators to changes in magma composition, and can record open system processes (magma mixing, assimilation), crystal fractionation, the degree of partial melting and the composition of an assimilant added during magmatic evolution. Melt inclusion compositions have provided a highly useful avenue to study magma evolution (see Taylor et al., 1997; Halter, et al., 2002), because these inclusions can record the change in melt composition during crystallization. These melt inclusions represent the melt from which the host phenocryst grew, and the melt inclusion compositions may record changes in melt composition due to crystal fractionation, magma mixing or assimilation (Roedder and Weibblen, 1970; Urusov and Dudnikova, 1998; Frezzotti, 2001). Not all melt inclusions are accurate representatives of the melt composition at the time of entrapment; recognition of melt inclusion compositions altered by post-entrapment re-equilibration is important (Qin et al., 1992; Lu et al., 1995; Nielsen

A)

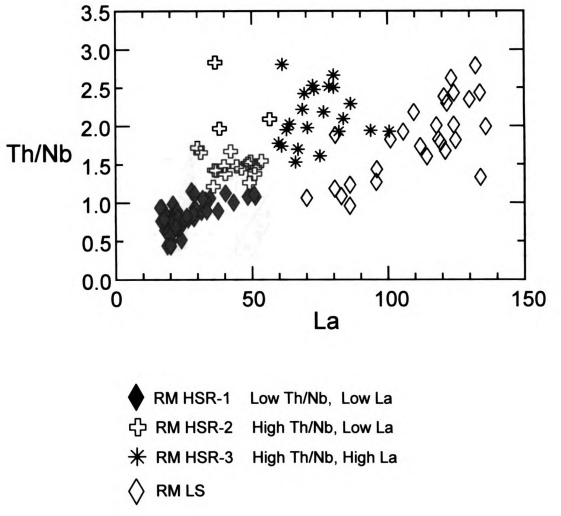

Figure 2 A). Th/Nb versus La plot showing division of Rainier Mesa high-silica rhyolite pumice fragments into three groups (HSR-1, HSR-2, and HSR-3). B). Cumulative frequency plot shown as a normal probability diagram for Rainier Mesa pumice fragments.

B)

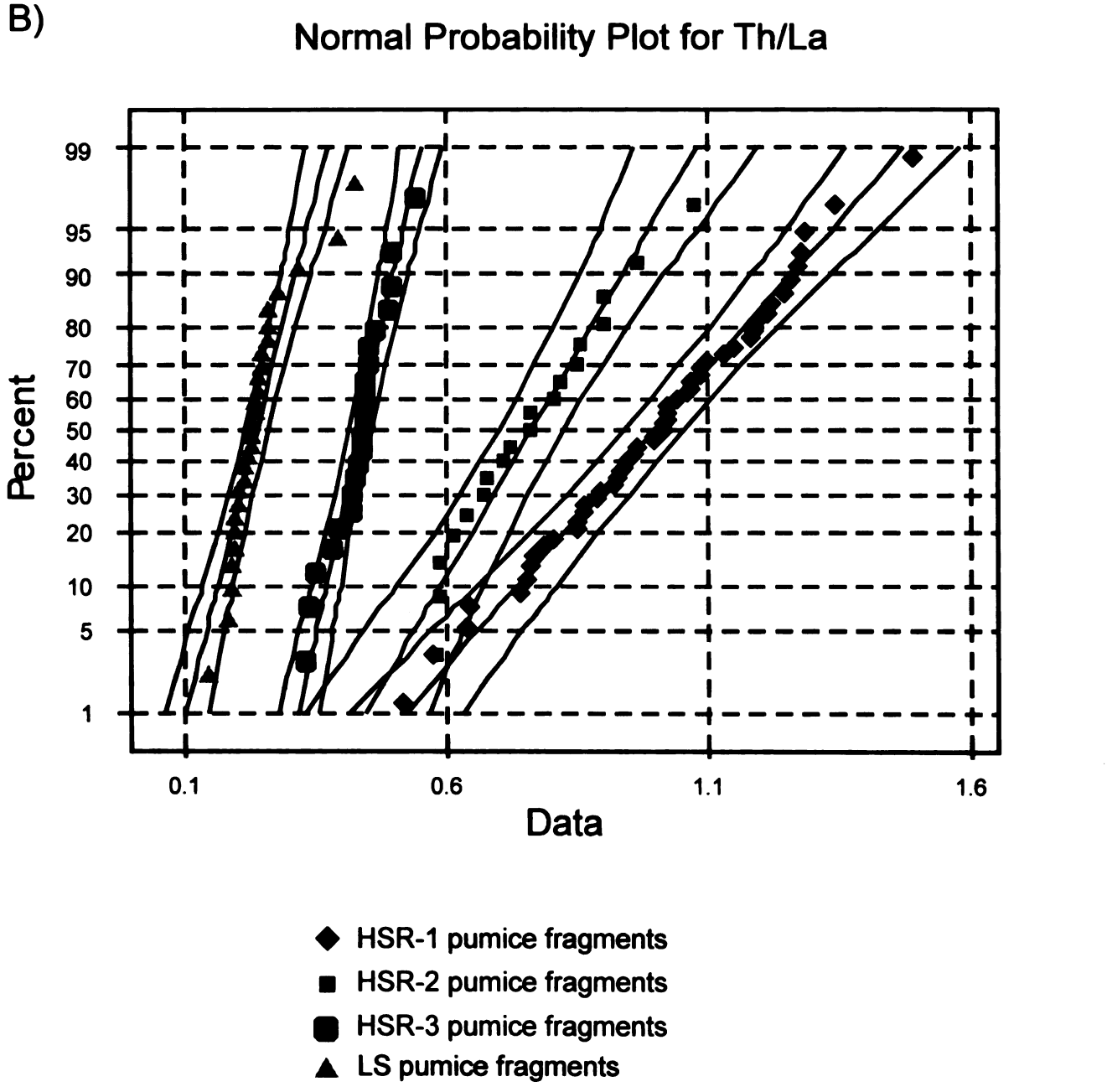

Figure 2. continued.

et al., 1998). Melt inclusions can have regular shaped walls defining a negative-crystal shape that may indicate post-entrapment crystallization. In this study, only those inclusions with rounded shapes were selected for analysis in order to eliminate melt inclusions with post-entrapped altered compositions. Furthermore, the compositions of sanidine-bearing melt inclusions were compared with quartz-bearing and plagioclase-bearing melt inclusions in order to identify which melt inclusions may be altered due to interaction with the host phenocryst. Bacon (1989) suggested that the melt trapped during crystallization of the host phase is not representative of the bulk melt due to the formation of a 'boundary layer' adjacent to the growing host crystal that is enriched in those elements that diffuse slowly through the melt. However, several researchers report that this boundary layer effect is negligible or absent on melt inclusions of ≥ 25 μm in size (Anderson, 1974; Lu et al., 1995; Thomas et al., 2001; Fedele et al., 2003). The melt inclusions chosen in this study all have diameters of ≥ 35 μm.

In addition to trace element compositions in the melt, trace element compositions within the solid phases are also useful in modeling changes in magma evolution. Trace element compositions of plagioclase phenocrysts have been used as evidence of open system processes within a magma chamber such as assimilation and magma mixing Singer et al., 1995; Ginibre et al., 2002; plagioclase phenocrysts can record changes in magma compositions during crystal growth due to the low diffusivities within plagioclase attributed to the Al-Si bond (Grove et al., 1981).

Geologic Setting

The Timber Mountain/Oasis Valley magmatic complex (Figure 1) formed between 13 Ma and 9.5 Ma in the Southern Great Basin, and is part of the 37 Ma to 5 Ma

volcanic activity of the Basin and Range, which has been related to subduction of the Farallon Plate and subsequent regional extension of continental crust (Eaton, 1984; Lipman et al., 1972). Numerous calderas and associated magmatic deposits are collectively called the Southwest Nevada Volcanic Field (SWNVF); the Timber Mountain/Oasis Valley caldera is one of the more recent major calderas within the SWNVF (Christiansen et al., 1977; Byers et al., 1989). The Oasis Valley caldera formed as a result of the eruption of the Paintbrush Group, of which the Topopah Spring (12.8 Ma, 1200 km^3) and the Tiva Canyon (12.7 Ma, ~900 km^3) members are associated. Eruption of the Rainier Mesa tuff (11.6 Ma, 1200 km^3) and Ammonia Tanks tuff (11.45 Ma, 900 km^3) formed the Timber Mountain caldera. Each ash-flow sheet contains high-silica rhyolite pumice fragments (HSR), and a lower silica (LS) pumice fragment composition (Figure 3). In addition, Tiva Canyon and Ammonia Tanks contain an intermediate (INT), rhyolitic pumice fragment population. Rainier Mesa is unique among these ash-flows in that three high-silica rhyolite pumice fragment compositions can be identified based on Th/Nb and La (HSR-1, HSR-2, and HSR-3).

Geochemistry

New pumice fragment geochemistry of Rainier Mesa samples have been added to the existing database and are reported in Appendix 1. Large compositional ranges were reported for the pumice fragments within the Ammonia Tanks (59-78 wt% SiO_2) and Rainier Mesa (57-80 wt% SiO_2) tuffs of the Timber Mountain group (Mills et al., 1997) (Figure 3). The lower silica pumice fragments range from 59.4-66.9 and 56.8-72.1 wt% SiO_2 for the Ammonia Tanks (AT-LS) and Rainier Mesa (RM-LS) tuffs, respectively.

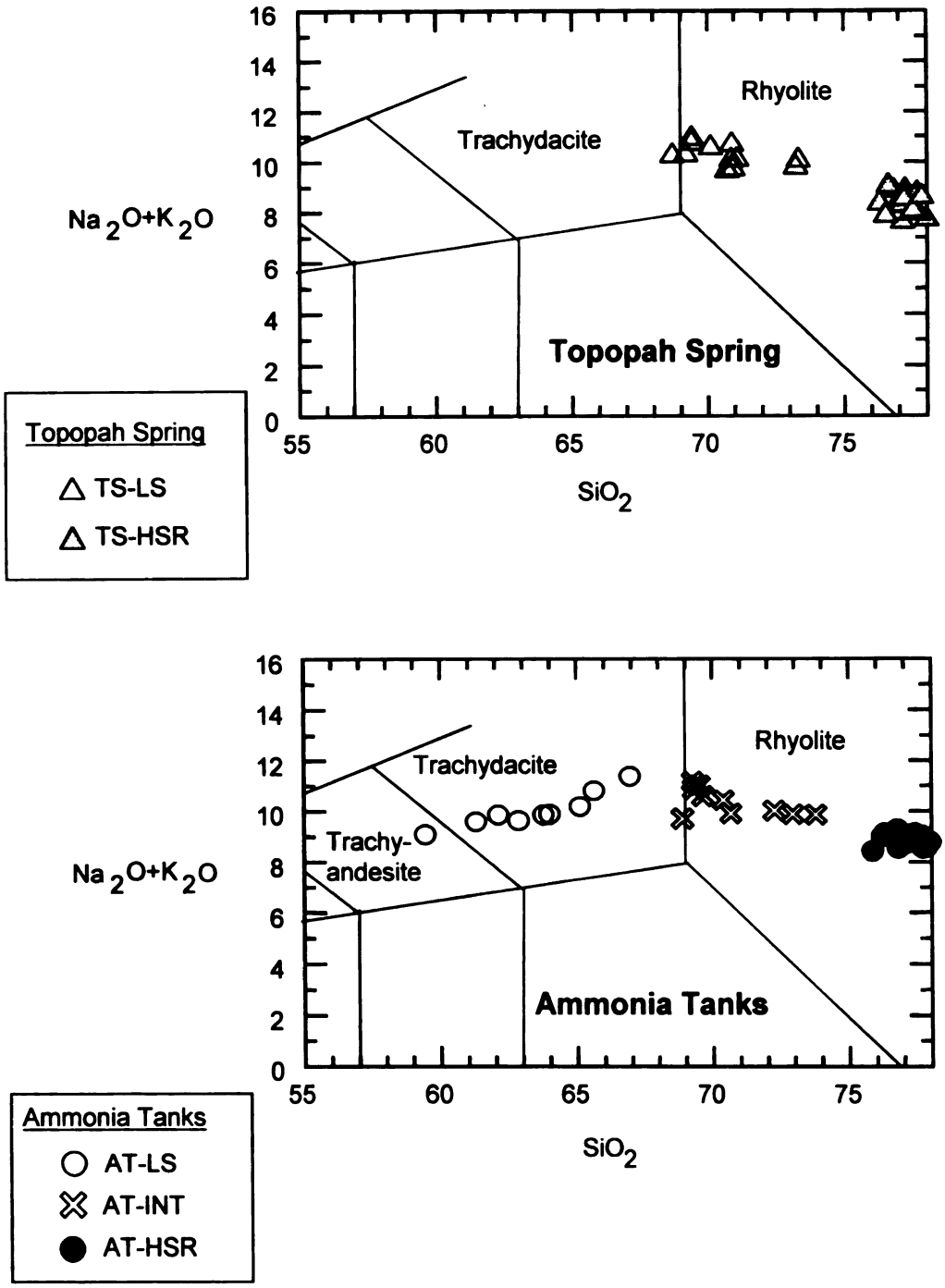

Figure 3. Total alkali diagram of pumice fragment compositions of the major ash-flow sheets of the southwest Nevada volcanic field. (LS = low silica, INT = intermediate, HSR = high-silica rhyolite.

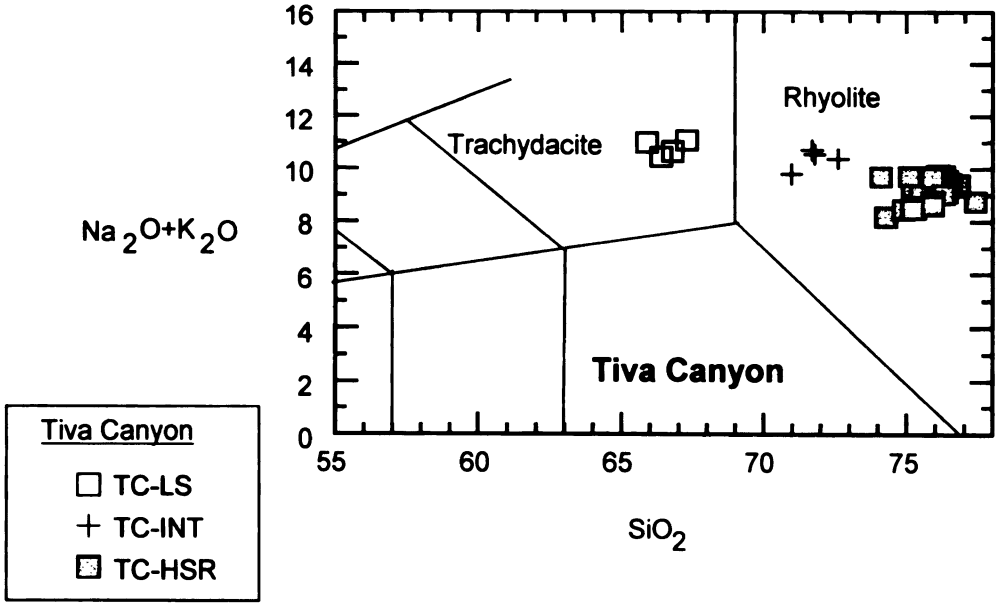

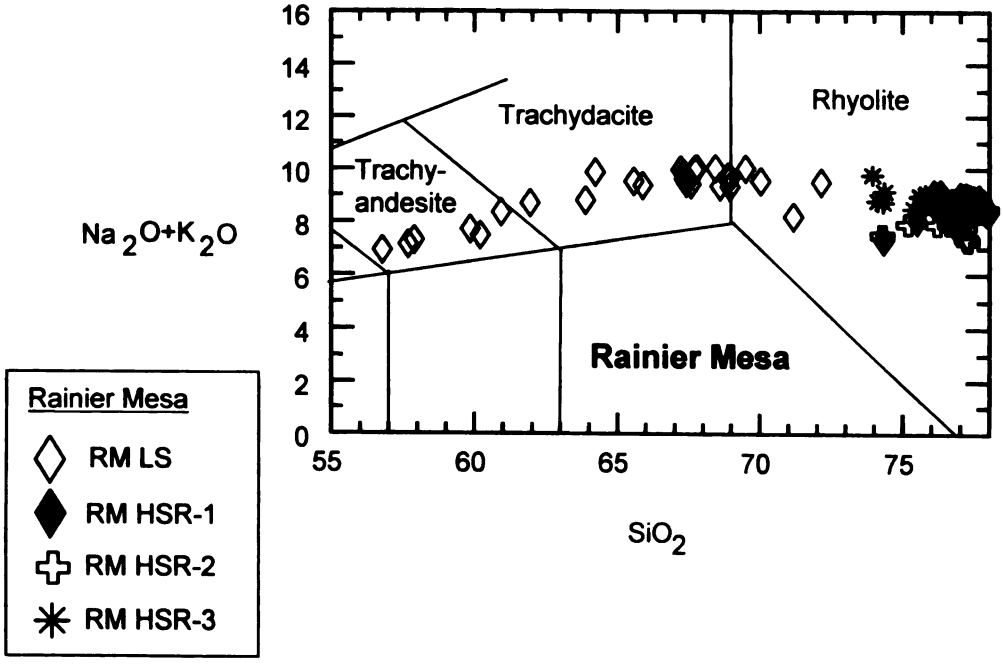

Figure 3. continued.

The high-silica rhyolite (HSR) pumice fragments within the Ammonia Tanks (AT-HSR) tuff have >75.8 wt% SiO_2. There is also an intermediate pumice fragment group (AT-INT) of 68.9-73.8 wt% SiO_2. Within Rainier Mesa, three separate high-silica rhyolite compositional groups are defined, based on trace element (Th, Nb, and La) concentrations (Figure 2A): a high Th/Nb, high La group (RM-HSR-3), a high Th/Nb, low La group (RM-HSR-2), and finally the low Th/Nb group (RM-HSR-1). Pumice fragment compositions in cumulative frequency plots shown as normal probability diagrams confirms the existence of the separate RM-HSR-1, RM-HSR-2, and RM-HSR-3 compositions within the Rainier Mesa ash-flow (Figure 2B).

The range of compositional zoning is not as large for the Topopah Springs and Tiva Canyon tuffs (Figure 3); the Topopah Spring tuff contains pumice fragments that range in composition from 69-79 wt% SiO_2 (Flood et al., 1989a; Schuraytz et al., 1989), and the Tiva Canyon tuff contains pumice fragments that range in composition from 65.9-77.4 wt% SiO_2, (Flood et al., 1989a). The low silica pumice fragment compositions range from 69.0-73 wt% SiO_2 for Topopah Springs (TS-LS) and 65.9-68 wt% SiO_2 for Tiva Canyon (TC-LS). The high-silica rhyolite pumice fragments within the Topopah Springs (TS-HSR) and Tiva Canyon (TS-HSR) have >75.9 wt% SiO_2 and >74.1 wt% SiO_2, respectively. Within the Tiva Canyon tuff, there is also a pumice fragment group (TC-INT) with intermediate silica compositions between 71.0-72.6 wt% SiO_2.

Mineralogy

The pumice fragments from these ash flows are nearly aphyric, with sanidine, albite plagioclase and quartz dominating the RM and AT phenocryst assemblages within

the high-silica rhyolite samples (Mills et al. 1997), and sanidine and albite plagioclase (no quartz) dominating the TS and TC phenocryst assemblages within the high-silica rhyolite samples (Flood et al., 1989a). High-silica rhyolite pumice fragments from TS, TC and AT have allanite, chevkinite and perrierite as the LREE-bearing accessory phases, however within the RM high-silica pumice fragments, monazite represents the major LREE-bearing accessory phase (Warren, et al., 1989; Mills et al., 1997). Sphene is also present in AT and TC high-silica rhyolite pumice fragments; it has been noted by others that there is an antipathetic relationship between monazite and both allanite and sphene (Lyakhovich, 1967; Mackie, 1928; McAdams, 1936; Rapp and Watson, 1986). A more comprehensive report of mineralogy for each of these ash flows can be found in the above cited publications on SWNVF. New analyses of sanidine and plagioclase phenocrysts from pumice fragments of all four ash-flow sheets are listed in Appendix 2.

Isotopic Studies

The earliest isotopic studies of SWNVF ash flows were on $^{87}Sr/^{86}Sr_i$ variations using whole rock and feldspar separates (Noble and Hedge, 1969); these authors reported more radiogenic (higher $^{87}Sr/^{86}Sr_i$) values for the lower portion (more silicic) versus the upper portion (more mafic) of each ash-flow sheet. Nd and Sr isotopic variations for these ash-flow sheets are reported by Farmer et al. (1991); these authors report lower initial ε_{Nd} values and higher $^{87}Sr/^{86}Sr_i$ for the lower portions of these ash flows as compared to the upper, less evolved portions. Oxygen isotope data was reported by Farmer et al. (1991) and more recently by Bindeman and Valley (2003). Bindeman and Valley (2003) interpret their data to indicate that the lower silica and high-silica rhyolite

magmas involved in the formation of each ash flow are not related by fractional crystallization and assimilation within a single magma chamber, and that these magmas most likely represent independent magma batches. Furthermore, Bindeman and Valley (2003) report that the low silica magmas involved in the generation of each ash flow cannot be related by fractional crystallization, and that the high-silica rhyolite magmas of each ash flow likewise cannot be related by fractional crystallization.

Over time, both the low silica and the high-silica rhyolite magmas of the Topopah Spring, Tiva Canyon, and Ammonia Tanks tuffs show a decrease in $\delta^{18}O$, which is consistent with these magmas representing an increase in the contribution of mantle-derived melts; however, Rainier Mesa magmas (both low silica and high silica) have an elevated $\delta^{18}O$ isotopic signature. Bindeman and Valley (2003) proposed that the Rainier Mesa magmas were derived from an ^{18}O-enriched crustal source; this source region dominates the isotopic signature of the Rainier Mesa magmas, thereby obscuring the isotopic contribution from mantle-derived melts.

Radiogenic isotopic analyses also provide a stratigraphic framework for these ash flow sheets. Sawyer et al. (1994) reported $^{40}Ar/^{39}Ar$ isotopic ages to constrain the timing of eruptive events of the SWNVF. More recently, Huysken et al. (2001) reported $^{40}Ar/^{39}Ar$ isotopic ages for the Post-Grouse Canyon tephra (oldest age at 13.52 ± 0.06 Ma) and the Pre-Rainier Mesa tephra sequences (between 12.79 and 11.84 Ma) that place age constraints on the overlying Topopah Springs and Rainier Mesa tuffs, respectively. Of particular interest is the reported geochemistry of the Pre-Rainier Mesa tephra, which has a lower portion (12.79 ± 0.10 Ma) that is geochemically the equivalent of a mixture between Tiva Canyon low silica magma (TC-LS) and Rainier Mesa HSR-1, and an upper

portion of the tephra sequence (11.84 ± 0.18 Ma) with a geochemistry similar to Rainer Mesa HSR-1, indicating that the 11.6 Ma Rainier Mesa magmas were rapidly generated (within 100,000 years) after eruption of the 12.7 Ma Tiva Canyon magmas.

Sampling and Analytical Techniques

Most of the pumice fragments were collected by previous workers (Flood et al., 1989a; Flood et al., 1989b; Schuraytz, et al., 1989; Mills et al., 1991; Bindeman and Valley, 2003), and they report bulk pumice and mineral analyses. Melt inclusion and matrix glass compositions were reported by Vogel and Aines (1996). Additional Rainier Mesa pumice fragments were collected for this study. For new bulk chemistry analyses of these additional samples, the pumice fragments were leached in a glacial acetic acid/sodium acetate solution to remove secondary carbonate precipitation, and then ground by hand using a ceramic mortar and pestle into a fine powder for fusing into glass disks for analysis. Major and minor elements of pumice fragments were measured using a Rigaku S-Max X-ray fluorescence spectrophotometer (XRF) at Michigan State University. New trace element data was collected by a laser ablation-inductively coupled mass spectrometer (LA-ICPMS) at Michigan State University (Cetac LSX 200+ and Micromass Platform ICP-MS). Earlier reported trace element compositions of pumice fragments were collected by XRF (Rb, Sr, Y, Zr, Nb, La, Ba) and instrumental neutron activation analysis (INAA) at Michigan State University (see above references). All major element data have been normalized to 100% anhydrous conditions.

For melt inclusion and phenocryst studies, phenocrysts were liberated from lightly crushed portions of pumice fragments and placed in immersion oil for microscopic

examination to select melt inclusion-bearing grains. Only phenocrysts with melt inclusions >35 μm were isolated and later mounted in resin on a microscope slide for analysis. After the resin hardened, the grains were exposed by hand grinding using abrasive paper, and later polished using diamond paste on a grinding wheel. Major and minor element analyses for melt inclusions and host sanidine and plagioclase were obtained using a Cameca SX-100 electron microprobe at University of Michigan. Microprobe operating conditions were 15 kv accelerating voltage, counting times were 30 seconds per element, with Na and analyzed first, using a beam spot size was 5 μm. Trace element analyses of melt inclusions and the phenocryst host were obtained by depth profiles on a LA-ICPMS at Michigan State University; depth profiles were 25 μm in diameter, with 10 seconds ablation, at a rate of 1 μm/sec. Element concentrations were calculated using Ca and Al as internal standards and a NIST 612 glass disc as an external standard.

CHAPTER 2

PVA RESULTS

Topopah Spring

An initial dataset containing all pumice fragments from the low silica (LS) and high-silica rhyolite (HSR) groups were analyzed (Figure 3); the average pumice fragment compositions of these samples are given in Table 1A. PVA for this dataset (labeled TS-ALL), generated five different end members (EM), the compositions of which are listed in Table 1B. The proportion of each of these end members within each individual pumice fragment is also generated by PVA, and an example of the variation in these proportions is shown in Figure 4. Note that the LS and HSR pumice fragments have different trends; in this figure, the proportion of EM1 versus EM2 within each individual pumice fragment shows that the HSR pumice fragments have very little variation in EM2 (0-4%), and a wide range of EM1 proportions (10-47%). On the other hand, the LS pumice fragments have more variation in EM2 (13-32%) and low proportions of EM1 (0-18%). Different trends for these two pumice fragment groups are also evident in EM2 versus EM5 (Figure 4). Each trend describes the evolution of each magma group, which indicates that the Topopah Spring low silica and high silica samples represent separate magma batches with their own evolutionary trends. If the two pumice fragment groups were related by mixing, they would display similar trends in these EM versus EM graphs.

The compositions of these 5 end members also reveal that the LS and HSR magmas are separate magma batches, because the compositions of the end members are

A)

Ash-flow tuff		TS	TS	TS	TS
pumice group		LS	LS	HSR	HSR
# samples		n = 12		n = 26	
		ave	st. dev.	ave	st. dev.
wt%:	SiO2	70.7	1.46	77.3	1.00
	TiO2	0.4	0.07	0.11	0.027
	Al2O3	15.4	0.81	12.7	0.963
	FeO	1.6	0.26	0.84	0.120
	MgO	0.4	0.13	0.17	0.104
	MnO	0.1	0.02	0.07	0.021
	CaO	1.1	0.43	0.63	0.347
	Na2O	3.8	0.26	2.97	0.340
	K2O	6.5	0.42	5.16	0.281
	P2O5	0.1	0.03	0.02	0.016
ppm:	Th	20.4	1.18	23.8	3.19
	La	169	40.6	34.4	4.33
	Nb*			33.2	3.14
	Rb	141	12.6	196	15.7
	Sr	88.3	59.0	20.3	10.0
	Zr	533	123	145	31.1
	Ce	280	57.5	73.0	10.9
	Ta	0.9	0.10	1.47	0.318
	Sm	11.2	1.54	5.75	0.746
	Eu	2.3	0.80	0.32	0.190
	Tb	0.9	0.05	0.77	0.135
	Yb	3.0	0.16	3.11	0.526
	Lu	0.5	0.10	0.51	0.093
	Sc	5.7	1.30	2.13	0.458
	Cs	3.5	0.51	5.74	1.31
	Hf	11.8	1.77	5.31	0.964
	Ba	954	972	93.6	47.5

Table 1 A). Average compositions of pumice fragments for the high-silica rhyolite (HSR) and lower silica (LS) compositions of Topopah Spring tuff. Also shown are the

*Nb analyzed in only 5 HSR pumice fragments.

B)

Dataset TS-ALL:

End member #		EM1	EM2	EM3	EM4	EM5
wt%:	SiO2	74.6	42.9	75.2	78.3	81.4
	TiO2	0.135	1.59	0.00	0.06	0.05
	Al2O3	17.0	28.1	4.09	12.5	8.87
	FeO	1.05	5.01	0.33	0.566	0.62
	MgO	0.087	1.26	1.78	0.109	0
	MnO	0.227	0.231	0	0.055	0
	CaO	0	1.91	11.0	0	0.10
	Na2O	1.47	6.47	4.60	2.65	4.20
	K2O	5.31	11.2	2.61	5.66	4.68
	P2O5	0	0.38	0.31	0	0.06
ppm:	Th	30	20	14	19	21
	La	28	697	0	5	32
	Nb					
	Rb	271	0	0	205	169
	Sr	0	338	351	0	13
	Zr	179	2050	21	84	48
	Ce	93	1135	7	3	59
	Ta	2	0	1	1	1
	Sm	7	35	1	3	5
	Eu	0	10	1	0	0
	Tb	1	2	1	0	1
	Yb	4	5	4	2	3
	Lu	1	1	1	0	0
	Sc	1	19	2	2	2
	Cs	9	0	0	4	6
	Hf	7	39	2	3	4
	Ba	340	4320	990	0	0

Table 1 B). End member compositions determined for all Topopah Spring pumice samples from the high-silica rhyolite and low silica pumice fragments, combined (TS-ALL).

C)

Dataset TS-HSR:

End member #		EM1	EM2	EM3
wt%:	SiO2	78.5	79.1	74.2
	TiO2	0.081	0.083	0.166
	Al2O3	12.2	9.52	15.1
	FeO	0.80	0.674	0.893
	MgO	0.055	0.284	0.304
	MnO	0.066	0	0.135
	CaO	0.219	1.7	0.811
	Na2O	2.88	3.8	2.84
	K2O	5.16	4.76	5.44
	P2O5	0	0.085	0.017
ppm:	Th	20.8	18.7	28.9
	La	27.1	34.5	50.0
	Nb			
	Rb	197	138	229
	Sr	3.69	49.4	36.2
	Zr	108	113	221
	Ce	54.5	58.6	114
	Ta	1.22	1.18	1.77
	Sm	5.16	4.76	6.88
	Eu	0.167	0.323	0.431
	Tb	0.659	0.651	0.878
	Yb	2.80	2.65	3.58
	Lu	0.484	0.499	0.537
	Sc	2.20	2.45	1.76
	Cs	5.49	3.25	7.84
	Hf	4.38	4.14	7.32
	Ba	73.5	0	249

Table 1 C). End member compositions determined for the dataset composed of all high-silica rhyolite pumice fragments (TS-HSR).

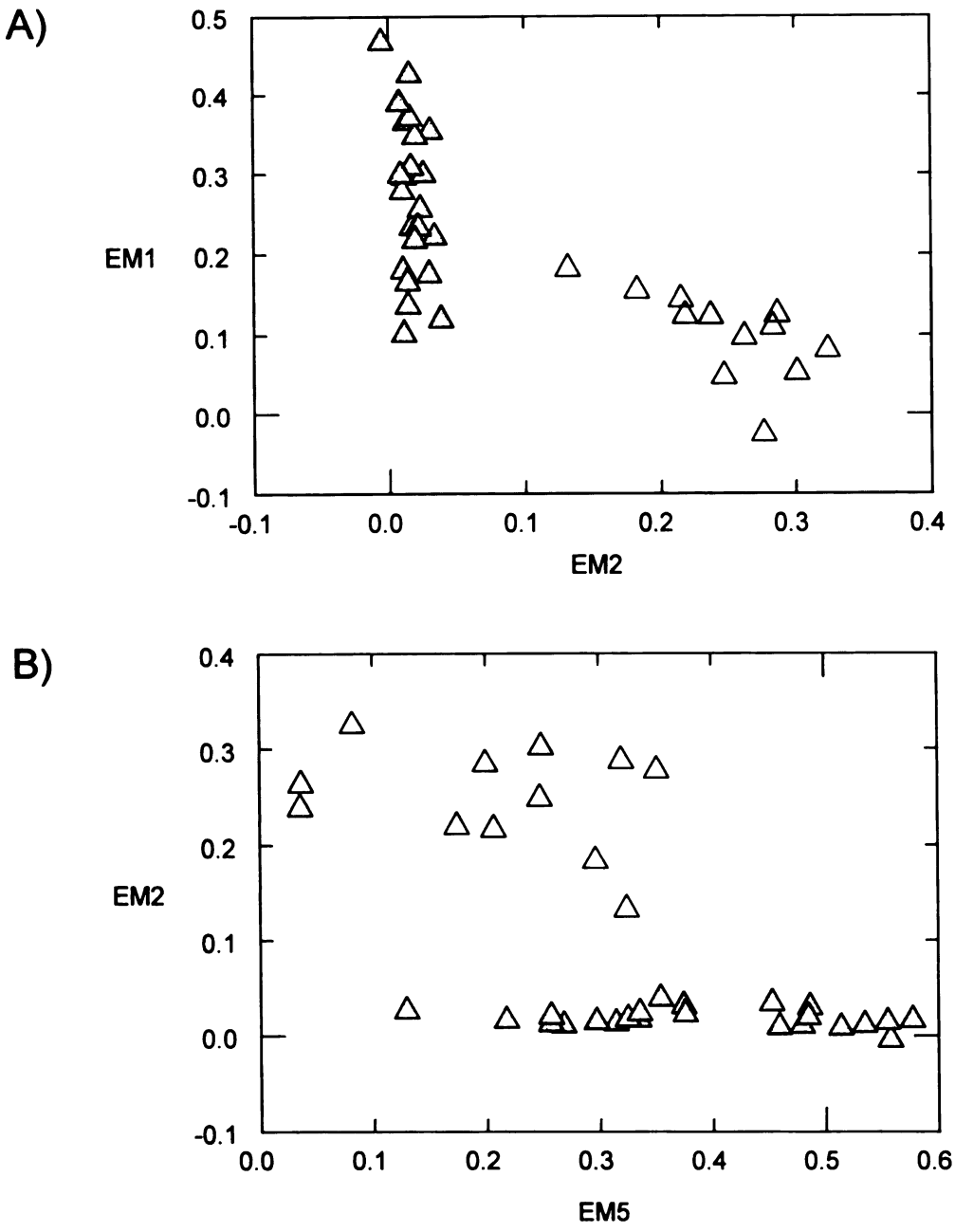

Figure 4. Example of the results of dataset TS-ALL, in which 5 end members were determined by PVA. Each pumice fragment in this dataset has its composition uniquely defined as some proportion of each of these 5 end members, so that the sum is 1 (a negative fraction is the result of preset parameters, and essentially means zero). In this example the proportion of EM1 versus EM2 in A), and EM2 versus EM 5 in B) are shown for each pumice fragment. Note the two different trends displayed for the low silica (LS, △) pumice versus the high-silica (HSR, △) pumice fragments, indicating that these two pumice fragment groups represent unrelated magmas.

unrealistic. End members that represent related magma batches should have compositions that closely constrain the sample populations that they represent; Figure 5 shows that one of the end members for the TS-ALL dataset has an extremely low SiO_2 content (Figure 5A), and a very high La content (Figure 5B), whereas the other four end members plot near or within the field of pumice fragment compositions (shaded region on figure). The results of a second dataset comprised of just the HSR samples (dataset TS-HSR) yields three end members, the compositions of which more accurately represent the range of HSR pumice fragment compositions (Table 1C, Figure 5A and B).

Tiva Canyon

Tiva Canyon pumice fragments represent a low silica magma (LS), a high-silica rhyolite magma (HSR), and an intermediate, rhyolitic magma composition (INT) (Figure 3, Table 2A). PVA of a dataset containing all three pumice fragment compositions (dataset TC-ALL, Table 2B) reveals that the HSR and LS are not related by mixing, as each of these compositional groups have a unique trend in EM proportions (Figure 6). This figure also shows that the INT pumice fragments cannot be the result of mixing between the LS and HSR magmas; note that the EM3 proportion within the INT samples is too low to be consistent with mixing between LS and HSR magmas. Although the compositions of these end members of the TC-ALL dataset are closer representatives of actual pumice fragment compositions (Figure 7) than the previous HSR and LS combined dataset for Topopah Spring (TS-ALL), there is still one end member with uncharacteristically low SiO_2 content for Tiva Canyon magmas. This is also evident in the trace element-trace element plot (Figure 7B). A second dataset composed of all HSR

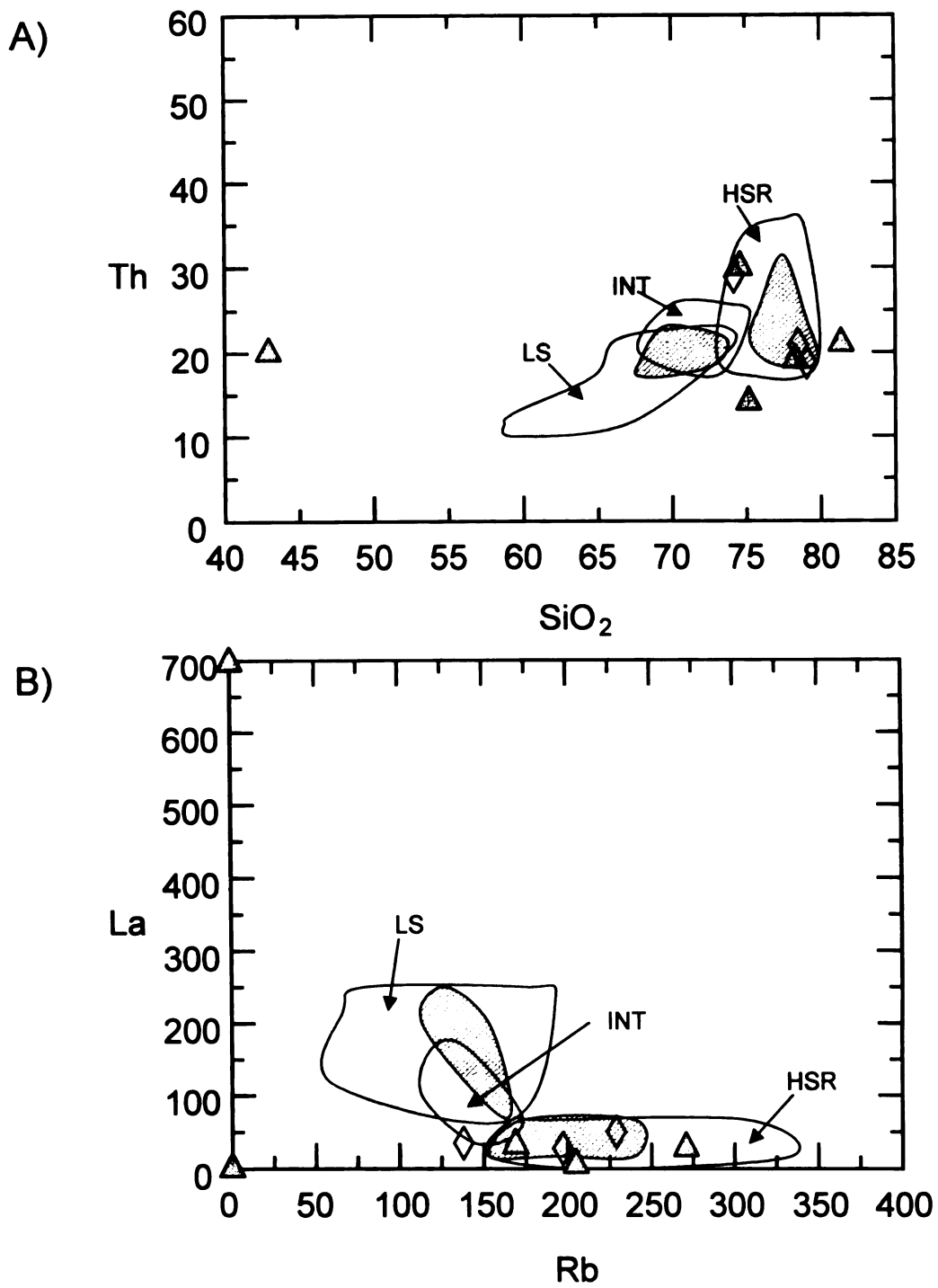

Figure 5. Graph of end member compositions determined for the TS-ALL (△) and TS-HSR (◊) datasets for Topopah Spring. Empty enclosed area defines the range of pumice fragment compositions for low silica, intermediate silica, and high-silica pumice fragments of Topopah Spring (TS), Tiva Canyon (TC), and Ammonia Tanks (AT), combined; shaded region is the range of pumice fragment compositions for Topopah Spring, only. A). Th versus SiO_2. B). La versus Rb.

A)

Ash-flow tuff		TC	TC	TC	TC	TC	TC
pumice group		LS	LS	INT	INT	HSR	HSR
# samples		n = 4		n = 5		n = 37	
		ave	st. dev.	ave	st. dev.	ave	st. dev.
wt%:	SiO2	66.6	0.594	72.2	1.18	75.9	0.60
	TiO2	0.613	0.005	0.32	0.06	0.15	0.01
	Al2O3	17.5	0.34	14.8	0.74	13.1	0.48
	FeO	2.02	0.173	1.30	0.25	0.90	0.14
	MgO	0.69	0.083	0.31	0.14	0.44	0.41
	MnO	0.13	0.022	0.12	0.03	0.09	0.02
	CaO	1.63	0.33	0.88	0.46	0.26	0.06
	Na2O	4.49	0.28	3.69	0.41	3.04	0.29
	K2O	6.3	0.31	6.53	0.14	6.12	0.64
	P2O5	0.11	0.041	0.02	0.01	0.01	0.00
ppm:	Th	13.9	1.28	20.2	0.81	24.1	2.78
	La	215	12.3	75.5	19.4	30.4	4.89
	Nb*					37.6	0.99
	Rb	123	51.1	144	12.9	212	37.0
	Sr**	222	62.5	69.3	10.3	14.1	4.33
	Zr	844	35.4	533	116	232	26.4
	Ce	400	22.4	165	30.2	67.4	11.3
	Ta	0.90	0.20	1.32	0.41	1.67	0.22
	Sm	13.5	0.82	9.80	1.52	6.01	0.99
	Eu	4.77	0.54	0.98	0.19	0.28	0.11
	Tb	0.9	0.0	1.10	0.20	0.95	0.13
	Yb	3.03	0.33	4.02	0.45	3.92	0.39
	Lu	0.53	0.21	0.76	0.15	0.68	0.14
	Sc	7.30	0.5	3.48	0.86	1.63	0.16
	Cs	2.88	1.31	3.74	0.49	5.34	0.68
	Hf	15.1	1.03	12.9	2.56	7.94	0.53
	Ba	2621	585	352	129	89.8	55.6

Table 2 A). Average compositions of pumice fragments for the high-silica rhyolite (HSR), intermediate silica (INT), and lower silica (LS) compositions of Tiva Canyon tuff.

*Nb analyzed in only 5 HSR pumice fragments.
**Sr analyzed in only 7 HSR pumice fragments.

B)

Dataset TC-ALL:

End member #		EM1	EM2	EM3	EM4
wt%:	SiO2	77.2	60.2	75.1	76.2
	TiO2	0.105	0.895	0.134	0.135
	Al2O3	11.9	19.9	13.9	13
	FeO	0.746	2.79	0.992	0.701
	MgO	0	0.49	1.7	0.01
	MnO	0.038	0.137	0.128	0.127
	CaO	0.106	2.49	0.151	0.416
	Na2O	2.17	4.89	3.45	3.79
	K2O	7.67	7.45	4.39	5.58
	P2O5	0.01	0.15	0.01	0
ppm:	Th	22.6	7.14	22.6	26.6
	La	22.1	308	25.8	11.1
	Nb				
	Rb	207	0	183	272
	Sr				
	Zr	116	1230	191	368
	Ce	35.8	570	51.5	69.4
	Ta	1.47	0.18	1.62	2
	Sm	2.93	17.3	5.53	10.1
	Eu	0.172	6.7	0.276	0
	Tb	0.584	0.771	0.877	1.57
	Yb	3.09	2.11	3.57	5.81
	Lu	0.416	0.274	0.665	1.24
	Sc	1.27	10.6	1.49	1.22
	Cs	5.07	0	5.33	6.21
	Hf	5.29	20	6.96	12.4
	Ba	120	3620	140	0

Table 2 B). End member compositions determined for the dataset of all Tiva Canyon high-silica rhyolite, intermediate, and low silica pumice fragments combined (TC-ALL).

C)

Dataset TC-HSR+INT:

End member #		EM 1	EM 2	EM 3	EM 4
wt%:	SiO2	77.5	68.7	75.6	76.5
	TiO2	0.079	0.471	0.108	0.162
	Al2O3	11.7	16	13.6	13
	FeO	0.747	1.74	0.914	0.632
	MgO	0	0	1.68	0.051
	MnO	0.046	0.143	0.125	0.089
	CaO	0.029	1.47	0.076	0.383
	Na2O	2.02	4.01	3.42	3.79
	K2O	7.83	7.25	4.35	5.27
	P2O5	0.00	0.04	0.01	0.01
ppm:	Th	21.2	16.9	23.1	29.2
	La	10.2	123	16.2	41.0
	Nb				
	Rb	177	47.8	196	364
	Sr				
	Zr	70.5	792	153	359
	Ce	8.60	263	33.1	119
	Ta	1.4	1.01	1.66	2.15
	Sm	1.98	14.2	4.97	9.88
	Eu	0	1.72	0.101	0.556
	Tb	0.508	1.27	0.872	1.49
	Yb	2.73	4.17	3.59	5.98
	Lu	0.368	0.748	0.673	1.19
	Sc	0.723	5.15	1.14	2.22
	Cs	4.65	1.56	5.6	7.73
	Hf	4.43	17.2	6.45	11.6
	Ba	19.8	601	80.3	29.6

Table 2 C). End member compositions determined for the dataset composed of all high-silica rhyolite and intermediate pumice fragments, combined (TC-HSR+INT).

D)

Dataset TC-HSR:

End member #		EM1	EM2	EM3	EM4
wt%:	SiO2	77.1	74.8	76.6	74.6
	TiO2	0.147	0.148	0.113	0.196
	Al2O3	12.8	14	12.1	13.3
	FeO	0.478	0.986	0.721	1.3
	MgO	0.19	1.45	0	0.601
	MnO	0.080	0.132	0.045	0.109
	CaO	0.344	0.191	0.079	0.611
	Na2O	3.76	3.63	2.44	2.53
	K2O	5	4.58	7.77	6.68
	P2O5	0.011	0.014	0.005	0.015
ppm:	Th	29.8	21.9	20.0	23.8
	La	45.3	24.4	5.91	66.7
	Nb				
	Rb	365	184	223	88.7
	Sr				
	Zr	365	212	129	313
	Ce	125	52.0	10.4	128
	Ta	2.27	1.5	1.2	1.79
	Sm	10.1	5.46	1.62	9.63
	Eu	0.675	0.214	0	0.935
	Tb	1.45	0.864	0.540	1.09
	Yb	5.81	3.47	2.65	4.55
	Lu	1.18	0.683	0.559	0.416
	Sc	2.45	1.48	0.722	2.64
	Cs	7.75	5.24	5.36	3.03
	Hf	11.1	7.37	5.59	9.59
	Ba	0	140	35.3	258

Table 2 D). End member compositions determined for the dataset composed of all high-silica rhyolite pumice fragments (TC-HSR).

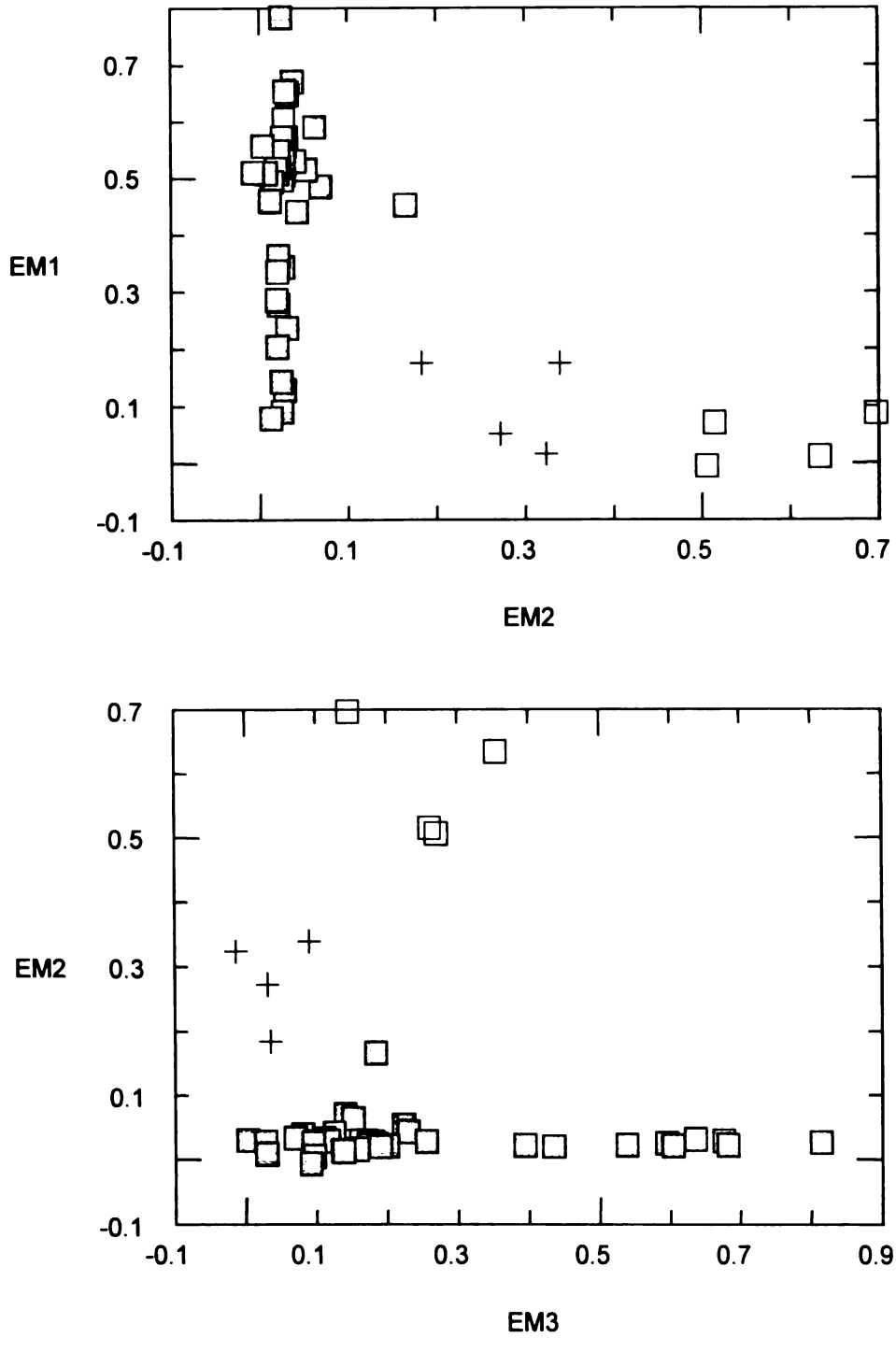

Figure 6. Example of the results of dataset TC-ALL, in which 4 end members were determined by PVA. Note the intermediate (INT, +) pumice fragments fail to plot between the HSR (□) and LS (□) pumice samples in EM1 versus EM3. two different trends displayed for the low silica (LS) pumice versus the high-silica (HSR) pumice fragments, indicating that the intermediate magmas result from mixing between HSR and LS magmas. Notice also the different trends for the HSR and LS magmas, indicating that these are unrelated magma batches.

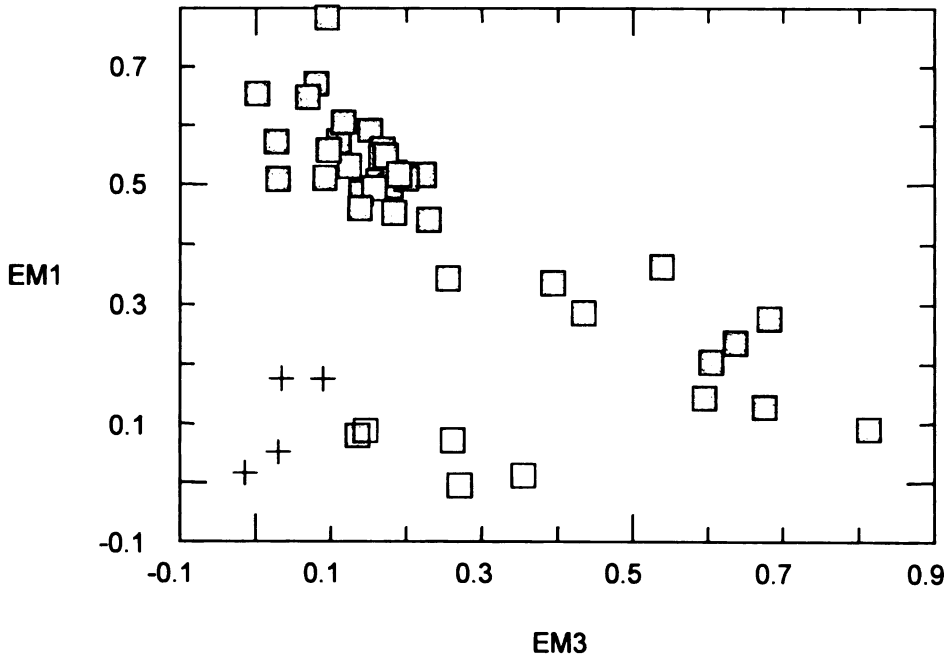

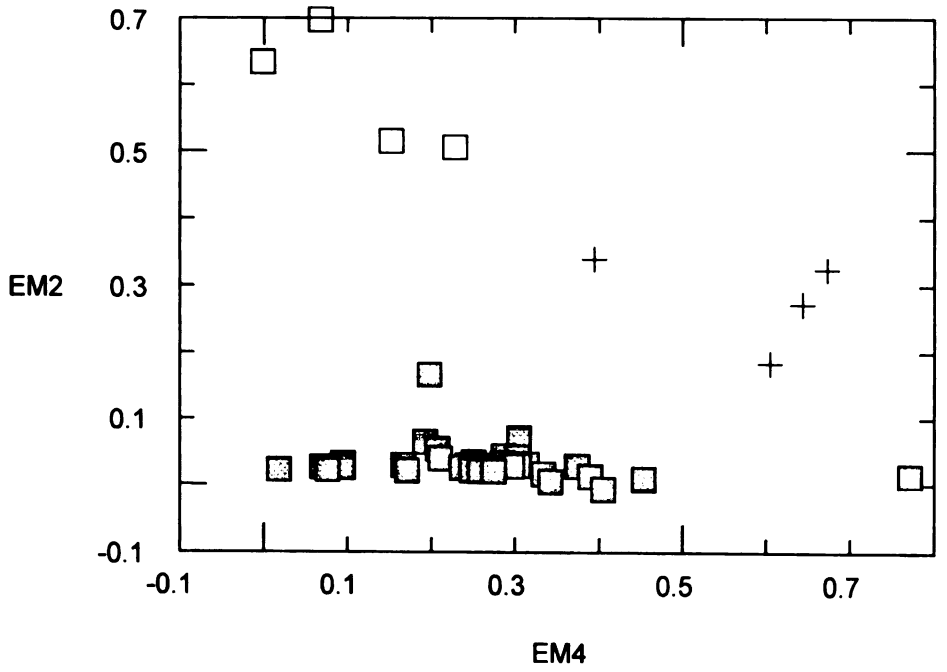

Figure 6. continued.

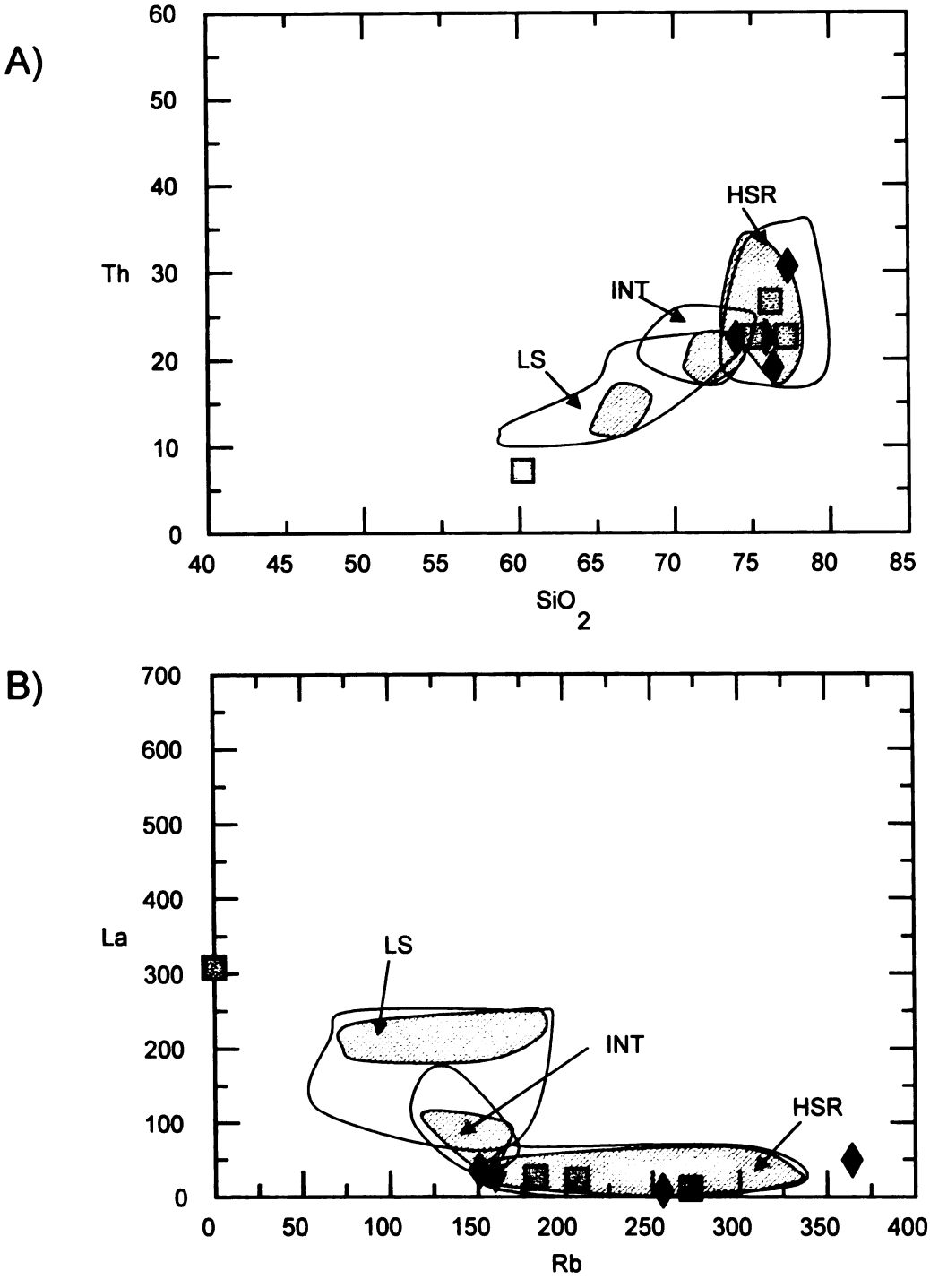

Figure 7. Graph of end member compositions determined for the TC-ALL (◻) and TC-HSR (◆) datasets for Tiva Canyon. Empty enclosed area defines the range of pumice fragment compositions for low silica, intermediate silica, and high-silica pumice fragments of Topopah Spring (TS), Tiva Canyon (TC), and Ammonia Tanks (AT), combined; shaded region is the range of pumice fragment compositions for Tiva Canyon, only. A). Th versus SiO_2. B). La versus Rb.

and INT pumice fragments was next analyzed (TC-HSR+INT, Table 2C); end member-end member plots also reveal different trends in end member proportions for these pumice fragment groups, again indicating that these magma types represent separate magma batches (not shown). PVA results on a dataset with only the LS and INT samples are inconclusive due to the small number of pumice fragments with these compositions (not shown), therefore, the relationship of LS with INT cannot be established, although there seems to some relationship, based on the similar trends in EM proportions between these two pumice fragment groups (Figure 6). However, it is clear that the INT and HSR are unrelated. PVA of the HSR dataset (TC-HSR, Table 2D) yields four end member compositions that have compositions that closely constrain the range of Tiva Canyon HSR pumice fragment compositions (Figure 7). Note that at least one end member composition lies close to the intermediate field; sanidine phenocrysts in the HSR pumice fragments have trace element compositions that indicate mixing with a less evolved magma occurred (see following section). Limited mixing between the HSR and less evolved magma is indicated based on sanidine compositions, and the end member compositions support this.

Ammonia Tanks

In addition to a low silica pumice fragment (LS) and high-silica rhyolite pumice fragment (HSR) group, Ammonia Tanks also has an intermediate pumice fragment group (INT) of rhyolitic composition (Figure 3, Table 3A). PVA of a dataset comprising all three groups (dataset AT-ALL, Table 3B) results in the generation of three end member compositions that better constrain the Ammonia Tanks pumice fragment compositional

A)

Ash-flow tuff		AT	AT	AT	AT	AT	AT
pumice group		LS	LS	INT	INT	HSR	HSR
# samples		n = 9		n = 10		n = 34	
		ave	st. dev.	ave	st. dev.	ave	st. dev.
wt%:	SiO2	63.47	2.32	70.67	1.73	77.26	0.58
	TiO2	0.81	0.18	0.37	0.08	0.15	0.02
	Al2O3	17.82	0.37	15.44	0.81	12.42	0.29
	FeO	3.41	0.97	1.50	0.29	0.73	0.14
	MgO	1.35	0.54	0.41	0.26	0.09	0.14
	MnO	0.12	0.02	0.10	0.01	0.08	0.01
	CaO	2.70	0.88	1.11	0.36	0.44	0.12
	Na2O	4.63	0.19	4.05	0.30	3.32	0.28
	K2O	5.40	0.79	6.29	0.31	5.50	0.39
	P2O5	0.29	0.12	0.06	0.02	0.01	0.01
ppm:	Th	14.27	2.91	21.59	1.81	29.2	5.96
	La	165.7	41.72	102.6	33.52	33.5	7.60
	Nb	16.98	3.29	25.56	2.17	36.7	5.97
	Rb	86.50	17.74	140.4	15.68	220.0	16.93
	Sr	493.0	207	115.9	42.96	11.11	12.96
	Zr	815.0	140.9	344.5	89.03	137.8	20.64
	Ce	272.0	69.40	176.0	59.31	65.84	16.51
	Sm	10.56	1.36	9.09	1.40	5.63	1.49
	Eu	3.23	0.28	1.14	0.41	0.21	0.10
	Tb	0.68	0.07	0.70	0.06	0.77	0.26
	Yb	2.43	0.08	2.63	0.48	3.05	0.95
	Lu	0.41	0.06	0.44	0.09	0.48	0.15
	Sc	6.79	0.62	3.19	1.01	1.33	0.35
	Hf	17.18	2.31	9.43	2.35	5.30	1.28
	Ba	3282	1122	569.6	171.4	115.6	71.37
	Y	31.14	2.80	32.09	1.71	36.51	6.55

Table 3 A).Average compositions of pumice fragments for the high-silica rhyolite (HSR), intermediate silica (INT), and lower silica (LS) compositions of Ammonia Tanks tuff.

B)

Dataset AT-ALL:

End member #		EM1	EM2	EM3	EM4	EM5	EM6
wt%:	SiO2	78.8	36.3	80.8	52.1	77.8	80.1
	TiO2	0	2.27	0.013	1.02	0.177	0.043
	Al2O3	11.4	25.8	10.9	24.1	11.9	11.3
	FeO	0.114	10.2	0.315	3.32	0.786	0.489
	MgO	0.222	5.19	0	0.912	0	0
	MnO	0.057	0.196	0.075	0.145	0.071	0.085
	CaO	0.323	8.92	0.051	2.41	0.331	0.014
	Na2O	1.59	6.17	3.07	6.26	3.87	4.09
	K2O	7.42	2.15	4.76	9.17	4.93	3.76
	P2O5	0	1.09	0	0.163	0	0
ppm:	Th	38.1	0	19.6	3.51	24.7	39.3
	La	0	260	0	377	36.1	8.93
	Nb	41.8	0.3	34.8	0	54.1	34.3
	Rb	223	0	258	0	221	274
	Sr	0	1870	0	341	0	0
	Zr	0	2270	0	1020	1810	36.2
	Ce	17.4	400	0	629	95	24.7
	Sm	3.74	11.9	3.28	21.6	10.4	2.91
	Eu	0	8.93	0	4.69	0.214	0
	Tb	0.825	0.64	0.030	0.771	1.84	0.689
	Yb	4.49	2.13	0	2.45	5.65	2.80
	Lu	0.647	0.24	0	0.542	0.53	0.733
	Sc	0	16.6	0.595	9.69	0.182	1.20
	Hf	3.24	41.8	0	23.3	8.13	4.36
	Ba	0	12000	0	1930	0	0
	Y	25.1	29.3	29.6	22.1	88.1	27.1

Table 3 B). End member compositions determined for datasets composed of all samples of high-silica rhyolite, low silica, and intermediate pumice fragments (AT-ALL).

C)

Dataset AT-HSR+INT:

End member #		EM1	EM2	EM3
wt%:	SiO2	77.7	65.9	78.1
	TiO2	0.129	0.543	0.116
	Al2O3	12.2	17.8	12.2
	FeO	0.66	2.08	0.65
	MgO			
	MnO			
	CaO	0.404	1.59	0.332
	Na2O	3.21	4.65	3.36
	K2O	5.61	7.07	5.13
	P2O5	0.009	0.094	0.006
ppm:	Th	34.7	15.5	21.9
	La	29.8	156	25.4
	Nb	40.1	18.6	29.5
	Rb	224	72.3	229
	Sr	3.4	209	0.0
	Zr	125	518	103
	Ce	69.7	266	30.8
	Sm	5.75	12.5	4.66
	Eu	0.18	1.89	0.025
	Tb	1.06	0.87	0.14
	Yb	4.33	2.94	0.37
	Lu	0.69	0.46	0.06
	Sc	1.00	4.44	1.70
	Hf	6.3	13.2	2.4
	Ba	37.1	944	147
	Y	41.2	33.4	24.4

Table 3 C). End member compositions determined for datasets composed of all high-silica rhyolite and intermediate pumice fragments (AT-HSR+INT).

D)

Dataset AT-LS+INT:

End member #		EM1	EM2	EM3
wt%:	SiO2	59	73.1	66.2
	TiO2	1.07	0.238	0.575
	Al2O3	18.6	14.4	17.7
	FeO	4.81	1.04	1.85
	MgO	2.15	0.223	0.426
	MnO	0.128	0.084	0.121
	CaO	4.03	0.815	1.10
	Na2O	4.74	3.79	4.75
	K2O	4.28	6.26	6.96
	P2O5	0.467	0.018	0.080
ppm:	Th	8.91	22.6	20.3
	La	134	58.7	248
	Nb	15.1	27.9	18.2
	Rb	65.7	160	93
	Sr	806	70	110
	Zr	1070	214	601
	Ce	212	101	420
	Sm	9.25	7.68	13.6
	Eu	3.96	0.446	2.89
	Tb	0.67	0.698	0.697
	Yb	2.29	2.47	2.85
	Lu	0.35	0.415	0.502
	Sc	7.95	1.84	6.53
	Hf	21	6.7	14.9
	Ba	5210	151	1040
	Y	32.3	32.6	29

Table 3 D). End member compositons for the dataset composed of all low silica and intermediate pumice fragments (AT-HSR+INT), respectively.

fields than the TS-ALL or TC-ALL datasets did for their respective pumice fragment populations (Table 3 and Figure 8). Furthermore, the EM plots in Figure 9 confirm that the INT magmas can be described as a mix between HSR and more evolved portions of the LS magma (as first proposed by Mills et al., 1991). In this figure, the circled region indicates LS and HSR pumice fragments with compositions that can generate intermediate (INT) magmas by mixing. The more extensive mixing between the LS and HSR magmas explain why AT-ALL end members are more reasonable in terms of representing all three pumice fragment compositional fields (Figure 8). A breakdown of the dataset into HSR and INT pumice fragments (AT-HSR+INT, Table 3C), and LS and INT pumice fragments (AT-LS+INT, Table 3D) reveals: 1) the most evolved end member in the LS+INT dataset has a HSR-like magma composition, and 2) the least evolved end member in the HSR+INT has a LS magma composition (notice that it falls in the more evolved end of the LS composition field). In other words, PVA recognizes a HSR end member in the LS+INT dataset, and an evolved LS end member for the HSR+INT dataset, which reflects the mixed origin of the INT pumice fragments, confirming earlier major-element multi-linear regression results on specific Ammonia Tanks pumice fragment samples by Mills, et al. (1997).

The CIPW normative compositions of all end members can be used to summarize the PVA results for Topopah Spring, Tiva Canyon, and Ammonia Tanks (Figures 10A and B). Note the extreme compositions of several end members in Figure 10A which result from PVA of datasets containing unrelated pumice fragments (or, unrelated magma batches). For comparison, Figure 10B shows only those end member compositions that resulted from analysis of either a single (in the case of Topopah Springs and Tiva

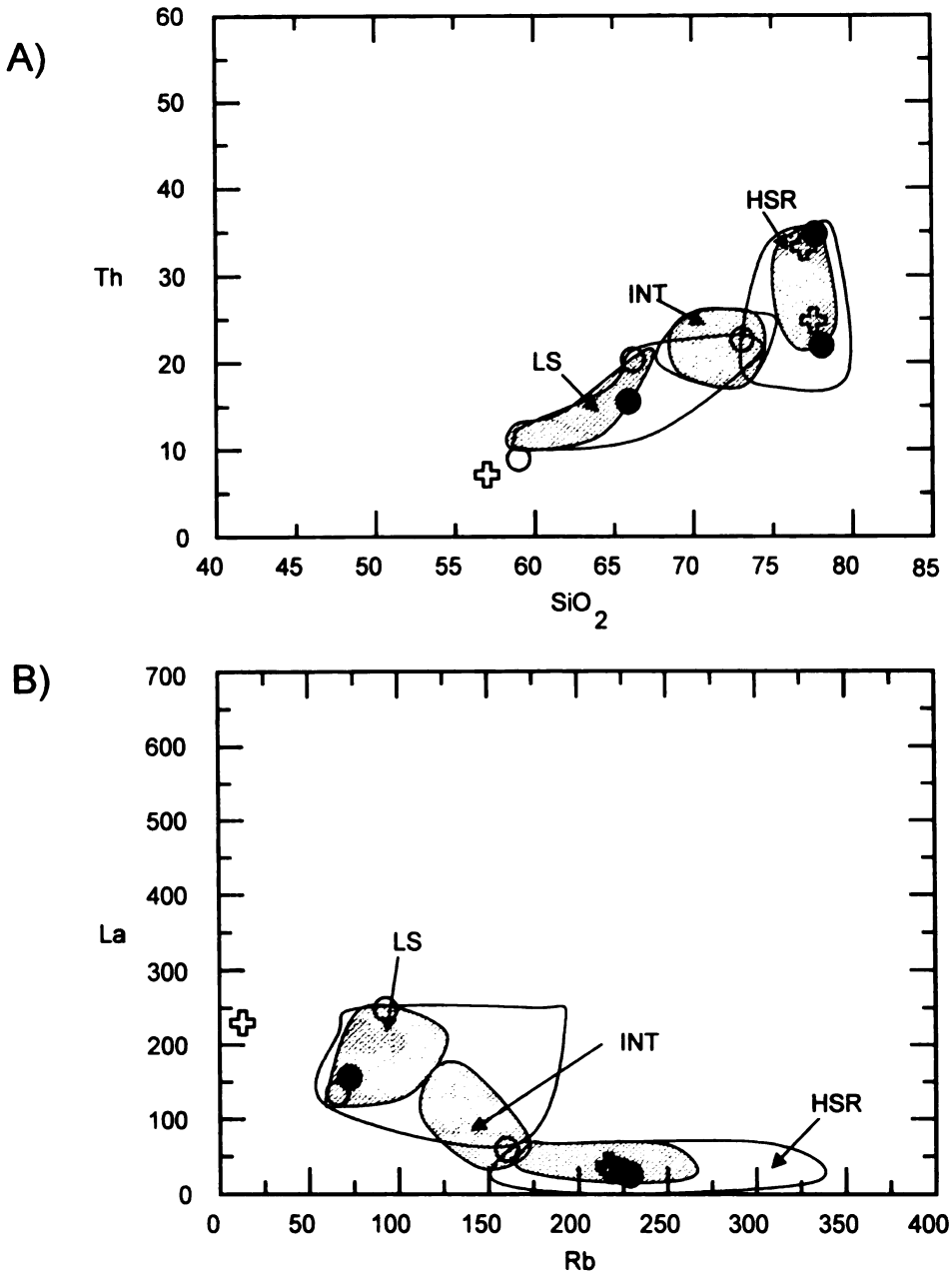

Figure 8. Graph of end member compositions determined for the AT-ALL (✣), AT-LS and INT (○), and AT-HSR and INT (●) datasets for Ammonia Tanks. Empty enclosed area defines the range of pumice fragment compositions for low silica, intermediate silica, and high-silica pumice fragments of Topopah Spring (TS), Tiva Canyon (TC), and Ammonia Tanks (AT), combined; shaded region is the range of pumice fragment compositions for Ammonia Tanks, only. A). Th versus SiO_2. B). La versus Rb.

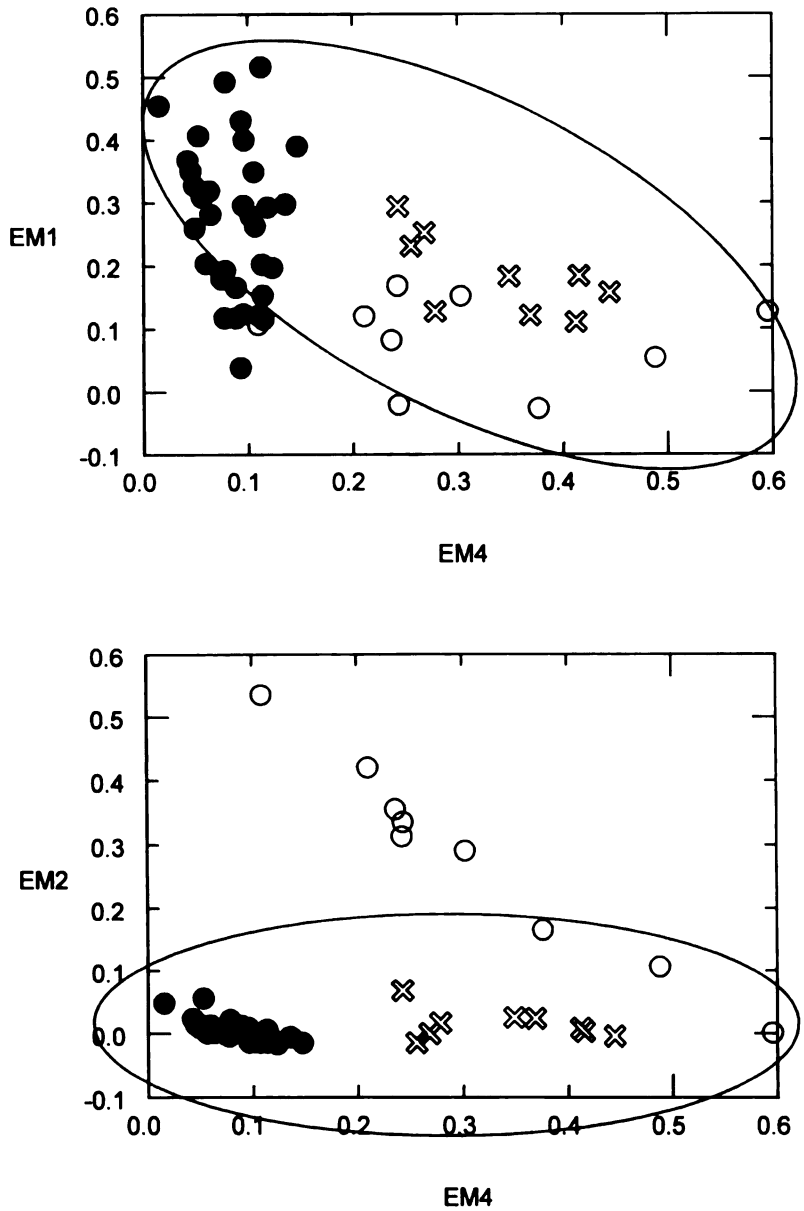

Figure 9. Example of the results of dataset AT-ALL, in which 6 end members were determined by PVA. Note the intermediate (INT,⊗) pumice fragments plot between the HSR (●) and three of the LS (○) pumice samples in EM1 versus EM4 and EM2 versus EM4, indicating that the intermediate magmas result from mixing between HSR and more evolved compositions of the LS magmas. Notice also the different trends for the HSR and LS magmas, indicating that these are unrelated magma batches.

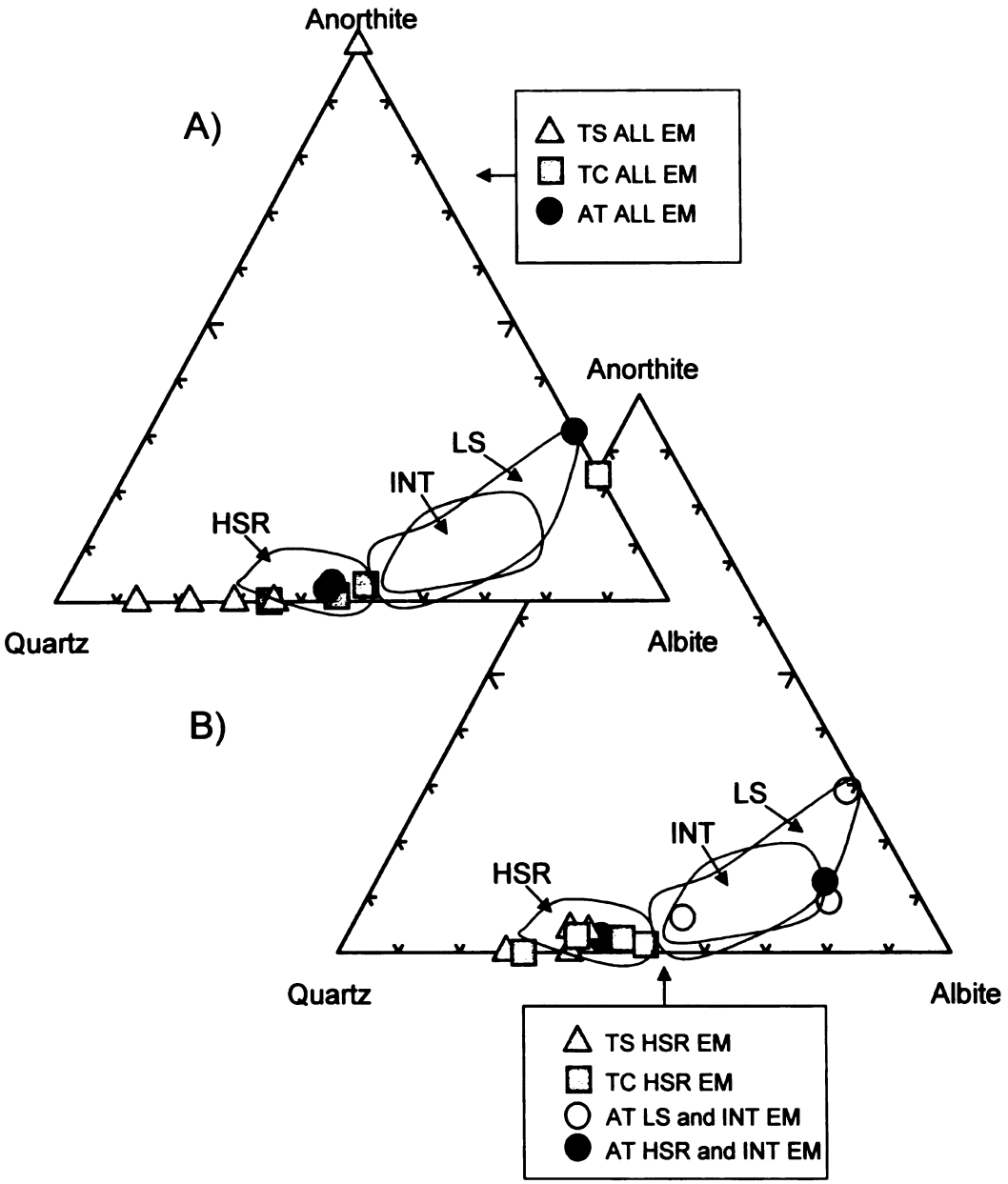

Figure 10. CIPW normative compositions of pumice fragments and end members for each dataset of Topopah Spring (TS), Tiva Canyon (TC), and Ammonia Tanks (AT). The open circled areas are the compositional ranges of TS, TC, and AT, combined, and are included here for reference. A). Notice the extreme compositions of several TS and and one TC end member (see text for explanation). B). Notice that separating the Ammonia Tanks pumice fragments into two separate datasets (one without HSR samples, the other without LS samples), results in end member compositions that define almost the same compositional space as the AT-ALL dataset (which contains all pumice fragment samples); this is attributed to the extensive mixing among the representative magma batches, which generated an intermediate (INT) magma.

Canyon) magma batch, or more than one related (in the case of Ammonia Tanks) magma batches.

Rainier Mesa

Rainier Mesa proved to be more complex than the other three ash-flow sheets; this ash flow contains three high-silica rhyolite pumice fragment compositions (HSR-1, HSR-2, and HSR-3) in addition to a lower silica (LS) pumice fragment group (Table 4A). Combining all pumice fragment samples into one dataset (RM-ALL) yielded five end member compositions (Table 4B). The compositions of these end members poorly constrain the actual range of pumice fragment compositions, as demonstrated in Figure 11A. A second dataset (RM-ALL HSR) excluding the LS pumice fragments was analyzed by PVA, and this time six end members were recognized (Table 4C, and Figure 11A). Most of these end member compositions are also poor representatives of the HSR pumice fragment compositions and have non-magma-like compositions. However, the end member-end member plots showed interesting results: 1) the HSR-1 pumice fragments are clearly unrelated to HSR-2 and HSR-3 based on the observed trends in EM proportions, and 2) the HSR-2 and HSR-3 pumice fragments are related, based on their similar trend (Figure 12A and B). The failure of dataset RM-HSR-ALL to closely define the compositional fields shown in Figure 11A is the direct result of analyzing a dataset that contains unrelated pumice fragments. Breaking down the sample population into a dataset comprised of just the HSR-1 pumice fragments (dataset RM-HSR1, Table 4D), and PVA of another dataset for the HSR-2, HSR-3 pumice fragments combined (dataset RM-HSR2+HSR3, Table 4E), and a third dataset of just LS samples (RM-LS, Table 4F)

A)

Ash-flow tuff		RM	RM	RM	RM	RM	RM	RM	RM
pumice group		LS	LS	HSR-1	HSR-1	HSR-2	HSR-2	HSR-3	HSR-3
# samples		n = 29		n = 45		n = 25		n = 22	
		ave	st. dev.	ave	st. dev.	ave	st. dev.	ave	st. dev.
wt%:	SiO2	65.9	4.22	77.3	0.539	76.9	1.32	75.9	1.01
	TiO2	0.663	0.34	0.115	0.018	0.174	0.026	0.240	0.032
	Al2O3	16.9	0.85	12.8	0.355	13.3	1.28	13.1	0.511
	FeO	3.18	1.71	0.569	0.111	0.803	0.180	0.989	0.154
	MgO	1.21	0.83	0.081	0.150	0.270	0.250	0.195	0.141
	MnO	0.092	0.024	0.068	0.011	0.042	0.010	0.051	0.008
	CaO	2.69	1.43	0.431	0.156	0.373	0.192	0.691	0.167
	Na2O	4.05	0.38	3.18	0.417	2.79	0.335	2.89	0.296
	K2O	5.04	0.85	5.45	0.427	5.28	0.448	5.89	0.425
	P2O5	0.255	0.209	0.018	0.019	0.045	0.042	0.033	0.013
ppm:	Th	26.3	8.04	23.1	3.91	33.5	4.44	31.8	3.38
	La	111	19.1	23.6	5.61	43.2	7.79	74.3	10.8
	Nb	14.6	4.27	30.8	8.31	24.6	8.37	15.3	2.76
	Rb	104	25.7	250	26.2	154	24.5	134	34.7
	Sr	535	280	5.45	8.97	23.8	10.6	64.0	28.5
	Zr	432	77.4	83.0	17.9	129	22.2	183	29.1
	Ce	180	27.7	51.9	8.66	87.5	18.0	121	19.3
	Ta	1.37	0.662	3.29	0.411	1.96	0.484		
	Sm	7.70	1.03	5.14	0.535	5.39	0.708	5.88	0.500
	Eu	1.85	0.517	0.147	0.063	0.320	0.125	0.602	0.141
	Tb	0.77	0.298	0.624	0.188	0.607	0.200	0.545	0.222
	Yb	2.12	0.565	2.88	0.803	2.22	0.410	1.53	0.382
	Lu	0.31	0.123	0.423	0.119	0.334	0.076	0.199	0.069
	Sc	4.91	2.87	3.33	0.960	2.40	0.702	1.80	0.376
	Hf	9.59	1.86	3.47	0.878	4.44	0.583	5.01	1.08
	Ba	1560	490	63.4	73.1	70.6	51.8	261	138
	Y	21.0	5.43	31.1	4.93	22.0	3.76	17.6	3.71

Table 4 A). Average compositions of pumice fragments for each of the high-silica rhyolite (HSR-1, HSR-2, and HSR-3) and lower silica (LS) compositions of Rainier Mesa tuff.

B)

Dataset RM-ALL:

End member #		EM1	EM2	EM3	EM4	EM5
wt%:	SiO2	78.3	35.1	84.2	82.9	5.54
	TiO2	0	1.5	0	0	3.84
	Al2O3	11.9	29	7.94	11.6	35.4
	FeO	0	7.04	0	0	19.5
	MgO	0	1.69	0	0.12	9.47
	MnO	0.103	0.235	0	0	0.342
	CaO	0	7.39	0	0	17
	Na2O	5.34	13.3	0	1.28	2.97
	K2O	4.23	3.24	7.86	4.05	2.53
	P2O5	0	0.409	0	0	2.05
ppm:	Th	4.79	8.88	28.7	68.9	0
	La	0.0	378	28.4	11.8	240
	Nb	51.9	0	2.04	50.6	5.23
	Rb	477	0	142	44.7	0
	Sr	0	1770	0	0	3710
	Zr	0	1590	0	0	1420
	Ce	0	525	46.6	77	389
	Sm	2.93	11.8	4.34	4.18	22.8
	Eu	0	5.86	0	0	9.84
	Tb	0.437	0	0	1.58	3.46
	Yb	4.82	0	0	4.88	5.87
	Lu	0.792	0.087	0	0.784	0.767
	Hf	1.14	28.4	0	4.3	28.3
	Ba	0	6760	0	0	7690
	Y	48.9	0	7.42	26.7	63.6

Table 4 B). End member compositions determined for the dataset composed of all samples from the HSR-1, HSR-2, HSR-3, and low silica pumice fragments (RM-ALL).

C)

Dataset RM-ALL HSR:

End member #		EM1	EM2	EM3	EM4	EM5	EM6
wt%:	SiO2	75.9	65.7	69.1	82.4	89	71.8
	TiO2	0.024	0.57	0.411	0.242	0.027	0
	Al2O3	14.4	17.7	20.5	7.92	3.99	15.6
	FeO	0.359	2.48	1.98	0.671	0	0.301
	MgO	0	0	2.39	0	0	0.529
	MnO	0.108	0.077	0	0.012	0	0.126
	CaO	0.2	2.09	0	0	0	1.39
	Na2O	4.74	3.46	0	8.67	0	0
	K2O	4.25	7.65	5.36	0	6.99	10.2
	P2O5	0.002	0.042	0.220	0.020	0	0
ppm:	Th	18.7	48.9	82.6	38.3	12.9	0.0
	La	0.0	196	86.3	78.1	33.8	0.0
	Nb	60.5	0.0	39.9	0.0	0.0	32.2
	Rb	387	0.0	0.0	0.0	132	515
	Sr	0.0	263	52.0	29.1	0.0	0.0
	Zr	0.0	451	311	162	31.4	0.0
	Ce	0.0	304	197	92.7	41.3	4.4
	Sm	4.50	9.02	6.94	2.50	3.53	7.54
	Eu	0	2.01	0.86	0	0.31	0
	Tb	1.15	0.59	1.61	0	0.33	0
	Yb	6.13	0	2.89	1.78	0	0.65
	Lu	0.96	0	0.48	0.68	0	0
	Hf	3.4	9.5	11.1	5.6	0.5	0
	Ba	12.0	1210	0	0	20.5	96.1
	Y	53.2	0	25.3	0	2.8	51.1

Table 4 C). End member compositions determined for the dataset composed of all samples from the HSR-1, HSR-2, and HSR-3 pumice fragments (RM-ALL HSR).

D)

Dataset RM-HSR1:

End member #		EM1	EM2	EM3	EM4
wt%:	SiO2	76.9	78.6	78.2	74.2
	TiO2	0.143	0.0723	0.128	0.135
	Al2O3	13.4	11.9	11.6	14.5
	FeO	0.616	0.314	0.741	0.786
	MgO	0	0	0	0.931
	MnO	0.076	0.052	0.060	0.089
	CaO	0.127	0.503	0.51	0.688
	Na2O	5.01	2.14	3.22	2.2
	K2O	3.63	6.44	5.48	6.37
	P2O5	0.036	0	0.002	0.041
ppm:	Th	30.8	13.3	24.8	26.5
	La	22.8	17.4	50.2	10.7
	Nb	47.3	19.8	6.1	46.8
	Rb	267	282	152	253
	Sr	0	2.92	7.36	18.3
	Zr	67.8	56.6	132	104
	Ce	47.1	40.3	68.3	62.9
	Sm	3.88	5.95	7.14	3.57
	Eu	0.090	0.148	0.049	0.299
	Tb	1.25	0.234	0	1.14
	Yb	5.79	1.73	0	3.46
	Lu	0.932	0.099	0	0.647
	Hf	5.58	1.18	3.29	4.27
	Ba	21.4	157	0	10.0
	Y	40.2	25.2	15.1	41.4

Table 4 D). End member compositions determined for the dataset composed of all HSR-1 pumice fragments (RM-HSR-1).

E)

Dataset RM-HSR2+HSR3:

End member #		EM1	EM2	EM3	EM4
wt%:	SiO2	71.0	75.3	77.1	80.2
	TiO2	0.431	0.232	0.109	0.120
	Al2O3	14.5	15.5	12.6	10.7
	FeO	1.65	0.944	0.560	0.593
	MgO	0	1.06	0	0.093
	MnO	0.071	0.026	0.057	0.038
	CaO	1.57	0	0.730	0.254
	Na2O	3.59	2.86	3.65	1.84
	K2O	6.97	3.89	5.18	6.15
	P2O5	0.034	0.108	0.018	0.003
ppm:	Th	32.3	43.4	22.2	29.7
	La	146	42.3	14.5	45.7
	Nb	3.49	35.6	10.4	19.1
	Rb	80.6	155	218	125
	Sr	184	20.6	5.65	0
	Zr	337	175	63.9	90.1
	Ce	218	87	56.9	72.9
	Sm	7.54	5.93	4.47	4.73
	Eu	1.32	0.259	0	0.412
	Tb	0.303	0.903	0	0.888
	Yb	0	3.3	1.47	2.04
	Lu	0	0.521	0.259	0.285
	Hf	6.38	6.31	1.55	4.49
	Ba	786	44.9	0	32.1
	Y	7.17	28.4	15.9	22.1

Table 4 E). End member compositions determined for the dataset composed of all HSR-2 and HSR-3 pumice fragments, combined (RM-HSR-2+HSR-3).

F)

Dataset RM-LS:

End member #		EM1	EM2	EM3
wt%:	SiO2	65	56	73
	TiO2	0.504	1.47	0.36
	Al2O3	17.9	18.1	14.7
	FeO	2.46	7.32	1.51
	MgO	0.63	3.27	0.704
	MnO	0.100	0.135	0.052
	CaO	2.51	6.06	0.761
	Na2O	4.98	3.6	2.97
	K2O	5.37	2.89	5.87
	P2O5	0.155	0.766	0.068
ppm:	Th	20.3	9.94	42.7
	La	124	67.4	114
	Nb	6.45	15.8	25.6
	Rb	104	74.2	123
	Sr	604	1220	49.5
	Zr	590	365	241
	Ce	172	133	212
	Sm	6.53	10.4	7.79
	Eu	2.08	2.99	0.854
	Tb	0.463	1.47	0.811
	Yb	1.16	3.56	2.66
	Lu	0.150	0.631	0.358
	Hf	12.8	8.77	5.26
	Ba	2520	1770	64.9
	Y	13.9	32.3	24.4

Table 4 F). End member compositions determined for the dataset composed of all low silica pumice fragments (RM-LS).

G)

Dataset for RM-HSR2:

End member #		EM1	EM2	EM3	EM4
wt%:	SiO2	75.7	77.5	75.5	81.1
	TiO2	0.218	0.107	0.231	0.144
	Al2O3	15.2	12.5	13.4	9.91
	FeO	0.828	0.597	0.959	0.793
	MgO	0.886	0.063	0.176	0.205
	MnO	0.024	0.060	0.037	0.043
	CaO	0	0.562	0.793	0.078
	Na2O	2.73	2.93	2.98	2.22
	K2O	4.25	5.63	5.89	5.39
	P2O5	0.073	0.020	0.047	0.034
ppm:	Th	39.6	26.3	34.1	26.6
	La	45.5	25.3	63.2	39.9
	Nb	30.5	14.4	16.6	21.5
	Rb	149	201	135	106
	Sr	23.3	0.0	48.8	31.8
	Zr	157	65.3	172	121
	Ce	75.0	58.1	133	69.3
	Sm	6.13	4.88	5.71	3.61
	Eu	0.297	0	0.567	0.374
	Tb	0.872	0.269	0.407	0.708
	Yb	2.83	2.03	1.40	1.94
	Lu	0.453	0.314	0.148	0.312
	Hf	5.33	2.82	5.35	3.92
	Ba	60.5	0.0	92.2	164
	Y	27.0	22.3	16.6	16.4

Table 4 G). End member compositions determined for the dataset composed of all HSR-2 pumice fragments (RM-HSR-2).

H)

Dataset for RM-HSR3:

End member #		EM1	EM2	EM3	EM4
wt%:	SiO2	71.8	78.9	75.4	75.5
	TiO2	0.337	0.135	0.233	0.291
	Al2O3	14.8	11.7	13.4	13.2
	FeO	1.51	0.54	0.969	1.14
	MgO	0.30	0	0.036	0.450
	MnO	0.059	0.034	0.041	0.071
	CaO	1.19	0.376	0.792	0.719
	Na2O	2.98	1.87	3.44	3.17
	K2O	6.74	6.46	5.53	5.36
	P2O5	0.074	0	0.035	0.043
ppm:	Th	34.2	35.8	21.1	36.7
	La	108	62.3	54.2	88.6
	Nb	17.4	19.5	10.8	14.0
	Rb	132	111	123	162
	Sr	161	0.0	112	36.9
	Zr	272	90.3	175	221
	Ce	165	104	78.8	156
	Sm	7.00	6.07	5.15	5.94
	Eu	1.15	0.694	0.463	0.447
	Tb	0.351	1.18	0.0	0.666
	Yb	1.28	2.50	0.157	2.00
	Lu	0	0.333	0.116	0.218
	Hf	6.29	6.04	2.10	6.06
	Ba	848	29.5	359	127
	Y	25.5	25.6	10.6	14.1

Table 4 H). End member compositions determined for the dataset composed of all HSR-3 pumice fragments (RM-HSR-3).

l)

Dataset RM-HSR2+3+LS:

End member #		EM1	EM2	EM3
wt%:	SiO2	80.3	39.3	75.6
	TiO2	0.124	1.86	0.124
	Al2O3	11.7	26.5	13.2
	FeO	0.593	9.36	0.316
	MgO	0.516	4.24	0
	MnO	0.024	0.197	0.0547
	CaO	0	8.10	0.408
	Na2O	1.98	6.54	3.41
	K2O	4.72	2.20	6.85
	P2O5	0.0637	0.907	0
ppm:	Th	33	9.85	32.9
	La	1.11	184	111
	Nb	27.3	16.4	8.11
	Rb	170	16.9	125
	Sr	0	1870	0
	Zr	0	993	278
	Ce	26.4	295	170
	Sm	4.71	13.2	5.65
	Eu	0	5.2	0.656
	Tb	0.742	1.78	0.202
	Yb	2.76	4.29	0.519
	Lu	0.446	0.720	0.00209
	Hf	2.27	20.9	5.79
	Ba	0	4700	538
	Y	26.7	35.7	9.53

Table 4 l). End member compositions determined for the dataset composed of all HSR-2, HSR-3, and low silica (LS) pumice fragments (RM-HSR2+3+LS).

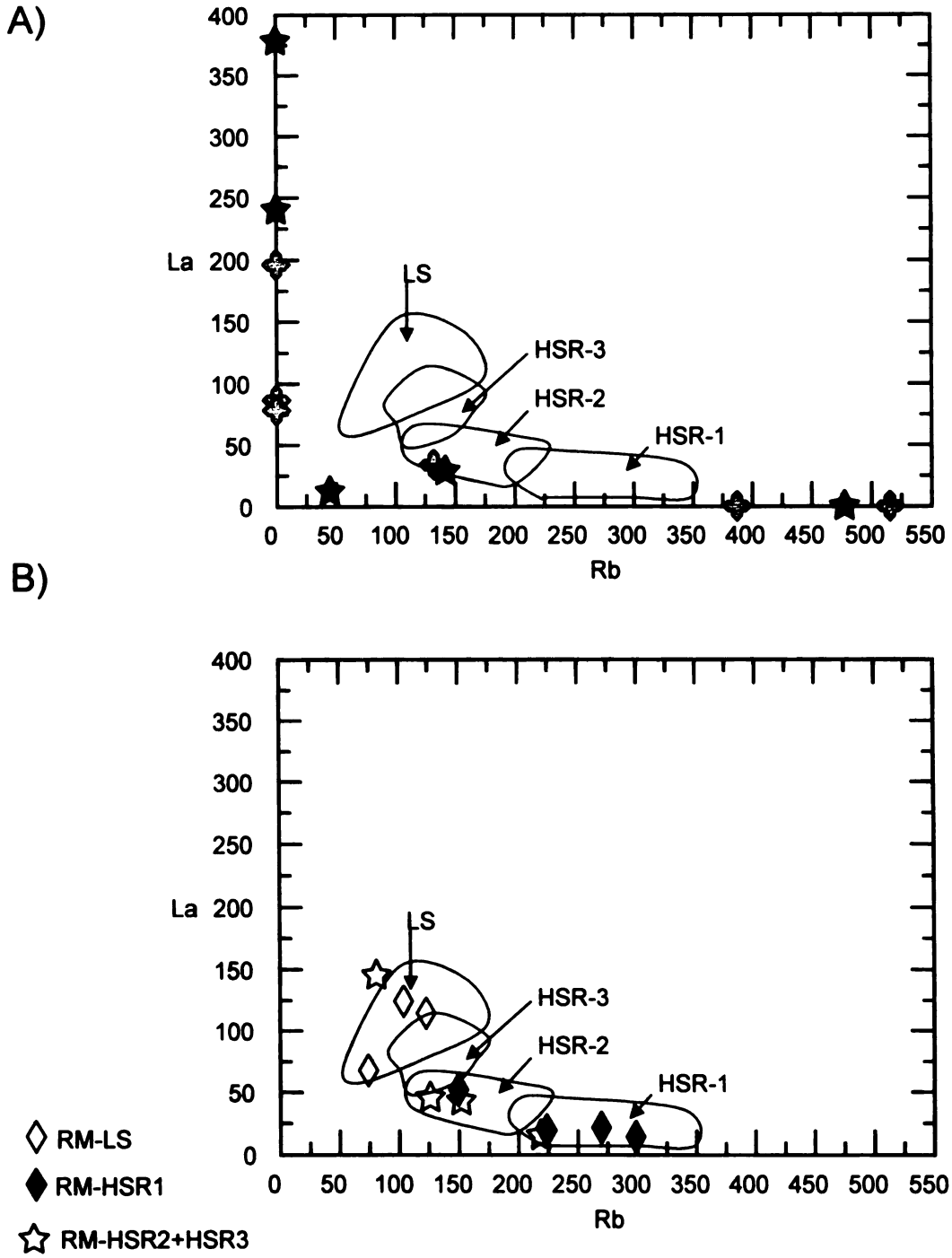

Figure 11. A). Graph of end member compositions determined for the RM-ALL (★) and RM-ALL-HSR (✦) datasets. Empty enclosed areas define the range of pumice fragment compositions for low silica (LS), and all three high-silica pumice fragments of Rainier Mesa (RM). B). Note how the end member compositions more accurately define the fields of pumice fragment compositions, as well as the tendency of some of the end members to overlap in composition (see text for explanation). C). End members determined for each separate pumice fragment group (RM-LS, RM-HSR1, RM-HSR2, and RM-HSR3).

C)

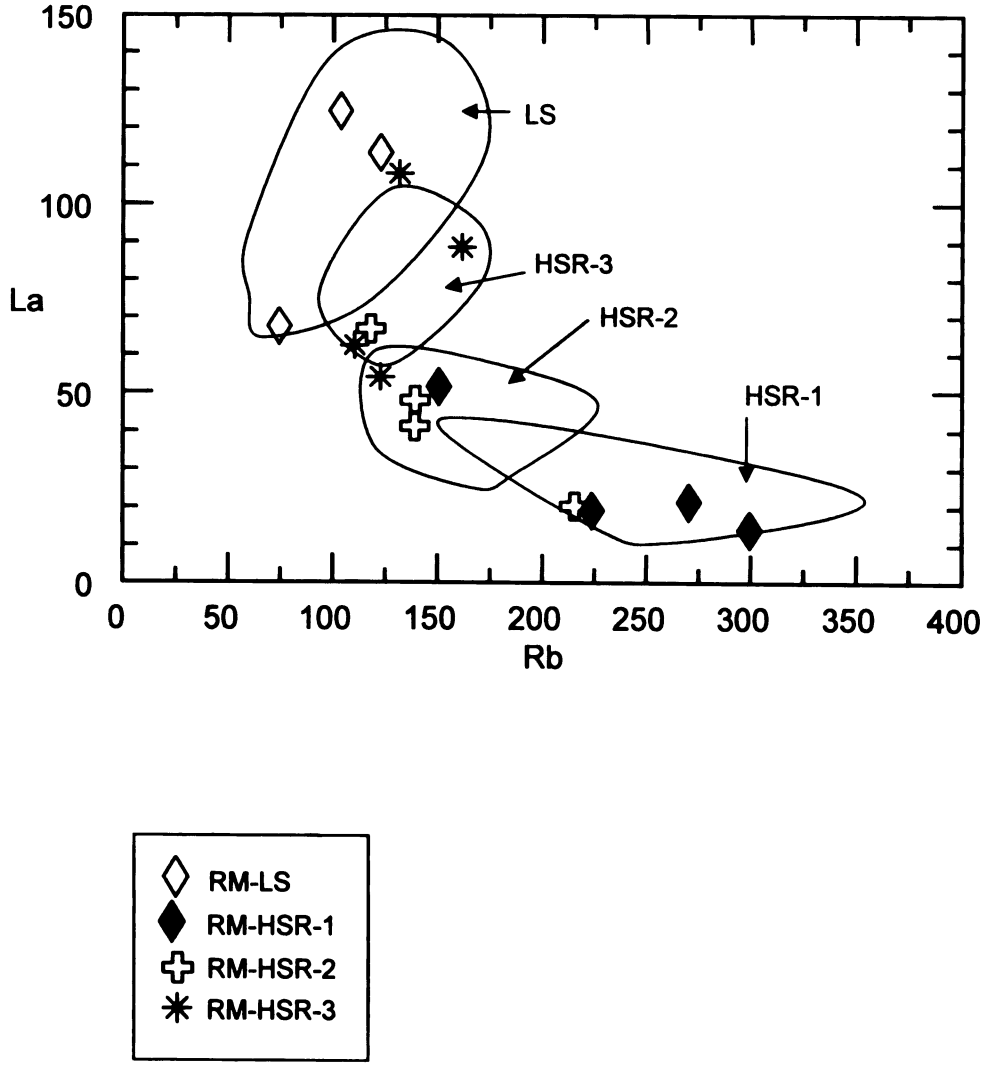

Figure 11. continued.

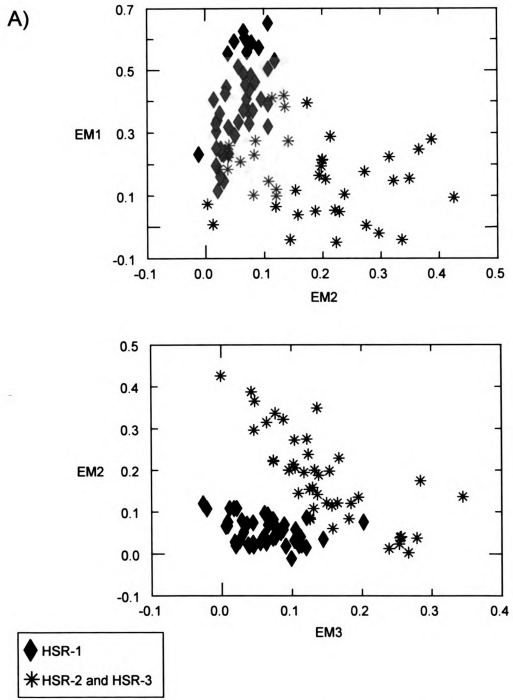

Figure 12. A). Example of the results of dataset RM-ALL-HSR, in which 6 end members were determined by PVA. In this example the proportion of EM1 versus EM2 and EM6, and EM2 versus EM3 and EM4 are shown for each pumice fragment. Note the two different trends displayed for the HSR-1 pumice fragments, and the second, more scattered trend of the HSR-2 and HSR-3 pumice fragments; the HSR-2 and HSR-3 pumice fragments do not separate into two groups statistically, and most likely represent the same, or a related magma batch. However, HSR-1 must represent a magma batch unrelated to HSR-2 and HSR-3. B). Same results from dataset RM-ALL-HSR, now with each HSR pumice fragment identified separately.

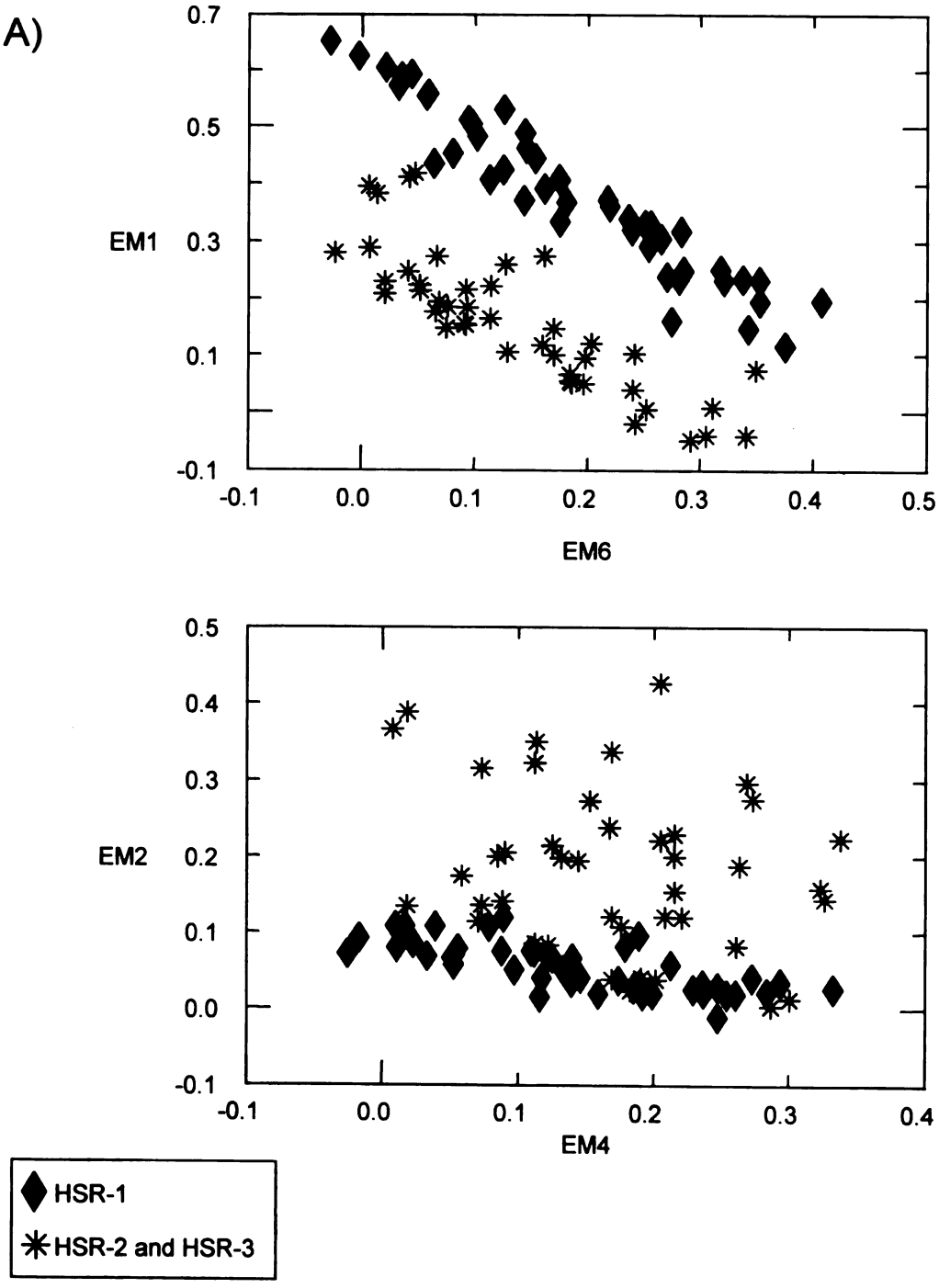

Figure 12. continued.

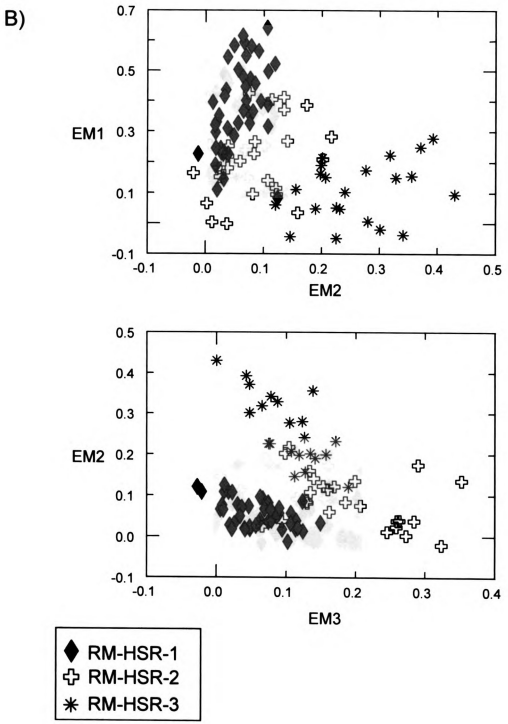

Figure 12. continued.

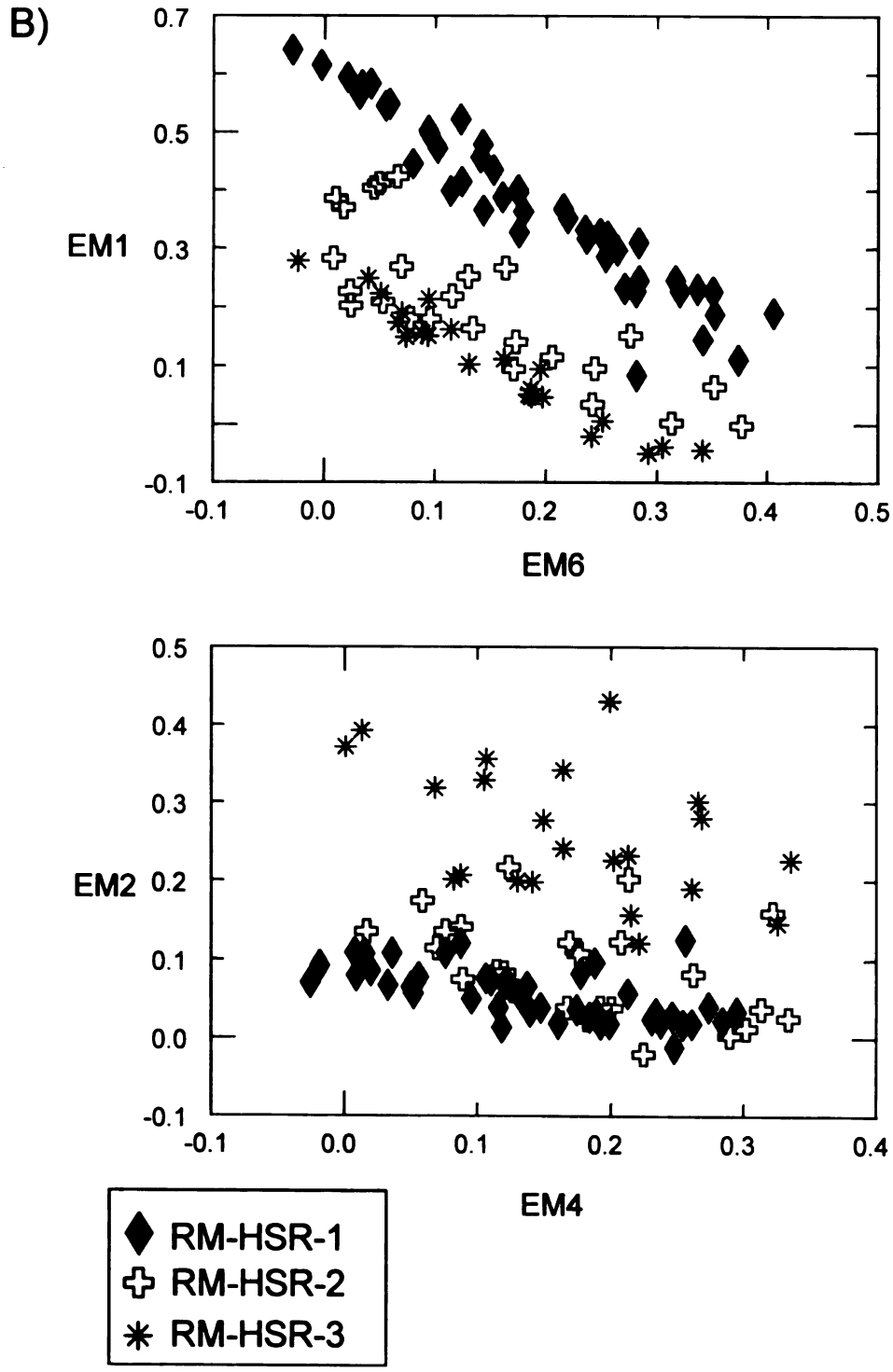

Figure 12. continued.

resulted in end member compositions that better constrain the field of represented pumice fragment compositions (Figure 12B). Note the overlap of end member compositions for each dataset; for example, one end member in the RM-HSR1 dataset has a composition that resembles HSR-2, and one end member in the RM-HSR2+HSR3 dataset closely resembles a LS magma, and a second end member resembles a HSR-1 magma. Although PVA rules out magma mixing between any two of these high-silica rhyolite magmas to generate a third high-silica rhyolite, it does indicate that limited mixing occurs between these three high-silica rhyolite magmas; separating HSR-2 and HSR-3 into two different datasets, RM-HSR2 (Table 4G) and RM-HSR3 (Table 4H), further demonstrates that mixing between the LS and HSR-3, between HSR-3 and HSR-2, and between HSR-2 and HSR-1 is indicated (Figure 11C). Further support of this interpretation is provided by the trace-element composition of sanidine phenocrysts, melt inclusions, and glass matrix from these pumice fragment groups (see following section).

Finally, Figure 13 summarizes the end member compositions (CIPW norm shown), determined by PVA on unrelated magma batches (Figure 13A), and related magma batches (Figure 13B). HSR-2 and HSR-3 remain grouped as one related magma batch, even though HSR-3 can be distinguished from HSR-2 by having elevated La concentrations. A dataset of HSR-2, HSR-3, and LS pumice fragments (RM-HSR2+3+LS, Table 4I) analyzed by PVA reveals that HSR-3 cannot be derived by mixing of LS magmas with HSR-2 magmas (Figure 14). However it is clear that HSR-3 was in more contact with LS magmas than HSR-2 based on sanidine and melt inclusion trace element analyses; further evidence of this mixing will be presented in later sections.

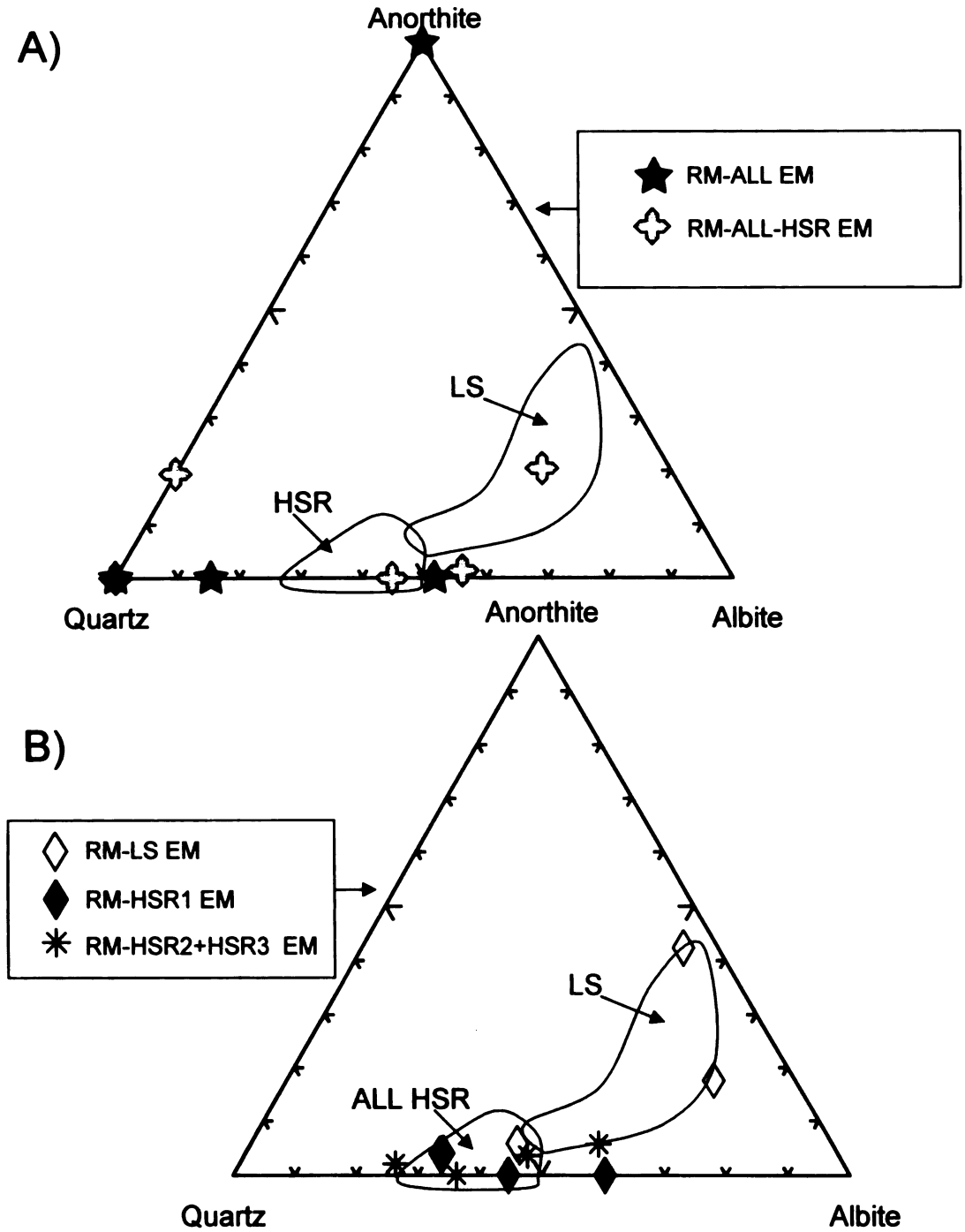

Figure 13. CIPW normative compositions of pumice fragments and end members for each dataset of Rainier Mesa (RM). The open enclosed areas are the compositional ranges of low silica pumice fragments and another area represents all three high-silica rhyolite pumice fragment compositions, combined. A). Notice the extreme compositions of most of the end members (see text for explanation). B). Notice that separating the low silica samples into one dataset, and separating the high-silica rhyolite samples into two different datasets (one with only HSR-1, the other dataset with HSR-2 and HSR-3 together) results in end member compositions that better defines the total range of pumice fragment compositions.

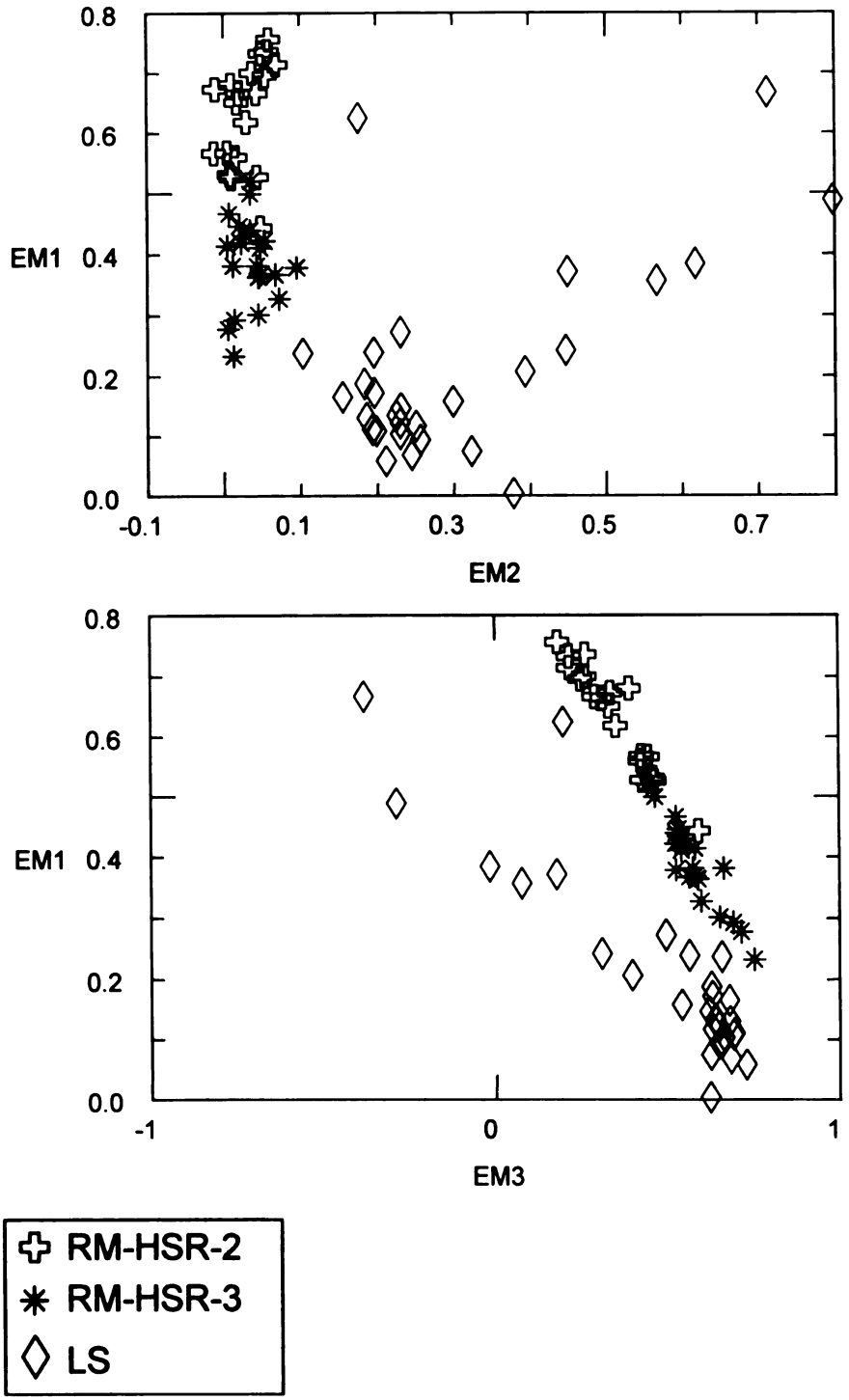

Figure 14. Example of the results of dataset RM-HSR2+3+LS, in which three end members were determined by PVA. Notice that the HSR-2 and HSR-3 pumice fragments have the same linear trend, and that many of the HSR-3 samples cannot be explained as mixing between the LS and HSR-2 samples based on their location in these graphs.

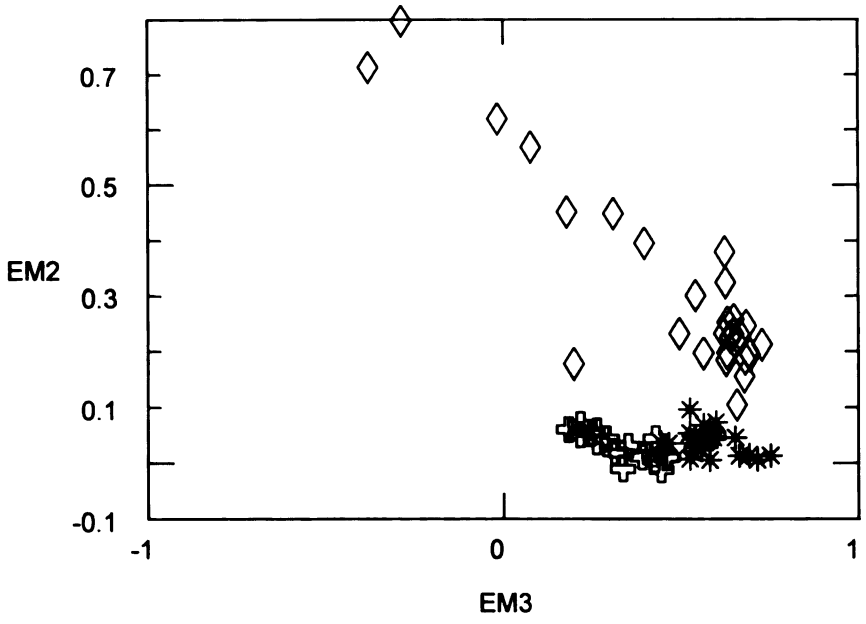

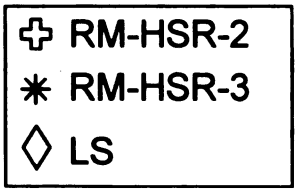

Figure 14. continued.

CHAPTER 3

SANIDINE ANALYSES

Topopah Spring

Trace element compositions (Ba, Sr, and Rb) of sanidine phenocrysts from high-silica pumice fragments are shown in Figure 15; sanidines from the low silica pumice fragments were not analyzed. Sanidine phenocrysts from TS-HSR can be grouped into three populations based on the trace element composition of the phenocryst core. Population 1 has low Ba (~200 ppm) and low Sr (~45 ppm) core compositions, whereas population 2 has elevated Ba (near 700 ppm) and Sr (~120 ppm) in the core. Both of these sanidine populations have similar Rb compositions (~70 ppm) from core to rim. Population 3 consists of sanidines that are xenocrysts derived from a more mafic magma, and these sanidines have very high Ba (> 2500 ppm) and Sr (~600 ppm); one grain from this group is unzoned with respect to Ba (12,000 ppm), the other grain is strongly zoned with a core composition of 2500 ppm Ba and a rim composition of 15,000 ppm Ba. Both of these grains are unzoned with respect to Sr (~600 ppm), and have very low Rb (~40 ppm). Zoning with respect to Ba and Sr is evident in the other sanidine populations as well, as some sanidines have core compositions that fall in population 2, but have decreasing Ba and Sr rimward so that the rim compositions match population 1 compositions. Likewise, one sanidine from population 1 has increasing Ba and Sr rimward and approaches the composition of population 2. The existence of a sanidine population (within the TS-HSR pumice fragments) with more than one core composition

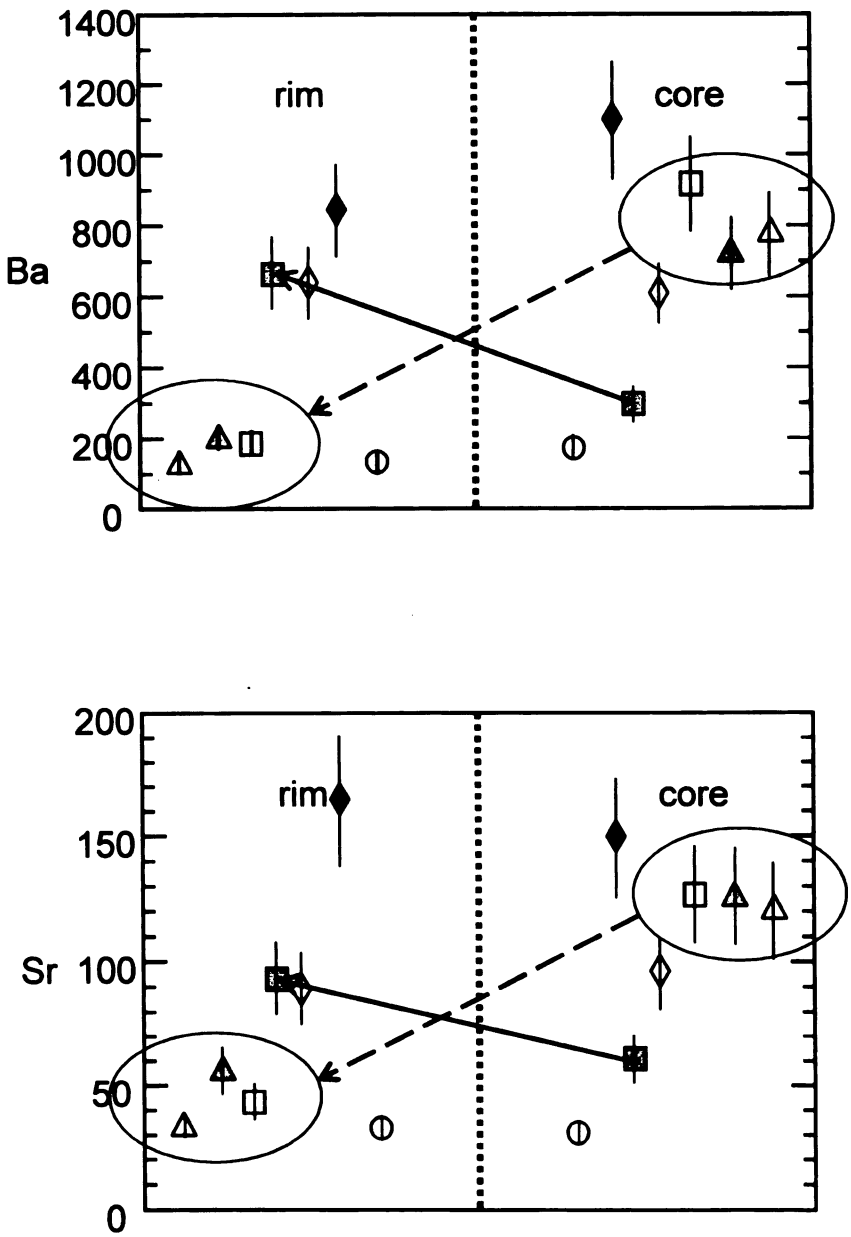

Figure 15. Ba, Sr, and Rb compositions of cores and rims of sanidines from high-silica rhyolite pumice fragments, Topopah Spring tuff. Each symbol denotes the core and rim of individual sanidines; 15% error indicated by bars on each symbol. Circled regions and arrows that connect cores and rims of grains are described in the text. LW4-10a-1 and LW4-10a-3 are not shown due to high Ba and Sr values (> 2500 ppm Ba and ~600 ppm Sr).

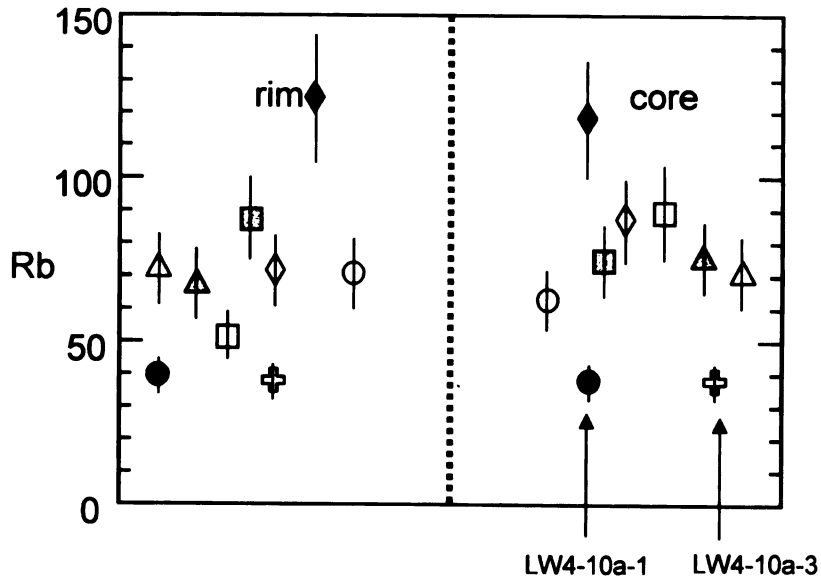

Figure 15. continued.

is consistent with open system processes such as magma mixing, with sanidines from a Ba- and Sr-enriched magma zoned with decreasing in Ba and Sr rimward, and sanidines from a Ba- and Sr-poor magma zoned with increasing Ba and Sr rimward as the phenocrysts continue to grow in the now hybrid magma.

Tiva Canyon

Only sanidines from the high-silica pumice fragments were analyzed, and these show smaller compositional ranges than the sanidines from high-silica pumice fragments of Topopah Springs (Figure 16). Most of these sanidines have low Ba (~300 ppm) and Sr (~100 ppm) and are unzoned with respect to Ba with the exception of two grains which have rimward increases to >550 ppm Ba. Most of the sanidines are unzoned with respect to Sr. One sanidine grain which has consistenly high Ba (~800 ppm) from core to rim, has high Sr with slight zoning from 145 ppm to 168 ppm core to rim; note that one sanidine with a core composition that matches the composition of the majority of sanidines has a rim composition that matches the trace element composition of this high Ba grain; in fact this zoned grain with the lower Ba core is the only grain that is zoned with respect to Ba, Sr, and Rb. The remainder of sanidines from this high-silica magma have either similar Sr concentrations in core and rim, or have slightly elevated Sr in the cores. Rb concentrations for most grains are low. One grain is zoned to > 150 ppm Rb at the rim; possibly a mineral inclusion or melt inclusion was inadvertently ablated during analysis of the rim, because Rb should decrease as Ba and Sr increase due to mixing with a magma of less evolved composition.

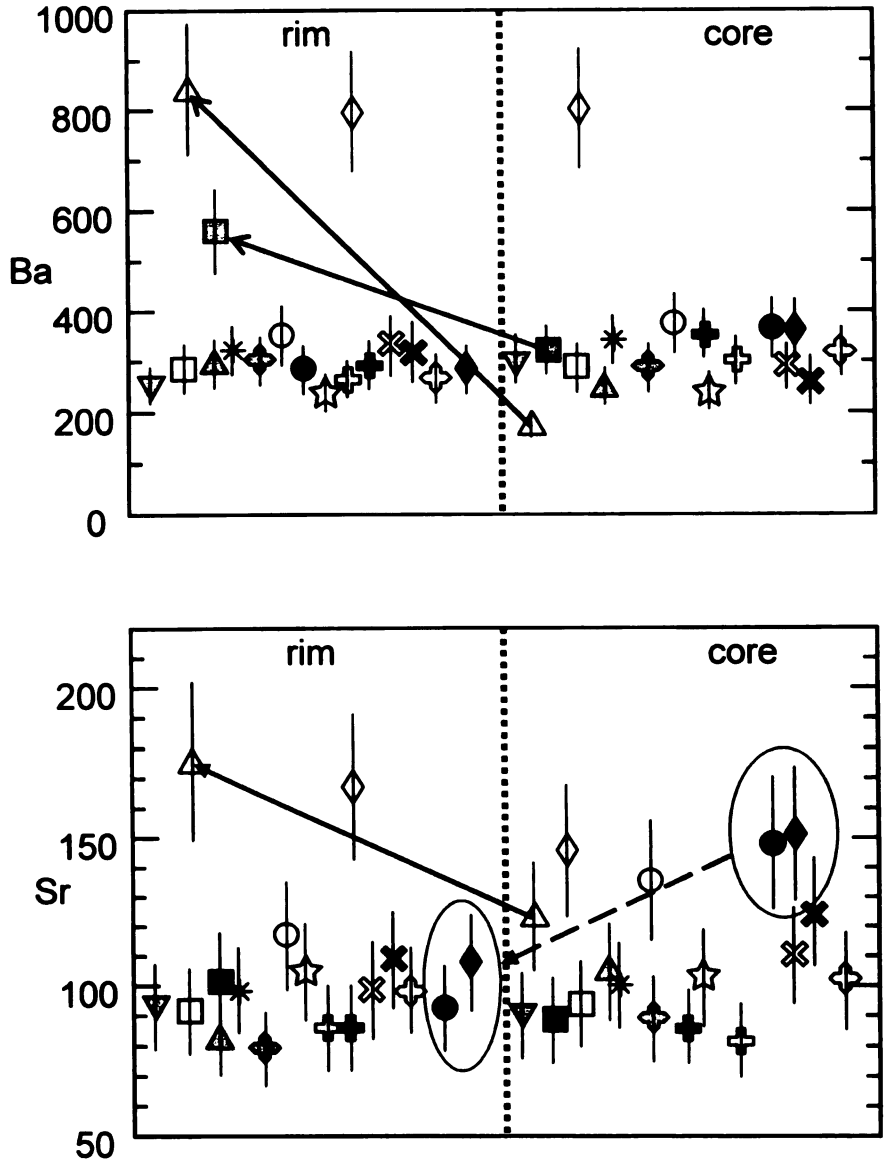

Figure 16. Ba. Sr, and Rb compositions of cores and rims of sanidines from high-silica rhyolite pumice fragments, Tiva Canyon tuff. Each symbol denotes the core and rim of individual sanidines; 15% error indicated by bars on each symbol. Arrows connect cores and rims of grains described in the text.

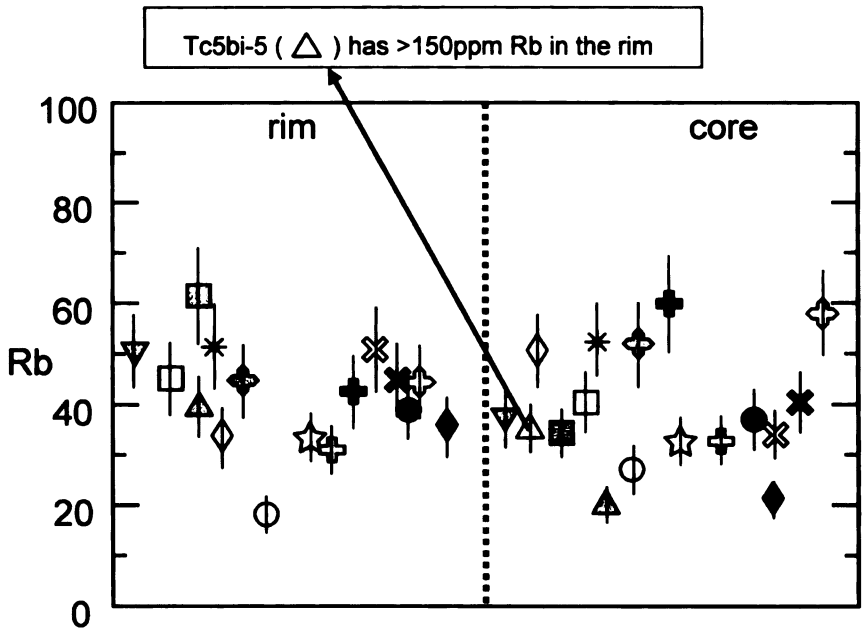

Figure 16. continued.

Ammonia Tanks

Only sanidines from the AT-HSR pumice fragments were analyzed, and trace element compositions are shown in Figure 17. The majority of sanidines have low Sr (~20 ppm) cores, and are unzoned with respect to either trace element. Three sanidines have slightly higher Ba cores (between ~100 and ~140 ppm), and decrease rimward to Ba concentrations that match the rest of the sanidines. These same grains have low Sr in the cores, with the exception of AT5-37-5, which is elevated (~40 ppm Sr), but decreases rimward to match the Sr compositions of the majority of sanidines. Also, one grain (AT5-37-4) was found to have relatively high Ba (~650 ppm core, ~300 ppm rim) and has a Sr concentration in both core and rim that matches the sanidine with elevated Sr (AT5-37-5). Rb concentrations of all sanidines in Ammonia Tanks are roughly similar, and show insignificant changes from core to rim in all but AT5-37-4 (which increases in Rb rimward). None of the sanidines have the high Ba and Sr compositions seen in the other high-silica pumice fragments within the other ash flows; this may be due to the small number of phenocrysts analyzed.

Rainier Mesa

One sanidine grain from a low silica pumice fragment was analyzed, and shows very high Ba concentrations (6930 to 11,300 ppm Ba, rim to core), a Sr composition between 913 and 1040 ppm, and Rb below detection limits (Table 5). Sanidines from all three high-silica rhyolite groups (RM-HSR-1, RM-HSR-2, and RM-HSR-3) are shown in Figures 18-20 and are summarized in Table 5.

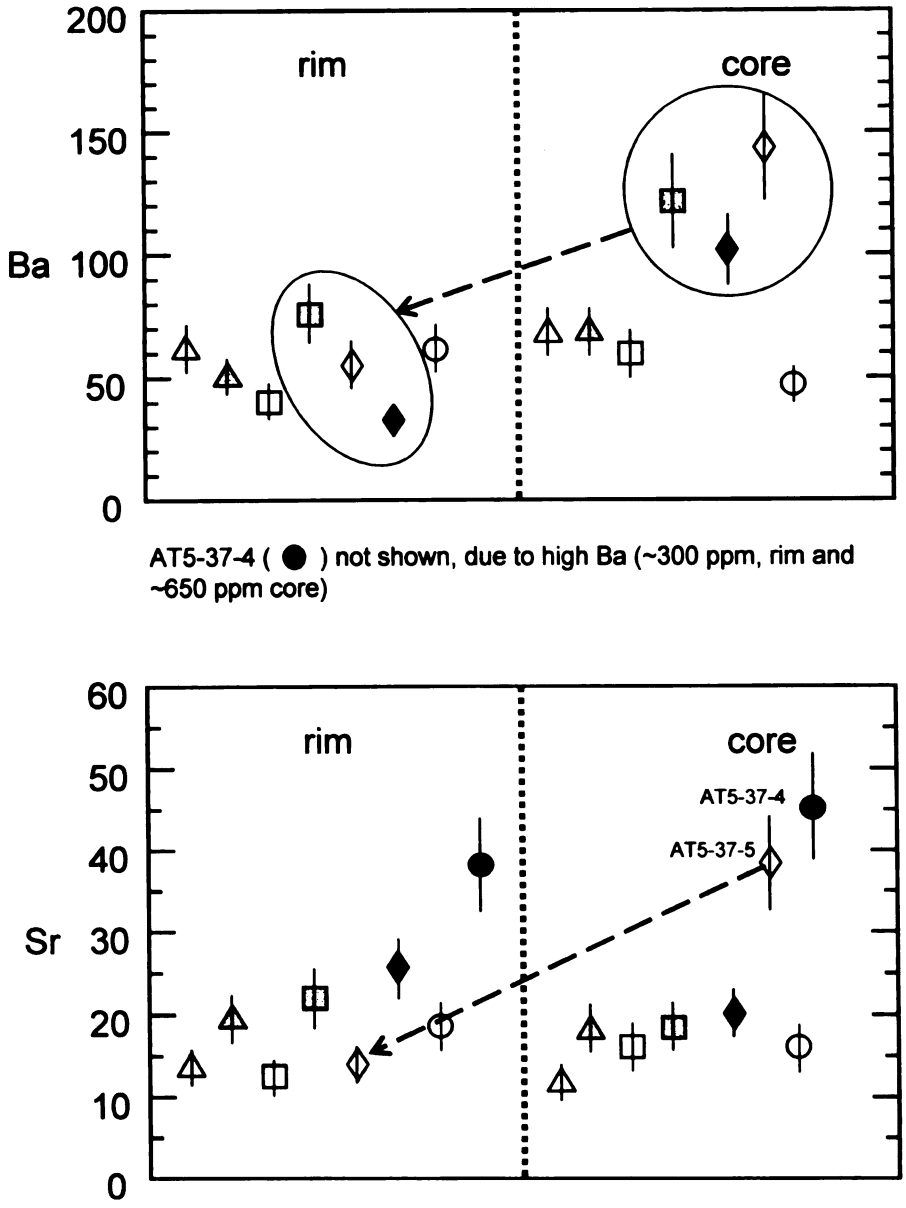

Figure 17. Ba, Sr, and Rb compositions of cores and rims of sanidines from high-silica rhyolite pumice fragments, Ammonia Tanks tuff. Each symbol denotes the core and rim of individual sanidines; 15% error indicated by bars on each symbol. Circled regions and arrows that connect cores and rims of grains are described in the text.

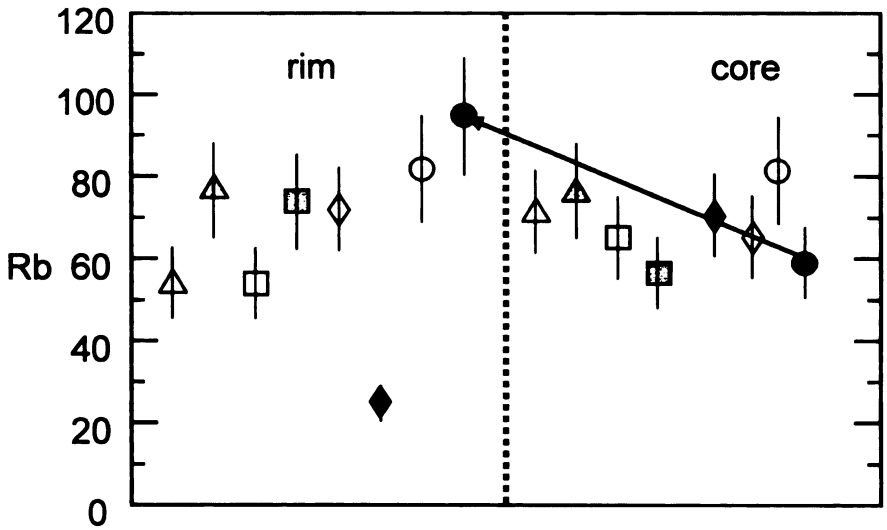

Figure 17. continued.

	Rim composition			Core composition		
	Ba	Sr	Rb	Ba	Sr	Rb
HSR-1	67.84 to 99.8 ppm	21.9 to 36.0 ppm	99.3 to 152 ppm	33.8 to 67.0 ppm	23.7 to 29.8 ppm	97.6 to 124 ppm
HSR-2	57.2 to 527 ppm	25.4 to 85.6 ppm	73.4 to 166 ppm	58.0 to 242 ppm	23.4 to 83.7 ppm	79.6 to 169 ppm
HSR-3	536 to 4368 ppm	178 to 633 ppm	< 80.3 ppm	134 to 4100 ppm	113 to 878 ppm	< 63.1 ppm
LS	6930 ppm	913 ppm	bdl	11300 ppm	1040 ppm	bdl

Table 5. Range of trace element compositions for rim and core analyses of sanidines from Rainier Mesa pumice fragments.

Most of the sanidines from the RM-HSR-1 pumice fragments are unzoned with respect to Ba, Sr and Rb, with variations within detection limits, although one grain is slightly zoned in all three trace elements, and another grain is zoned with respect to Ba only (Figures 18A, 19A, and 20A). The grain that is zoned with respect to Ba, Sr, and Rb has the lowest Ba core (38 ppm) and highest Sr and Rb rim composition compared to the other HSR-1 sanidines.

HSR-2 has two sanidine populations based on the trace element compositions of the rims (Figures 18B, 19B and 20B). Population 1 is relatively unzoned with respect to Ba, whereas population 2 has Ba compositions in the core similar to population 1, except for increased Ba and Sr at the rims (~525 ppm Ba and ~85 ppm Sr). Sr compositions generally increase rimward or are relatively constant from core to rim; however, one grain has decreasing Ba and Sr rimward. Still another grain with a low Ba core increases to ~240 ppm Ba, simlar to the normally zoned (with respect to Ba) grain mentioned previously. The presence of these two grains which display either normal or reverse zoning is not uncommon in phenocryst populations in magmas that have undergone mixing. The interpretation here is that there was limited mixing between HSR-1 and HSR-2 magmas; this observation is supported by the melt inclusions (see following section). In addition, the rimward increase in Ba (to ~525 ppm) and Sr (~85 ppm) seen in population 2 sanidines indicates that a second mixing event occurred, this time involving a Ba- and Sr-enriched magma.

Fewer grains were analyzed in the RM-HSR-3 pumice fragments, and their Ba compositions are highly variable between grains, with two of these showing extreme variations in Ba from core to rim (Figure 18C). One grain has Ba, Sr, and Rb

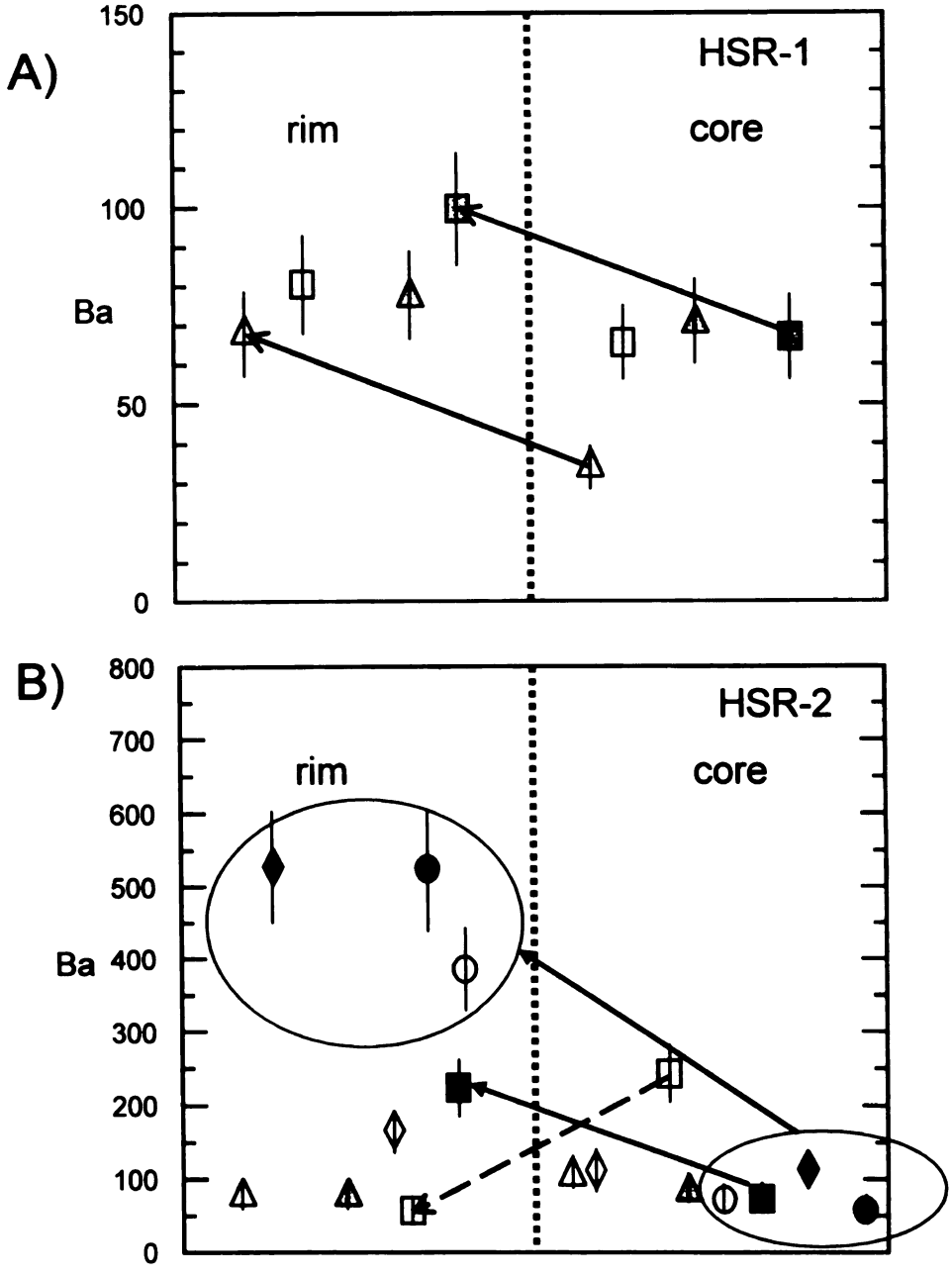

Figure 18. Ba concentrations of sanidine cores and rims from each of the three high-silica rhyolite pumice fragments of Rainier Mesa tuff. Each symbol denotes the core and rim of individual sanidines; 15% error indicated by bars on each symbol. Circled regions and arrows that connect cores and rims of grains are described in the text. A). HSR-1. B). HSR-2. C). HSR-3.

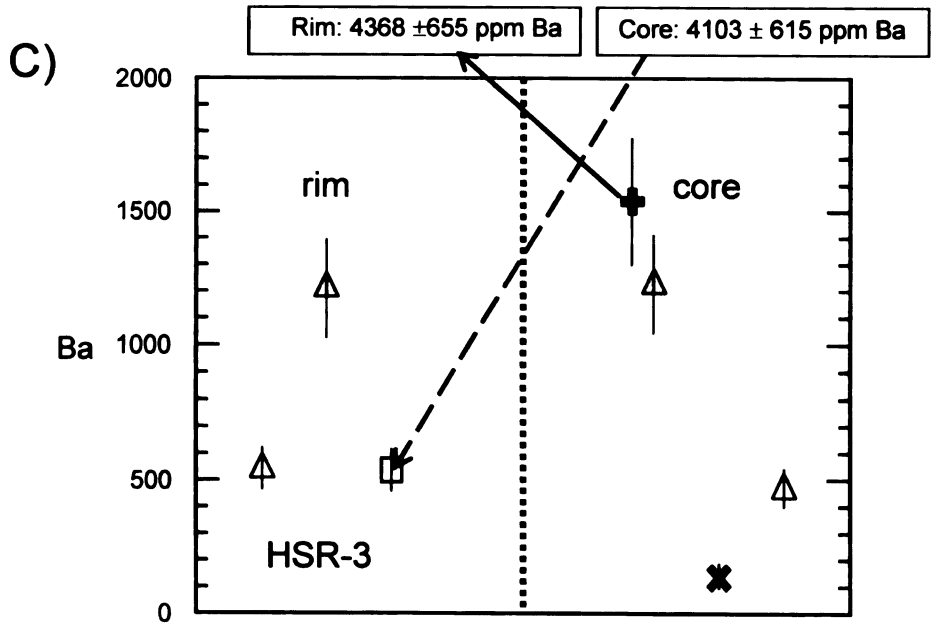

Figure 18. continued.

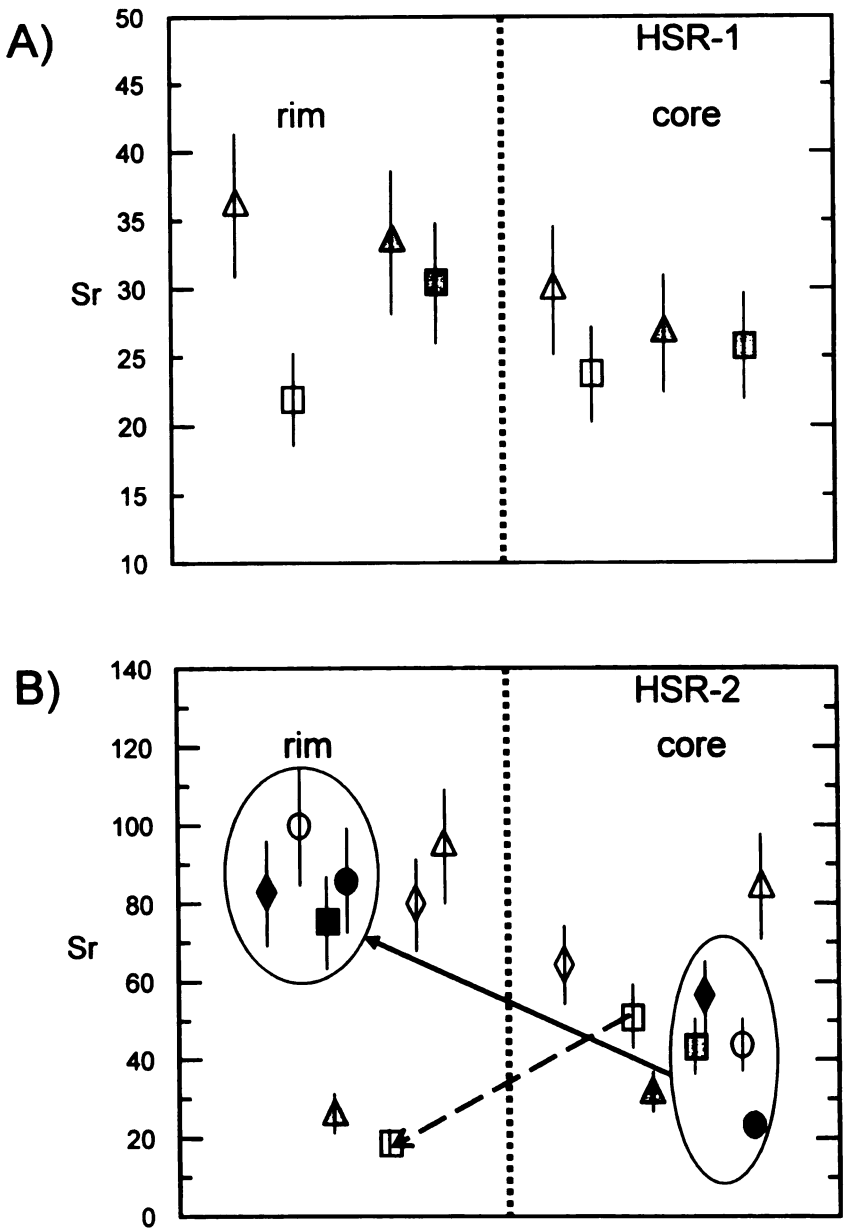

Figure 19. Sr concentrations of sanidine cores and rims, with each graph showing phenocrysts from each of the Rainier Mesa high-silica rhyolite pumice fragment groups. Each symbol denotes the core and rim of individual sanidines; 15% error indicated by bars on each symbol. Cirlced regions and arrows that connect cores and rims of grains are described in the text. A). HSR-1. B). HSR-2.C). HSR-3.

C)

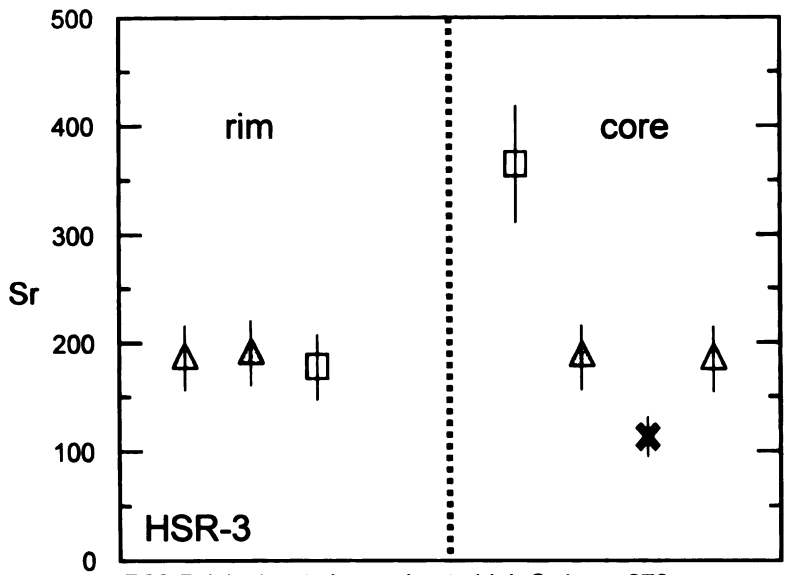

R23-7-1 (✚) not shown due to high Sr (core 878 ppm, rim 633 ppm)

Figure 19. continued.

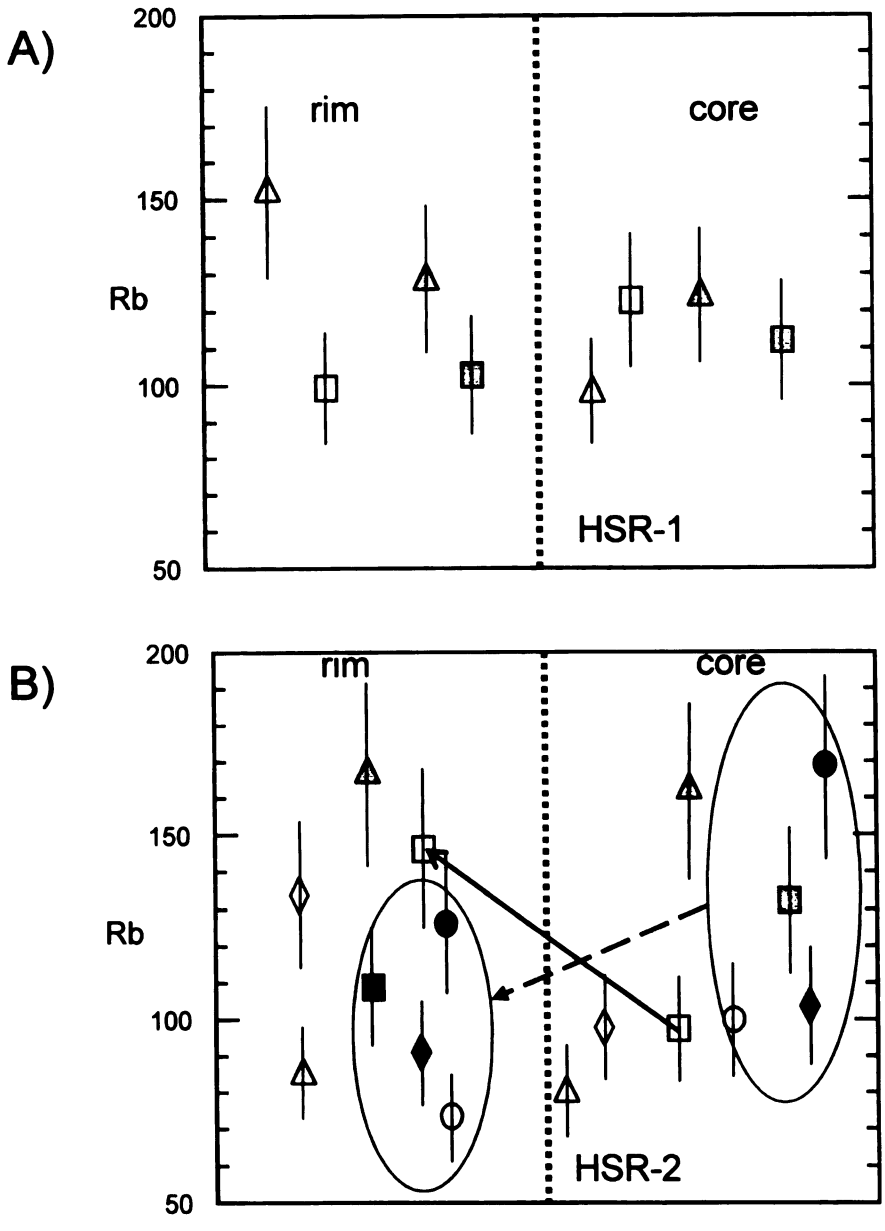

Figure 20. Rb concentrations of sanidine cores and rims, with each graph showing phenocrysts from each of the high-silica rhyolite groups of Rainier Mesa. Each symbol denotes the core and rim of individual sanidines; 15% error indicated by bars on each symbol. Circle regions and arrows that connect cores and rims of phenocrysts are described in the text. A). HSR-1. B). HSR-2. C). HSR-3.

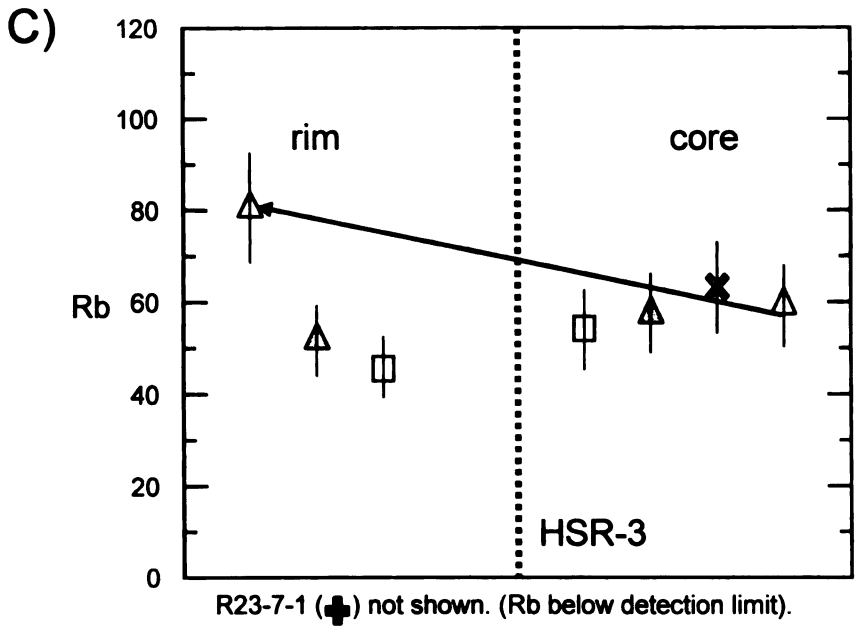

Figure 20. continued.

concentrations that are identical to the HSR-2 population 1 (Figures 18C, 19C, and 20C), and a second grain (with ~500 ppm Ba in the core and rim) is identical to HSR-2 population 2 in terms of Ba content. A third grain has elevated Ba (~1200 ppm) for the core and rim; another grain has a similar core composition, but is highly zoned with respect to Ba (4368 ppm Ba at the rim). A fifth grain has a similar Ba composition (4103 ppm Ba), but this grain is normally zoned, with a large decrease in Ba rimward (536 ppm); this same grain is the only sanidine zoned in Sr (325 ppm to 178 ppm core to rim). None of the sanidines in HSR-3 show significant zoning in Rb (Figure 20C). Based on the sanidine compositions of the HSR-3 pumice fragments, it appears that some mixing occurred between two different magmas, one resembling HSR-2 and one with an even more Ba- and Sr-enriched composition; this second magma type may be the RM-LS magma.

Evidence of Mixing in Rainier Mesa based on Sanidines and PVA

The composition of sanidines in equilibrium with each of the end members generated by PVA was calculated using the published partition coefficient for Ba between sanidine and high-silica rhyolite melt (Mahood and Hildreth, 1983). Ba was used for these calculations as sanidine is the dominant phenocryst type and is the only phase in these magmas that would contain significant amounts of Ba (see section on mineralogy). These calculated compositions were compared to measured values in core and rim and the results are shown in Table 6 and Figure 21A. In Figure 21A, the maximum and minimum Ba concentration of cores and rims are shown. The entire range of core and rim compositions of sanidines within HSR-1 falls near or between the

	measured composition		
		min	max
HSR-1	rim	67.8 ppm Ba	99.8 ppm Ba
	core	33.8 ppm Ba	67.0 ppm Ba
HSR-2	rim	57.2 ppm Ba	527 ppm Ba
	core	58.0 ppm Ba	242 ppm Ba
HSR-3	rim	536 ppm Ba	4370 ppm Ba
	core	134 ppm Ba	4100 ppm Ba

	equilibrium* composition			
	EM1	EM2	EM3	EM4
HSR-1	92.0 ppm Ba	675 ppm Ba	-	43.0 ppm Ba
HSR-2	260 ppm Ba	-	396 ppm Ba	705 ppm Ba
HSR-3	3650 ppm Ba	127 ppm Ba	1540 ppm Ba	546 ppm Ba

Table 6. Ba concentrations of sanidine phenocrysts within Rainier Mesa pumice fragments. HSR-1 EM3 and HSR-2 EM2 have 0 ppm Ba.

*Equilibrium composition= calculated (Ba) composition for sanidines in equilibrium with magma compositions represented by each end member. Calculations are based on a mineral/melt partition coefficient of 4.30 (Mahood and Hildreth, 1983) for Ba in sanidine in high-silica rhyolite magma.

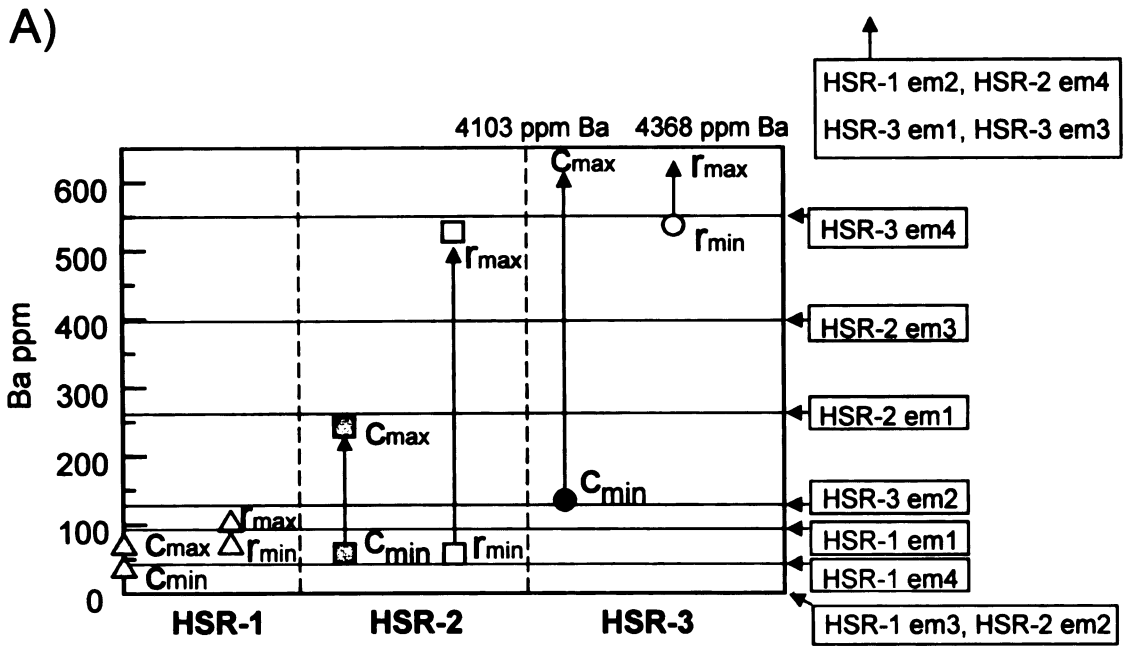

Figure 21. A) Maximum and minimum Ba concentrations measured in cores (Cmax and Cmin) and rims (rmax and rmin) of sanidines in the Rainier Mesa high-silica rhyolites. Horizontal lines indicate the calculated Ba concentration of a sanidine in equilibrium with each of the end members (end members HSR-1 em3 and HSR-2 em2 both have 0 ppm Ba). Note the increase in the range of Ba concentrations from HSR-1 to HSR-3. The large range in rim compositions indicates that eruption occurred prior to equilibration. Note shown: HSR-1 em2 (675 ppm Ba), HSR-2 em4 (705 ppm Ba), HSR-3 em1 (3646 ppm Ba), and HSR-3 em3 (1544 ppm Ba). B) La-Rb plot of end members and their location within the range of pumice fragment compositions representative of each Rainier Mesa magma composition (open areas on graph).

B)

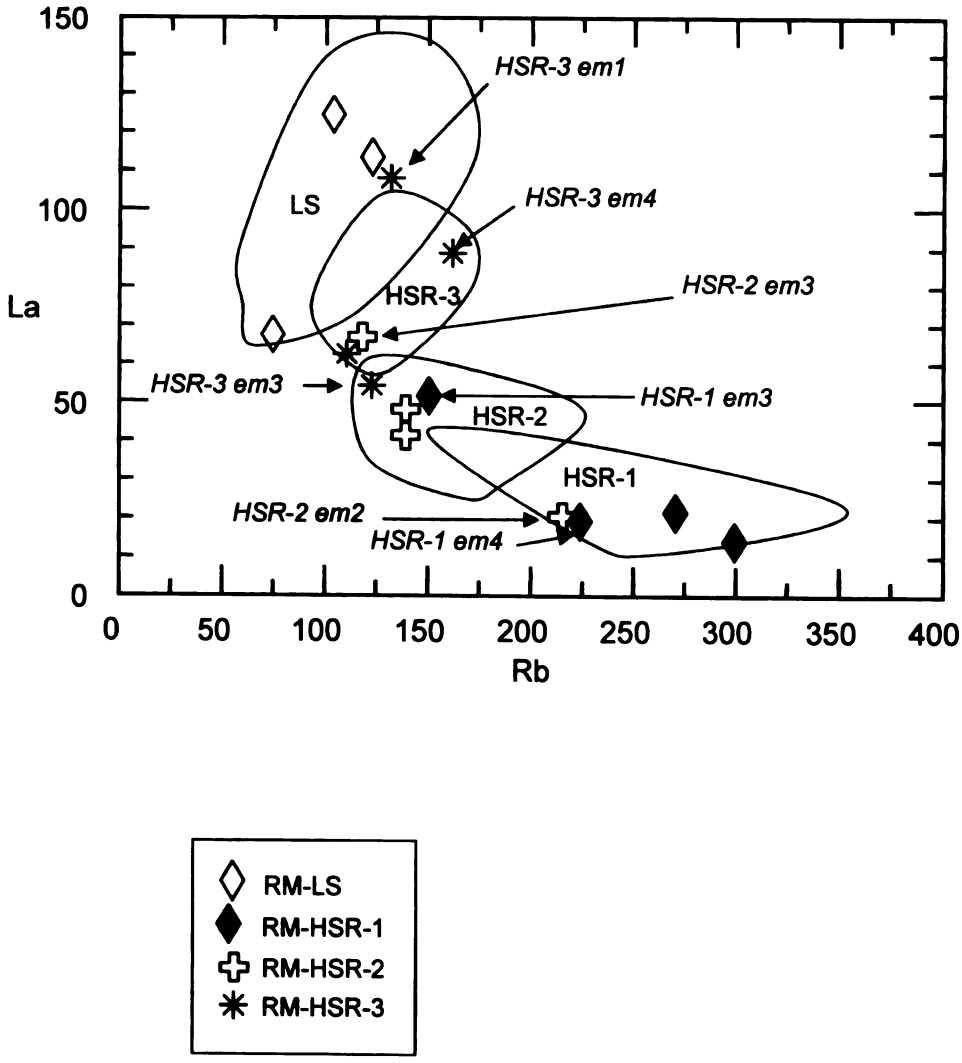

Figure 21. continued.

calculated compositions of sanidines in equilibrium with HSR-1 EM1 and EM4; note that both of these end members lie within the HSR-1 compositional field in La-Rb space (Figure 21B).

Sanidines from HSR-2 have a larger range of Ba concentrations within the cores and rims (Figure 21A). The lower Ba core and rim (c_{min} and r_{min}) compositions are not in equilibrium with any of the HSR-2 end members, but are near equilibrium compositions of HSR-1 EM4; note in Figure 21B that HSR-1 EM4 plots near HSR-2 EM2 in the HSR-1 compositional field in La-Rb space. The similarity of HSR-2 EM2 and HSR-1 EM4 is interpreted here as representing the mixing of magmas with HSR-1 and HSR-2 compositions. The HSR-2 cores with high Ba (c_{max}) have compositions that approach the compositions of sanidines in equilibrium with HSR-2 EM1, which lies in the compositional field of HSR-2 pumice fragments (Figure 21B). However, the maximum Ba concentration in the rims (r_{max}) are not in equilibrium with any of the HSR-2 end members, but their compositions approach that of the calculated concentrations of sanidines in equilibrium with HSR-3 EM4; this end member lies well within the HSR-3 compositional field (Figure 21B).

Sanidines from HSR-3 have the largest range of Ba compositions in both cores and rims, with maximum values in the 0.1wt% range (not shown). Lower Ba cores (c_{min}) have compositions that are close to the calculated composition of sanidines in equilibrium with HSR-3 EM2 (Figure 21A); this end member falls within the compositional field of HSR-3 pumice fragments in La-Rb space (Figure 21B). Higher Ba cores (c_{max}) have Ba concentrations that exceed all HSR-3 end member compositions (see Table 6 and figure caption for 21A) and are interpreted here as xenocrysts from the RM-LS magma. Rim

compositions are also very high in Ba; the minimum compositions (r_{min}) are near the HSR-3 EM4 calculated equilibrium compositions, but the higher Ba rims (r_{max}) have extremely high Ba concentrations (up to 4368 ppm Ba). The large range in core compositions of HSR-3 is interpreted here as representing sanidines derived from mixing events involving HSR-2 and LS magmas. Rim compositions of HSR-2 sanidines approach values for HSR-3 sanidines, so that maximum rim values in HSR-2 are similar to minimum values for HSR-3 sanidines. The range of rim compositions for HSR-2 from r_{min} to r_{max} and r_{min} to r_{max} in HSR-3 sanidines is a direct consequence of the relatively short time interval between mixing due to the limited contact of HSR-2 magmas with HSR-1 and HSR-3 magmas, and mixing due to limited contact of HSR-3 with HSR-2 and RM-LS magmas, prior to eruption which resulted in the zoned sanidines with disequilibrium compositions.

The trace element compositions of melt inclusions from Rainier Mesa magmas support the role of mixing between the HSR-1 and HSR-2 magmas, as well as mixing between HSR-2 and HSR-3. In the section below, melt inclusion analyses from Rainier Mesa are reported, and their compositions are compared with the melt inclusion compositions of the other ash-flow sheets.

CHAPTER 4

MELT INCLUSION ANALYSES

Major and trace element compositions of melt inclusions analyzed in each ash flow are reported in Appendix 3. Melt inclusions from all HSR pumice fragments of Topopah Spring, Tiva Canyon, and Ammonia Tanks typically have less Th, La, Nb and Rb than their respective pumice fragments, with the exception of one melt inclusion (LW4-10a-3-lb) from a Topopah Spring high-silica pumice fragment has elevated La (Figure 22A). The host phenocryst for the Topopah Spring melt inclusion mentioned above has extremely an high Ba and Sr composition; this phenocryst must be xenocrystic, and may indicate that some mixing has occurred between the low silica and high silica magmas, since the melt inclusion has a La content similar to the melt inclusions from the LS pumice fragments.

Melt inclusions in Rainier Mesa HSR pumice fragments show a larger range in trace element compositions than the melt inclusions from other ash flows, particularly in Rb and Nb (Figures 22B and 23). These melt inclusions are categorized into three groups (Groups A, B, and C) representing early-, mid-, to late-entrapped melts; Group A inclusions represent the earliest trapped melt, followed by Group B and Group C based on the occurrence of melt inclusions within phenocrysts that contain multiple melt inclusions. For example, a quartz grain (R18-16-5) and a sanidine (99TM14-3) both have a Group A inclusion located in the inner portion of each phenocryst, and both grains have a Group B inclusion located nearer the rim. Also, a quartz grain (R8-42-6) and

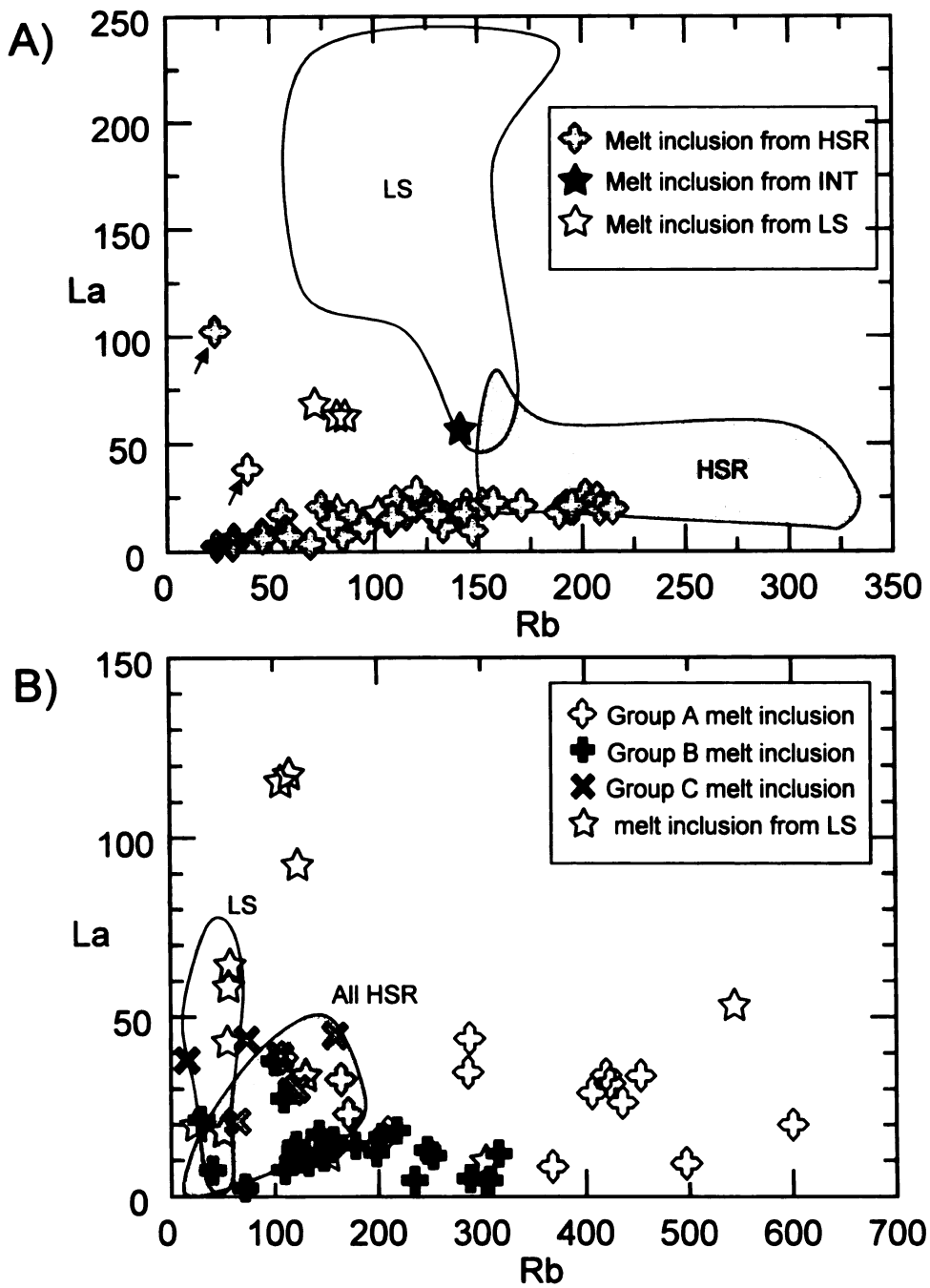

Figure 22. A) La versus Rb (ppm) for melt inclusions from high-silica rhyolite pumice fragments from Topopah Spring, Tiva Canyon, and Ammonia Tanks, and melt inclusions from low silica pumice fragments (Topopah Spring) and intermediate silica pumice fragments (Ammonia Tanks). Note that one, possibly two melt inclusions have elevated La contents (arrows), similar to melt inclusions from low silica pumice fragments. Open and shaded fields indicate the range of low silica and high-silica pumice fragment compositions, respectively. B). Melt inclusions from high-silica rhyolite and low silica pumice fragments of Rainier Mesa. Open and shaded regions represent the low silica and the high-silica pumice fragments (HSR-1, HSR-2, and HSR-3), respectively.

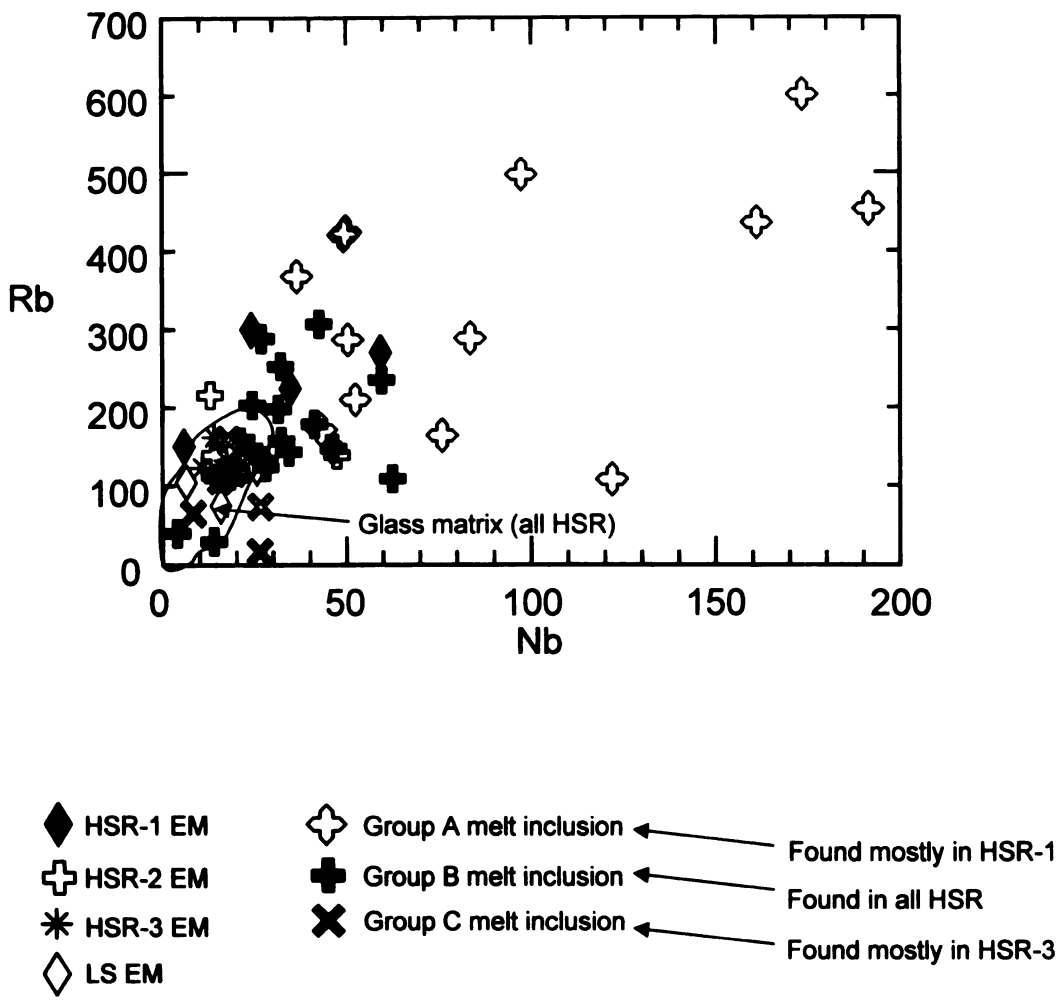

Figure 23. Graphs showing the trace element variation in melt inclusions from all high-silica rhyolite pumice fragments of Rainier Mesa, along with end member compositions for four separate datasets (HSR-1, HSR-2, HSR-3, and LS). Note the high Rb and Nb content of Group A inclusions. Glass matrix compositions of all high-silica rhyolite magmas are indicated on each graph. Concentrations are in ppm.

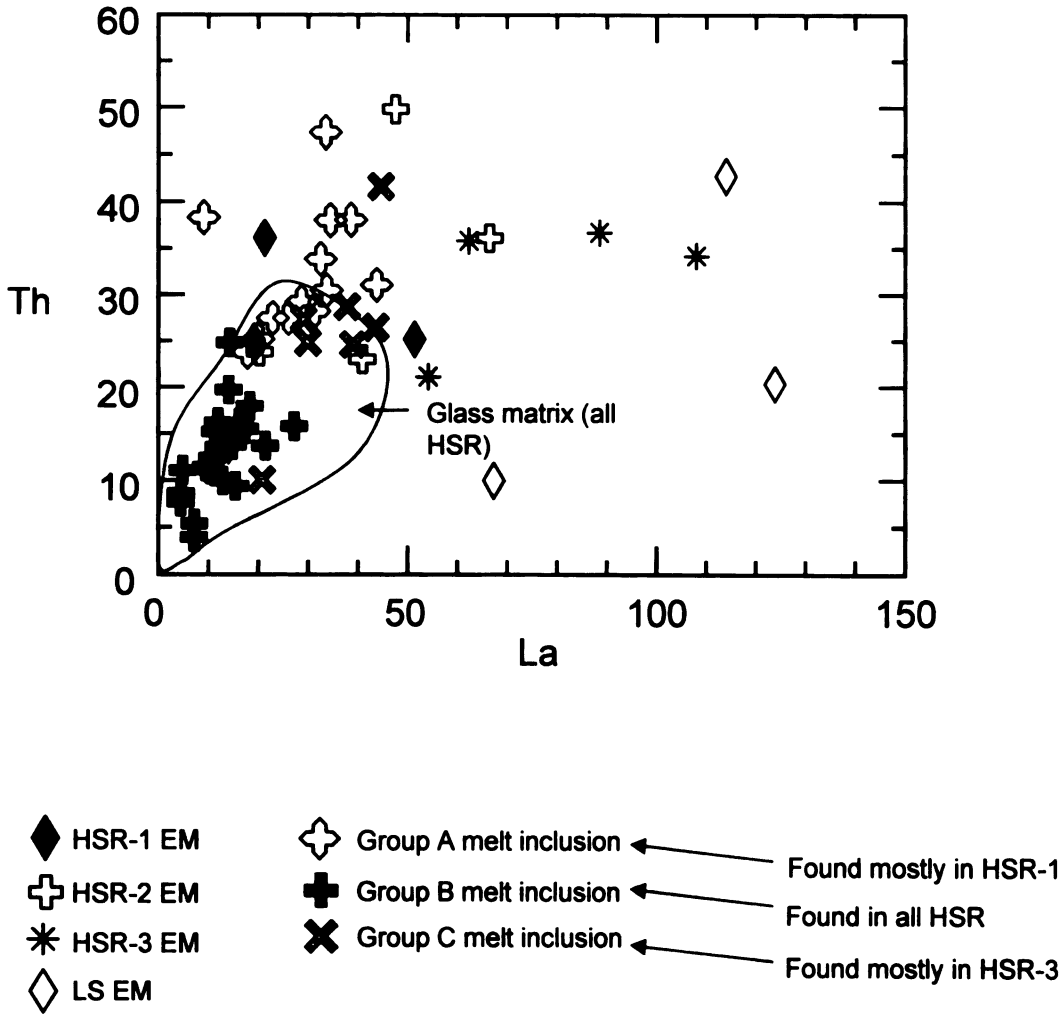

Figure 23. continued.

sanidine (R8-42-3) with a Group B inclusion in the inner portion of each grain both have Group C inclusions near the rim.

Group A inclusions have compositions that range to unusually high Rb and Nb contents (up to 3X and 20X higher than the host pumice fragment, respectively) (Figure 22B, and Figure 23A and B). These melt inclusions are predominately found in HSR-1 pumice fragments. The second group (Group B) describes melt inclusions that have La and Th concentrations that match the La and Th concentrations of the glass matrix of all three high-silica pumice fragment compositions; these melt inclusions are found in all three high-silica pumice fragment groups (HSR-1, HSR-2, and HSR-3). Group C consists of those melt inclusions that have Rb and Nb concentrations that match the glass matrix composition of all high-silica pumice fragment groups, except for elevated La and Th. These Group C melt inclusions are found almost exclusively in HSR-3 pumice fragments. It should be mentioned that not all Group B inclusions necessarily formed before Group C melt inclusions; those melt inclusions that have low Th and La, as well as low Rb and Nb, have compositions that are well within the compositional range of the glass matrix of all HSR pumice fragments, and therefore represent the last entrapped melts. What was important for this study was the identification of a group of melt inclusions that are the earliest trapped melts (Group A) and those inclusions that record an input of Th and La enriched melt (Group C). As the sanidine analyses indicate mixing has occurred among these high-silica magma types, the increase in Th and La recorded in Group C inclusions, as well as their occurrence in mainly the HSR-3 pumice fragments, most likely record the change in melt composition due to mixing with a Th-, La- enriched magma (as well as Ba- and Sr-enriched, as evidenced by the sanidine compositions) such

as the LS magma; the presence of a few Group C inclusions in HSR-1 and HSR-2, and the presence of a group A inclusion in HSR-2 is consistent with limited mixing among the magmas of Rainier Mesa prior to eruption. However, as shown by PVA, mixing between any two high-silica magmas does not generate the third high-silica magma type (nor can mixing between HSR-2 and LS magmas generate HSR-3 magma), and that at least two independent high-silica magmas were involved in the formation of Rainier Mesa.

Melt inclusion composition of all ash flows

Figure 22A shows La versus Rb concentrations of all melt inclusions from Topopah Spring, Tiva Canyon, and Ammonia Tanks tuffs along with the range of compositions represented by the pumice fragments in these ash flows. Notice that: 1) all melt inclusions from the high-silica pumice fragments of each ash flow are indistinguishable from one another, and plot along the same trend; 2) melt inclusions from low-silica pumice fragments appear to have a separate trend; and 3), at least one inclusion from a high-silica pumice fragment has a composition that more closely resembles the melt composition of a low-silica pumice fragment. Figure 22B shows the Rainier Mesa melt inclusions for comparison. All melt inclusions from the high-silica pumice fragments of all four ash flows were analyzed as one dataset by PVA, and the results show two distinct melt populations: one group is comprised of only Group A melt inclusions from Rainier Mesa, and the second group contains all the remaining melt inclusions from the high-silica pumice fragments of all four ash flows. Group B and Group C melt inclusions from Rainier Mesa were excluded, as these inclusions have

compositions that reflect mixing between HSR-2, HSR-3, and LS magmas, and therefore result in a lot of scatter in the EM plots in Figure 24. It is worth mentioning that PVA utilizes the entire geochemistry of the melt inclusions when determining relationships, not just a few key trace elements, and still the Group A inclusions are singled out as unique. Also, the fact that all remaining melt inclusion compositions are grouped as one related melt implies that the high silica magmas of Topopah Spring, Tiva Canyon, Ammonia Tanks, share a common end member.

Finally, the compositions of end members generated by PVA of melt compositions are compared in Figure 25. The dataset composed of melt inclusions from high-silica rhyolite pumice fragments of Topopah Spring, Tiva Canyon, and Ammonia Tanks (TSTCAT-ALL) is described by four end members, all of which are similar in terms of their compositions (Figure 25A). The Rainier Mesa inclusions were first analyzed together (RM-ALLHSR), and then subdivided into two subsets, one with all the Group A inclusions (RM-GPA), and another dataset with the remainder of inclusions (RM-GPB+GPC) (Figure 25B). Notice the wide range in end member compositions; as with the pumice fragment compositions, the large range of Rainier Mesa end member compositions is most likely due to the input from LS magmas to HSR-3. It is therefore not surprising, as some end members of the RM-ALLHSR and RM-GPB+GPC datasets have either 0 ppm Rb or 0 ppm Nb; both of these trace elements are of low concentrations within the RM-LS magma, and those end members with 0 ppm Rb and 0 ppm Nb may represent the input of LS magma.

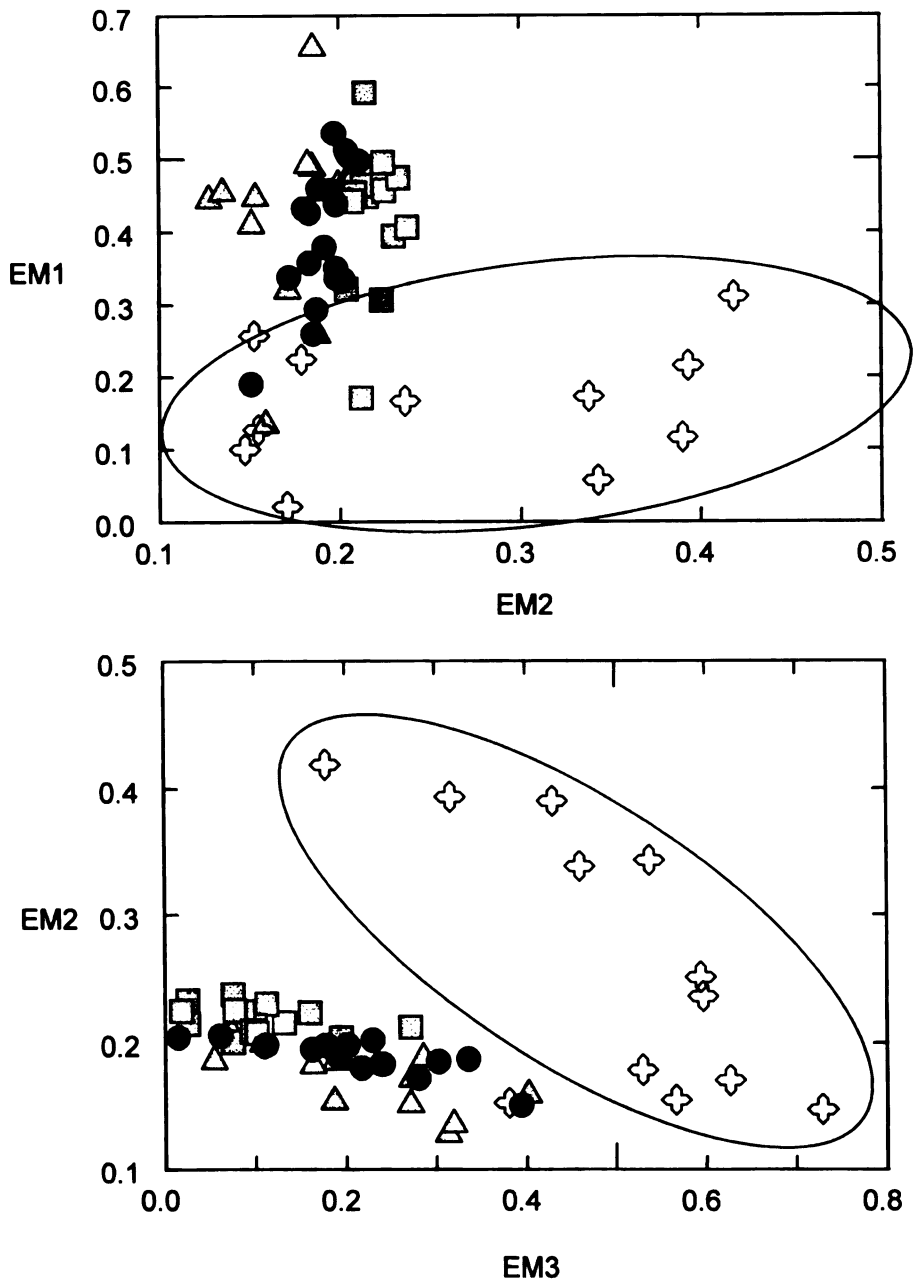

Figure 24. Graphs of end member proportions in melt inclusions from high-silica rhyolite pumice fragments: Topopah Spring (△), Tiva Canyon (□), Rainier Mesa Group A (◇), Ammonia Tanks (●). Only the Group A melt inclusions from Rainier Mesa are shown and have a distinctly different trend (circled region) in end member proportions than the melt inclusions from other ash flows, indicating that the melt compositions are related for all high-silica rhyolite magmas except for Rainier Mesa.

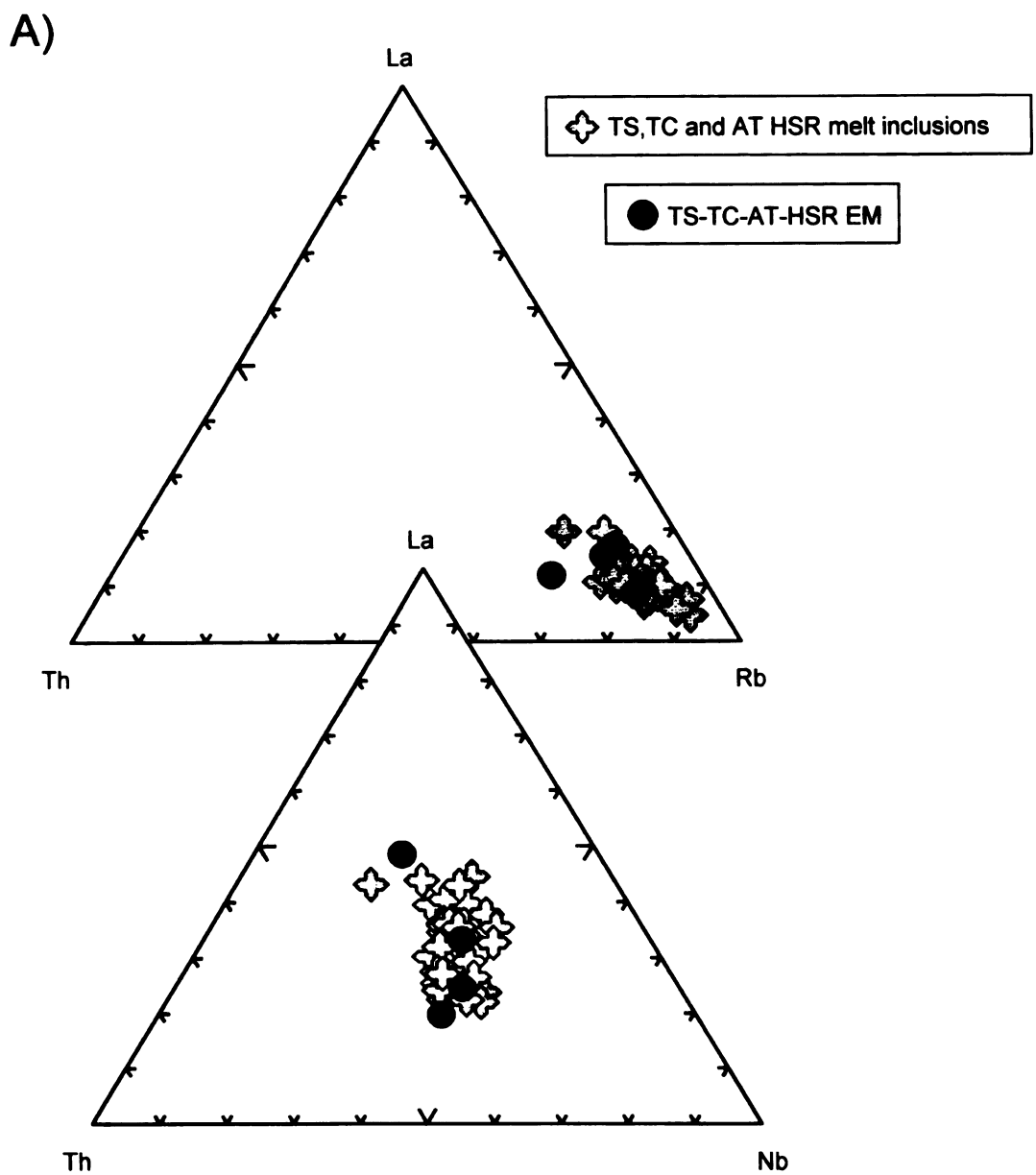

Figure 25. Triangular plots of trace element composition of melt inclusions and end members. A) TS, TC, and AT melt inclusions and the 4 end members generated from dataset TS-TC-AT-HSR. The two high La inclusions of TS, interpreted as trapped melt from xenocrysts, were excluded from the dataset, and therefore not shown on the graphs. B) Group A, Group B, and Group C inclusions with end members generated from the RM-GPA dataset, RM-GPB+C dataset, and RM-ALLHSR dataset. All inclusions are from high-silica rhyolite pumice fragments.

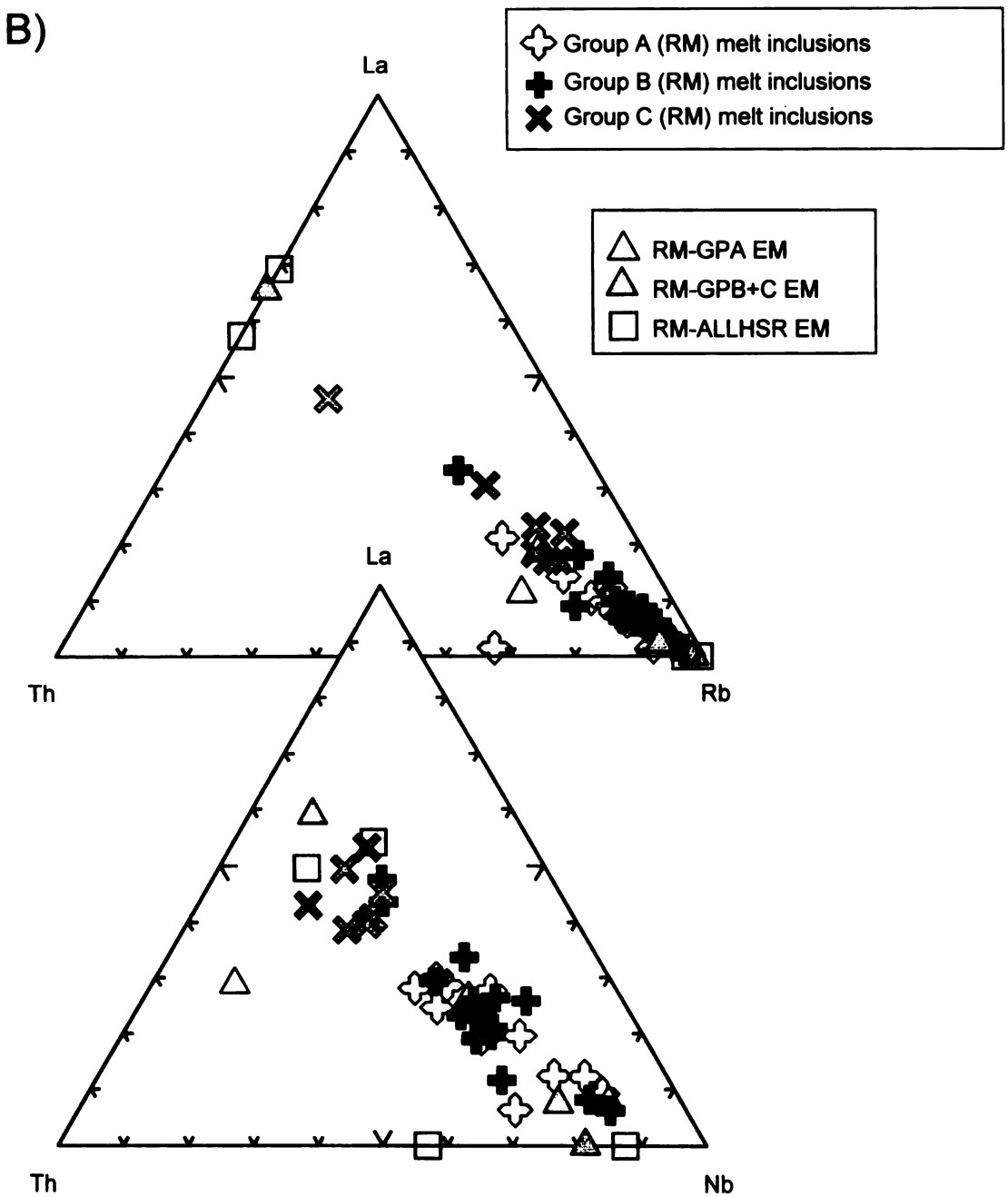

Figure 25. continued.

CHAPTER 5

DISCUSSION

Based on previous whole rock and pumice fragment geochemical and isotopic studies, the co-erupted low silica and high-silica rhyolite magmas associated with each of the four major ash-flow sheets of southwest Nevada volcanic field cannot be explained as magmas related by processes occurring within a single magma chamber, and therefore represent independently generated magma batches. That such magmas can erupt from the same nested caldera has been attributed to the extensional environment of this portion of the southern Great Basin (Cambray et al., 1995). These authors describe how releasing steps associated with, in this case, normal dip-slip detachment faults, can serve as magma chambers that expand during extension and can accommodate further influxes of magma (Figure 26). Lower rates of extension can result in a greater internal pressure within the releasing step (magma chamber), and with the addition of new magma, result in eruption. Such a mechanism for eruption in this tectonic regime explains why periods of major extension and major volcanism are not contemporaneous (Sawyer et al., 1994). Releasing steps along such a fault system can allow the spatial separation of discrete magma batches in different regions of the crust, which eventually mingle during the eruption process that results in the formation of the major ash-flow sheets in this study.

The hypothesis that the low silica and high-silica rhyolite magmas associated with each ash-flow sheet are unrelated is supported by PVA of the pumice fragments, based on 1) the identification of distinct trends in the variation of end member proportions in EM

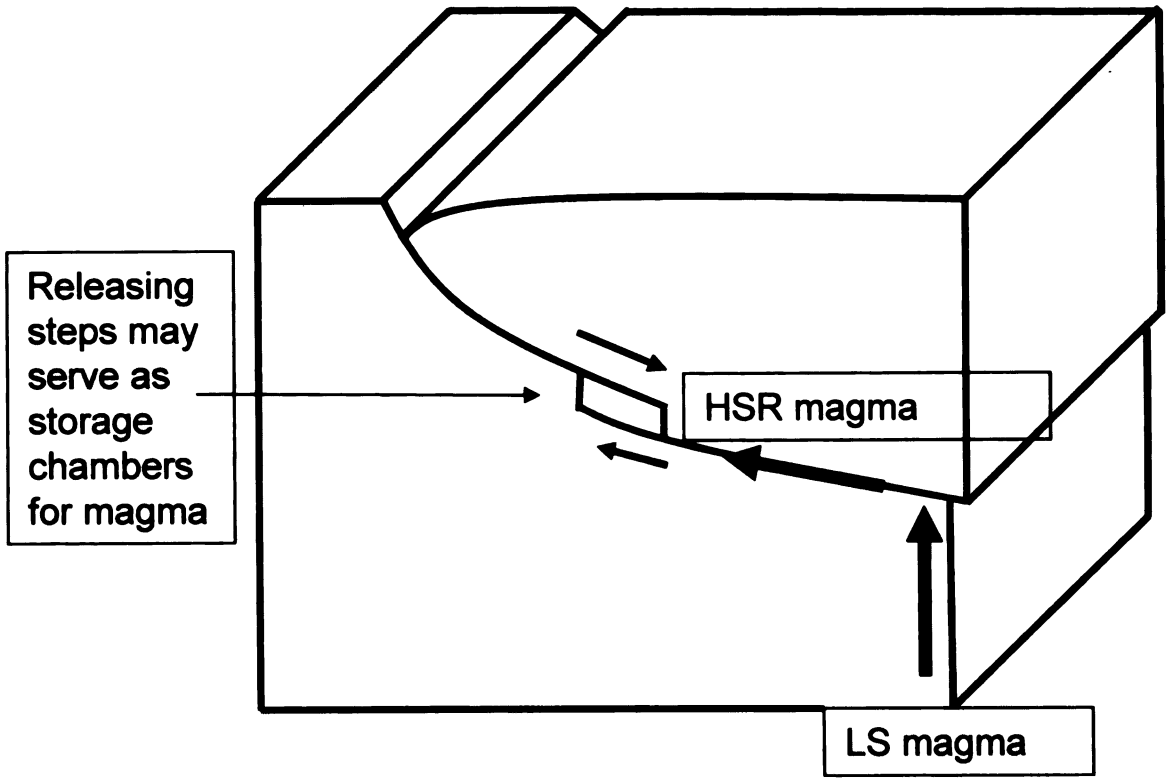

Figure 26. Model proposed by Cambray et al. (1995) showing normal dip-slip detachment fault with releasing step. As extension continues, releasing steps can accommodate more magma. Multiple releasing steps can allow the physical separation of magma batches that come into contact immediately preceding eruption.

plots, and 2) the generation of end members with unrealistic compositions, which fail to constrain the range of pumice fragment compositions in the dataset. Based on these same criteria, the relationship of the three high-silica rhyolite magmas of Rainier Mesa (HSR-1, HSR-2, and HSR-3) is also determined; HSR-1 is identified as a separate magma batch unrelated to the other coerupted magmas (HSR-2, HSR-3, and LS). HSR-3 cannot be explained as the result of magma mixing between HSR-2 and LS; however, HSR-3 and HSR-2 are very similar, and together may represent a second high-silica rhyolite magma batch. That limited mixing occurred among HSR-1, HSR-2, and HSR-3 is supported by the melt inclusions and sanidine trace element compositions. Furthermore, the determination of sanidine compositions that are in equilibrium with one of the end members allowed the identification of sanidines that are xenocrysts derived from the magma involved in mixing. In other words, if a sanidine from HSR-2 has a core composition that is in equilibrium with a HSR-2 end member that plots within the HSR-3 compositional field, then that sanidine first crystallized in HSR-3 magma, and later became incorporated in HSR-2 magma during a mixing event.

Not only does the use of PVA on datasets composed of pumice fragment samples confirm the existence of independently generated magma batches associated with each of the four major ash-flow sheets, but a relationship among the high-silica magmas can be determined. Both the trace element variation of melt inclusions from high-silica rhyolite pumice fragments, and PVA of these same melt inclusions, establishes that the high-silica rhyolite magmas of Topopah Spring, Tiva Canyon, and Ammonia Tanks have a common source, and followed similar evolutionary paths. Conversely, Rainier Mesa is unique among these ash-flow sheets in that 1) at least two high-silica rhyolite magma

compositions are determined, and 2) there are melt inclusions with high Rb and Nb (Group A inclusions) that are unique among these studied ash-flow sheets, and based on PVA, represent melt compositions that are distinct from the other ash-flow sheets, and finally, 3) Rainier Mesa magmas were derived from an ^{18}O-enriched crustal source, which dominates the isotopic signature of the Rainier Mesa magmas. Rainer Mesa magmas were generated during a relatively large time interval (1.1 My between Tiva Canyon and Rainier Mesa) at a time when extension rates in this region of the southern Great Basin were high; this explains the lack of significant eruptions during this time, as releasing steps can accommodate more magma during extension (Figure 26). What is proposed here is that, as a result of the large amount of extension, a different region of the lower to mid level crust underwent melting which produced the Rainier Mesa magmas; this region of the crust had an elevated $\delta^{18}O$, perhaps due to hydrothermal alteration. Following the caldera-forming eruption of the Rainier Mesa magmas, Ammonia Tanks magmas were quickly generated and erupted a short 150,000 years after the formation of the Rainier Mesa tuff; despite the short time span between these eruptions, Ammonia Tanks magmas are more alike Topopah Springs and Tiva Canyon in terms of pumice fragment and glass geochemistry, and PVA results on TS, TC, and AT pumice fragments and melt inclusion compositions. Thus it appears that whatever crustal source was involved in the generation of Rainier Mesa magmas was no longer involved in magma generation post-Rainier Mesa.

CHAPTER 6

CONCLUSIONS

End member compositions generated by PVA give valuable information as to whether or not a dataset comprises more than one magma batch (ie. whether or not the samples are related). If end member compositions adequately constrain the field of represented pumice fragment compositions, then the pumice fragments in the dataset (and therefore the magmas they represent) are related. Variations in the proportions of each of these end members within each pumice fragment sample result in the immediate recognition of one or more pumice fragment groups (if they represent unrelated magma batches). Breaking down a dataset into smaller subgroups is the next logical step in determining the relationship of, in this case, co-erupted magmas. As shown in Rainier Mesa, the interaction of three high-silica rhyolites and a low silica magma was detected. Furthermore, mixing between two magma batches was identified as the origin of the Ammonia Tanks INT pumice fragment group, whereas the Tiva Canyon INT pumice fragment group was not found to be a hybrid magma generated by mixing between high-silica rhyolite and low silica magmas. However, mixing is often subtle and not recognized in the sample geochemistry, such as within the Rainier Mesa high-silica rhyolite magmas. PVA-determined end member compositions for the HSR-1 and HSR2-HSR-3 datasets reveal an overlap in end member compositions that span more than one representative HSR composition field. These HSR pumice fragments have sanidine, melt inclusion, and glass matrix trace-element compositions that indicate mixing, which

involved all three HSR as well as a less evolved magma type, and PVA detects limited mixing among independent magma batches where conventional major and trace element least squares linear regression modeling fails. For the ash flows of SWNVF, independent magmas were involved in each ash flow formation, and PVA can establish a common source for the high-silica magmas of Topopah Spring, Tiva Canyon, and Ammonia Tanks despite limited mixing with less evolved magmas and the overprinting of the isotopic signature from mantle-derived melts. Until now, magma mixing has been detected by a combination of bulk geochemistry, phenocryst and glass geochemistry, and also by petrographic analysis; the results of this study show that PVA along with traditional methods of evaluation provides a powerful technique of evaluating magma petrogenesis.

APPENDICES

APPENDIX 1

APPENDIX 1. Major and trace element analyses of pumice fragments in Rainier Mesa tuff.

Sample ID	86RM6-16	02RM19-15B	99TM-13	020724-RM17	020724RM-18	02Rm19-10
Group	HSR-1	HSR-1	HSR-1	HSR-1	HSR-1	HSR-1
wt%:						
SiO2	77.4	76.8	77.2	77.0	77.2	77.3
TiO2	0.15	0.16	0.14	0.15	0.14	0.14
Al2O3	13.0	13.3	12.9	12.8	12.7	12.9
FeO	0.65	0.66	0.7	0.51	0.46	0.57
MgO	0	0	0	0	0	0
MnO	0.07	0.07	0.05	0.07	0.06	0.06
CaO	0.1	0.1	0.38	0.35	0.34	0.34
Na2O	3.7	3.8	3.4	3.27	3.51	3.66
K2O	4.85	4.9	5.04	5.71	5.44	4.93
P2O5	0.05	0.05	0.05	0.05	0.05	0.05
ppm:						
Th	24.0	24.2	28.6	25.9	24.5	25.3
La	19.0	19.9	26.3	20.2	19.0	19.9
Nb	39.6	42.8	34.9	59.6	55.8	57.1
Rb	259	260	256	284	276	267
Sr	4.37	3.94	15	7	8	6
Zr	76.7	80.0	92	80	73	81
Ce	38.8	39.4	65.9	55.9	55.7	54.2
Ta	3.19	3.40	2.51	3.52	3.66	3.45
Sm	4.33	4.67	4.68	4.83	4.77	4.49
Eu	0.13	0.16	0.16	0.33	0.23	0.24
Tb	0.85	0.94	0.78	0.93	0.94	0.92
Yb	3.36	3.50	3.23	3.63	3.73	3.71
Lu	0.51	0.54	0.45	0.60	0.59	0.60
Hf	3.46	3.63	3.62	3.59	3.54	3.57
Ba	15.2	12.4	45.4	42.0	31	34.4
Er	3.34	3.69	3.04	3.51	3.42	3.49
V			4.65	14.5	5.35	11.2
Cr			3.66	12.5	6.91	12.3
U	5.91	6.20	5.33	10.9	13.1	9.64
Pb			37.3	58.7	91.2	53.9
Nd	16.5	17.2	19.8	17.2	17.0	16.9
Pr	4.93	5.27	6.43	5.74	5.61	5.48
Dy	5.28	5.67	4.68	5.5	5.69	5.48
Ho	1.16	1.25	1	1.24	1.26	1.23
Gd	4.5	4.94	4.46	4.86	4.77	4.72
Y	37.1	40.0	32.6	38.1	37.1	37.4

APPENDIX 1. Continued.

Sample ID	86RM6-17	86RM27-6	86RM27-7	86RM27-8	86RM-27-9	86RM27-14
Group	HSR-2	HSR-2	HSR-2	HSR-2	HSR-2	HSR-2
wt%:						
SiO2	74.3	77.3	77.2	78.4	77.2	76.2
TiO2	0.21	0.19	0.21	0.19	0.18	0.17
Al2O3	16.2	13.5	13.7	12.8	13.0	13.9
FeO	1.3	0.56	0.63	0.44	0.86	1.03
MgO	0.15	0.93	0.63	0.62	0.66	0.51
MnO	0.04	0.02	0.02	0.02	0.04	0.05
CaO	0.14	0.14	0.12	0.11	0.13	0.15
Na2O	2.52	2.84	2.82	2.64	2.77	2.94
K2O	4.96	4.42	4.56	4.7	5.01	4.93
P2O5	0.05	0.05	0.05	0.05	0.05	0.05
ppm:						
Th	38.5	36.5	34.7	33.5	34.8	32.5
La	39.9	44.5	51.1	46.3	49.2	35.9
Nb	26.0	24.7	25.2	23.2	27.6	26.8
Rb	130	160	162	160	154	155
Sr	22.0	23.6	24.3	23.8	23.3	20.8
Zr	147	135	160	153	133	113
Ce	70.5	78.0	82.0	77.0	80.7	68.4
Ta	2.19	1.77	1.74	1.71	1.87	1.9
Sm	5.43	5.83	5.92	5.48	6.12	4.74
Eu	0.29	0.27	0.34	0.31	0.33	0.26
Tb	0.72	0.76	0.74	0.71	0.82	0.69
Yb	2.5	2.59	2.38	2.26	2.6	2.32
Lu	0.40	0.40	0.36	0.35	0.4	0.36
Hf	5.14	4.62	4.98	4.98	4.49	4.03
Ba	69.4	51.9	66.2	72.0	60.3	55.9
Er	2.37	2.51	2.27	2.18	2.65	2.26
V						
Cr						
U	2.8	2.28	2.21	2.28	3.09	3.48
Pb						
Nd	28.4	30.1	32.4	30.3	33.0	25.1
Pr	8.61	9.39	10.33	9.5	10.36	7.78
Dy	3.86	4.14	3.93	3.68	4.22	3.67
Ho	0.84	0.91	0.84	0.79	0.96	0.82
Gd	4.97	5.48	5.51	5.14	5.68	4.68
Y	22.7	26.5	23.1	22.8	27.3	23.4

APPENDIX 1. Continued.

Sample ID	86RM27-36	99TM-14	99TM-16	020725RM-23	02RM19-2	02RM19-3
Group	HSR-2	HSR-2	HSR-2	HSR-2	HSR-2	HSR-2
wt%:						
SiO2	80.2	75.6	77.2	76.8	76.5	75.5
TiO2	0.15	0.16	0.19	0.18	0.14	0.16
Al2O3	10.9	14.7	12.5	12.8	13.9	14.9
FeO	0.72	0.82	0.9	0.81	0.75	0.84
MgO	0.26	0.05	0.07	0.06	0.02	0
MnO	0.04	0.05	0.04	0.04	0.05	0.05
CaO	0.14	0.12	0.51	0.48	0.40	0.41
Na2O	2.25	2.85	3.55	3.21	2.90	2.52
K2O	5.21	5.55	4.93	5.51	5.27	5.51
P2O5	0.05	0.05	0.05	0.05	0.05	0.05
ppm:						
Th	28.3	33.0	34.2	32.9	37.7	41.1
La	37.1	29.0	53.6	51.3	37.6	43.3
Nb	19.9	29.8	22.1	30.6	42.4	41.1
Rb	124	170	124	125	171	173
Sr	22.4	12.4	50	42	17	18
Zr	122	107	162	157	113	132
Ce	67.9	60.2	119	112	95.5	104
Ta	1.4	2.4	1.28	1.59	2.68	2.88
Sm	4.15	4.53	5.11	5.03	6.00	7.34
Eu	0.32	0.12	0.47	0.6	0.31	0.34
Tb	0.54	0.70	0.60	0.61	0.84	1.00
Yb	1.96	2.58	1.96	2.00	2.81	3.06
Lu	0.3	0.39	0.26	0.33	0.43	0.46
Hf	3.98	4.22	4.55	4.54	4.5	5.06
Ba	78.5	36.4	186	187	74.7	74.2
Er	1.78	2.46	1.8	1.81	2.5	2.92
V			4.52	19.1	7.69	6.75
Cr			2.74	13.1	8.73	7.84
U	3.14	4.57	2.68	4.9	8.62	8.62
Pb			38.5	45.1	88.3	98.0
Nd	23.7	21.9	30.8	30.2	29.4	35.7
Pr	7.43	6.8	10.7	10.1	9.58	11.6
Dy	2.88	4.05	3.1	3	4.5	4.96
Ho	0.65	0.87	0.57	0.65	0.93	1.09
Gd	4.09	4.58	4.41	4.46	5.38	6.58
Y	17.9	25.8	18.8	17.6	27.2	30.3

APPENDIX 1. Continued.

Sample ID	02RM19-7	02RM19-11	86RM24-1	020725-RM5	020725RM-19F
Group	HSR-2	HSR-2	HSR-3	LS	LS
wt%:					
SiO2	74.4	77.4	76.3	72.2	71.2
TiO2	0.21	0.17	0.24	0.37	0.38
Al2O3	16.3	12.5	13.0	14.7	15.8
FeO	1.07	0.82	1	1.66	1.94
MgO	0.09	0.04	0.09	0.3	1.17
MnO	0.05	0.04	0.05	0.06	0.04
CaO	0.42	0.45	0.17	0.98	0.97
Na2O	2.63	2.6	2.74	3.55	3.34
K2O	4.67	5.9	6.33	5.93	4.84
P2O5	0.05	0.05	0.05	0.07	0.09
ppm:					
Th	45.4	38.4	36.3	51.3	35.2
La	48.6	51.0	67.1	130.1	82.9
Nb	42.3	34.8	21.4	21.9	32.5
Rb	123	179	145	112	93
Sr	27	24	42.2	131	219
Zr	159	136	213	359	301
Ce	109	117	110	259	176
Ta	2.58	1.89	1.5	1.22	2.09
Sm	6.38	6.1	5.33	7.5	7.3
Eu	0.45	0.47	0.51	1.07	1.21
Tb	0.82	0.77	0.59	0.74	0.95
Yb	2.77	2.4	2.06	2.01	3.3
Lu	0.41	0.36	0.32	0.26	0.47
Hf	5.57	4.44	5.92	8.62	7.36
Ba	101	101	173	497	792
Er	2.29	2.19	1.88	1.44	2.91
V	10.1	9.28		19.6	32.5
Cr	9.35	8.37		6.74	9.03
U	7.58	7.56	2.24	3.61	5.24
Pb	78.2	80.0		63.9	129
Nd	34.8	34.0	35.8	65.1	50.1
Pr	11.4	11.6	11.5	21.9	16.4
Dy	4.21	3.82	3.01	2.78	4.65
Ho	0.83	0.8	0.66	0.55	1.02
Gd	5.71	5.41	5.01	6.79	7.19
Y	24.2	22.4	19.0	15.3	33.2

APPENDIX 2

APPENDIX 2. Major and trace element geochemistry of sanidine and plagioclase grains.

Topopah Spring

ID	BB8-15b-1-P1	BB8-15b-1-P2	BB8-15b-1-P3	BB8-15b-1-P4	BB8-15b-1-P5	BB8-15b-1-P6	BB8-15b-1-P7	BB8-15b-1-P8
GROUP	HSR	HSR	HSR	HSR	HSR	HSR	HSR	HSR
distance to rim (μm)	1	50	100	150	200	250	300	350
wt%								
SiO2	66.0	65.6	65.7	65.6	65.7	65.4	65.6	65.5
TiO2	0.002	0.016	0.020	0.000	0.015	0.000	0.006	0.014
Al2O3	18.9	18.8	18.7	18.9	18.9	19.0	19.1	18.8
FeO	0.071	0.039	0.102	0.094	0.050	0.131	0.081	0.081
MgO	0.001	0.000	0.000	0.004	0.000	0.006	0.003	0.003
CaO	0.199	0.225	0.223	0.216	0.187	0.209	0.225	0.166
Na2O	4.00	4.17	4.27	4.17	4.20	4.27	4.29	4.33
K2O	10.8	11.1	10.8	10.8	10.7	10.9	10.6	10.9
ppm:								
Ba	844	829	825	1003	1016	1078	1099	1037
Sr	165	155	143	142	140	152	150	117
Rb	125	102	111	101	93.9	109	118	78.5

APPENDIX 2. Continued.

Topopah Spring

ID	BB8-3A-1-P1	BB8-3A-1-P2	BB8-3A-1-P3	BB8-3A-1-P4	BB8-3A-1-P5	BB8-3A-1-P6	BB8-3A-1-P7	BB8-3A-1-P8
GROUP	HSR	HSR	HSR	HSR	HSR	HSR	HSR	HSR
distance to rim (μm)	1	50	100	150	200	250	300	350
wt%								
SiO2	65.8	65.8	65.7	65.7	65.4	66.0	65.8	65.8
TiO2	0.021	0.004	0.000	0.010	0.000	0.009	0.018	0.000
Al2O3	19.0	18.9	19.2	19.1	19.2	18.6	18.8	18.7
FeO	0.119	0.139	0.129	0.023	0.078	0.048	0.056	0.093
MgO	0.006	0.000	0.000	0.005	0.000	0.000	0.002	0.000
CaO	0.248	0.286	0.238	0.179	0.186	0.234	0.213	0.214
Na2O	4.06	4.18	4.30	4.04	4.10	4.08	4.20	4.18
K2O	10.7	10.7	10.4	10.9	11.0	10.9	10.8	11.0
ppm:								
Ba	122	216	243	574	697	587	636	774
Sr	32.8	41.5	54.0	104	112	108	112	120
Rb	71.7	70.5	78.0	76.0	68.7	74.1	69.6	70.4

APPENDIX 2. Continued.

Topopah Spring

ID	LW4-10A-1-P1	LW4-10A-1-P2	LW4-10A-1-P3	LW4-10A-1-P4	LW4-10A-1-P5	LW4-10A-1-P6	LW4-10A-1-P7	CP3-1a-2 core
GROUP	HSR	HSR	HSR	HSR	HSR	HSR	HSR	HSR
distance to rim (μm)	1	50	100	150	200	250	300	600
wt%								
SiO2	64.0	64.6	64.6	64.5	64.5	64.5	65.2	63.3
TiO2	0.002	0.046	0.031	0.031	0.014	0.055	0.045	0.00
Al2O3	19.7	19.5	19.3	19.6	19.6	19.8	19.3	22.7
FeO	0.202	0.229	0.207	0.233	0.240	0.222	0.160	0.095
MgO	0.000	0.006	0.000	0.001	0.005	0.002	0.000	0.007
CaO	0.675	0.770	0.747	0.628	0.802	0.810	0.622	3.906
Na2O	4.78	4.74	4.77	4.75	4.82	5.06	4.97	8.85
K2O	9.09	8.99	9.32	9.21	9.07	8.67	9.29	1.17
ppm:								
Ba	15045	9102	7144	6343	6415	4472	2349	40.2
Sr	602	508	460	376	379	455	464	162
Rb	39.6	39.9	38.3	43.7	37.5	36.6	38.0	16.6

APPENDIX 2. Continued.

Topopah Spring

ID	CP3-1a-2 rim	BB8-3A-10-P1	BB8-3A-10-P2	BB8-3A-10-P3	BB8-3A-10-P4	BB8-3A-10-P5	BB8-3A-10-P6	BB8-3A-10-P7
GROUP	HSR	HSR	HSR	HSR	HSR	HSR	HSR	HSR
distance to rim (μm)	1	1	50	100	150	200	250	300
wt%								
SiO2	63.8	65.5	65.6	65.6	65.6	65.7	65.6	65.3
TiO2	0.01	0.02	0.01	0.01	0.01	0.01	0.01	0.00
Al2O3	22.5	18.8	18.8	18.9	18.9	19.0	19.0	18.8
FeO	0.116	0.093	0.095	0.078	0.083	0.103	0.060	0.076
MgO	0.000	0.000	0.013	0.000	0.000	0.001	0.000	0.004
CaO	3.559	0.243	0.265	0.253	0.206	0.230	0.205	0.240
Na2O	8.88	4.47	4.12	4.19	4.28	4.49	4.17	4.26
K2O	1.14	10.9	10.9	10.8	10.7	10.4	10.9	11.1
ppm:								
Ba	68.6	196	728	707	705	807	718	758
Sr	139	55.4	104	114	121	128	125	111
Rb	9.51	66.8	72.3	78.1	66.8	74.9	75.1	72.3

APPENDIX 2. Continued.

Topopah Spring

ID	BB8-3A-6-P1	BB8-3A-6-P2	BB8-3A-6-P3	BB8-3A-6-P4	BB8-3A-6-P5	BB8-3A-6-P6	BB8-3A-6-P7	BB8-3A-6-P8
GROUP	HSR	HSR	HSR	HSR	HSR	HSR	HSR	HSR
distance to rim (μm)	1	50	100	150	200	250	300	350
wt%								
SiO2	65.6	65.5	65.5	65.5	65.6	65.8	65.6	65.4
TiO2	0.02	0.01	0.02	0.01	0.00	0.00	0.00	0.00
Al2O3	19.0	18.8	18.9	18.9	19.0	18.9	19.1	19.2
FeO	0.154	0.077	0.120	0.066	0.117	0.081	0.088	0.122
MgO	0.005	0.006	0.015	0.002	0.002	0.000	0.004	0.000
CaO	0.256	0.204	0.246	0.205	0.212	0.183	0.186	0.184
Na2O	4.13	4.18	4.20	4.11	4.15	4.09	4.03	4.14
K2O	10.8	11.2	11.0	11.2	10.8	10.9	10.8	10.9
ppm:								
Ba	185	238	280	579	715	745	796	819
Sr	43.1	50.3	68.8	76.6	85.3	92.9	101	112
Rb	51.2	43.3	87.1	89.0	66.5	129	84.5	72.3

APPENDIX 2. Continued.

Topopah Spring

ID	BB8-3A-6-P9	BB8-3A-6-P10	BB8-3A-6-P11	BB8-3A-6-P12	CP1-2E-3 core	CP1-2E-3 rim	BB8-15b-3-P1	BB8-15b-3-P2
GROUP	HSR	HSR	HSR	HSR	HSR	HSR	HSR	HSR
distance to rim (μm)	400	450	500	550	600	1	1	50
wt%								
SiO2	65.6	65.7	65.7	65.9	63.9	63.1	62.9	63.2
TiO2	0.00	0.00	0.00	0.01	0.00	0.00	0.02	0.01
Al2O3	19.0	19.0	18.9	19.0	22.2	22.2	22.0	22.5
FeO	0.095	0.075	0.032	0.105	0.185	0.209	0.213	0.167
MgO	0.002	0.000	0.000	0.001	0.000	0.000	0.003	0.010
CaO	0.196	0.198	0.237	0.189	3.647	3.818	3.665	3.830
Na2O	4.16	4.09	4.14	4.26	8.55	9.34	9.92	8.99
K2O	10.8	10.9	10.8	10.5	1.42	1.30	1.23	1.20
ppm:								
Ba	808	789	750	917	59.6	45.8	96.4	182
Sr	111	114	107	127	162	163	191	251
Rb	76.7	51.0	72.2	89.3	0.00	0.00	11.9	0.00

APPENDIX 2. Continued.

Topopah Spring

ID	BB8-15b-3-P3	BB8-15b-3-P4	BB8-15b-3-P5	BB8-15b-4-P1	BB8-15b-4-P2	BB8-15b-4-P3	BB8-15b-4-P4	BB8-15b-4-P5
GROUP	HSR	HSR	HSR	HSR	HSR	HSR	HSR	HSR
distance to rim (μm)	100	150	200	1	50	100	150	200
wt%								
SiO2	63.2	63.5	63.6	65.5	65.7	65.6	65.7	65.7
TiO2	0.00	0.01	0.00	0.02	0.00	0.02	0.01	0.01
Al2O3	22.7	22.5	22.3	18.7	19.0	19.0	19.0	19.1
FeO	0.231	0.194	0.132	0.139	0.124	0.208	0.129	0.140
MgO	0.001	0.006	0.006	0.000	0.000	0.000	0.000	0.025
CaO	4.044	3.915	3.923	0.331	0.372	0.302	0.320	0.324
Na2O	8.76	8.80	8.81	5.25	4.87	4.98	4.80	4.73
K2O	1.04	1.07	1.24	10.1	10.0	9.84	10.0	10.0
ppm:								
Ba	215	173	119	132	168	183	172	154
Sr	273	254	219	32.7	35.2	35.3	30.4	32.2
Rb	0.00	0.00	0.00	70.8	61.4	48.5	73.5	60.9

APPENDIX 2. Continued.

Topopah Spring

ID	BB8-15b-4-P6	LW4-10a-3-P1	LW4-10a-3-P2	LW4-10a-3-P3	LW4-10a-3-P4	BB8-3A-9-P1	BB8-3A-9-P2	BB8-3A-9-P3
GROUP	HSR	HSR	HSR	HSR	HSR	HSR	HSR	HSR
distance to rim (μm)	250	1	50	100	150	1	50	100
wt%								
SiO2	65.7	64.1	63.7	63.9	63.6	65.9	65.6	65.9
TiO2	0.01	0.01	0.02	0.00	0.03	0.01	0.01	0.00
Al2O3	19.0	19.9	19.7	19.9	19.7	19.0	18.7	18.7
FeO	0.182	0.210	0.244	0.173	0.268	0.085	0.102	0.083
MgO	0.000	0.008	0.000	0.005	0.000	0.004	0.008	0.000
CaO	0.276	0.752	0.961	0.814	0.882	0.227	0.211	0.195
Na2O	4.54	4.90	4.90	4.76	4.99	4.09	4.61	4.07
K2O	10.2	8.30	8.77	8.97	8.88	10.6	10.6	10.9
ppm:								
Ba	172	12115	11866	11848	11776	639	678	607
Sr	30.7	587	590	583	572	88.9	96.9	92.5
Rb	62.7	37.9	37.7	44.7	38.0	71.6	79.9	75.9

APPENDIX 2. Continued.

Topopah Spring

ID	BB8-3A-9-P4	BB8-3A-9-P5	BB8-3a-5 core	BB8-3A-5-RIM	BB3A-4-CORE	BB8-3A-4 rim
GROUP	HSR	HSR	HSR	HSR	HSR	HSR
distance to rim (μm)	150	200	600	1	600	1
wt%						
SiO2	65.8	65.8	65.7	65.6	65.4	65.9
TiO2	0.02	0.03	0.00	0.00	0.00	0.00
Al2O3	18.8	18.9	18.9	19.4	18.9	19.4
FeO	0.088	0.056	0.084	0.126	0.071	0.076
MgO	0.007	0.011	0.000	0.000	0.012	0.000
CaO	0.219	0.199	0.269	0.270	0.215	0.204
Na2O	4.12	4.09	4.18	3.79	4.09	4.64
K2O	10.8	11.0	10.7	10.8	11.1	9.72
ppm:						
Ba	609	546		173	298	663
Sr	96.1	95.8		72.1	60.8	93.2
Rb	87.3	65.5		151	74.7	87.0

APPENDIX 2. Continued.

Tiva Canyon

ID	TC5BI-5 P1	TC5BI-5 P2	TC5BI-5 P3	TC5BI-5 P4	TC5BI-3 P1	TC5BI-3 P2	TC5BI-3 P3	TC5BI-3 P4
GROUP	HSR	HSR	HSR	HSR	HSR	HSR	HSR	HSR
distance to rim (μm)	1	50	100	150	1	50	100	150
wt%:								
SiO2	66.6	66.7	66.9	67.0	67.0	66.9	66.7	66.5
TiO2	0.000	0.009	0.010	0.023	0.026	0.008	0.016	0.017
Al2O3	19.3	19.6	19.2	19.7	19.7	19.3	19.2	19.4
FeO	0.247	0.237	0.228	0.278	0.258	0.234	0.209	0.262
MgO	0.004	0.000	0.004	0.036	0.011	0.004	0.005	0.000
CaO	0.337	0.653	0.528	0.676	0.451	0.391	0.356	0.401
Na2O	6.56	7.73	6.84	7.36	5.86	6.50	6.66	6.76
K2O	6.88	5.04	6.31	4.94	6.64	6.63	6.77	6.59
ppm:								
Ba	836	170	387	402	285	281	291	281
Sr	175	123	111	98.1	91.7	92.8	95.9	91.4
Rb	191	34.8	63.0	42.5	45.2	48.4	25.7	33.3

APPENDIX 2. Continued.

Tiva Canyon

ID	TC5BI-3 P5	TC5BI-3 P6	TC5BI-4 P1	TC5BI-4 P2	TC5BI-4 P3	TC5BI-4 P4	TC5BI-4 P5	TC5BI-4 P6
GROUP	HSR	HSR	HSR	HSR	HSR	HSR	HSR	HSR
distance to rim (μm)	200	250	1	50	100	150	200	250
wt%:								
SiO2	66.8	66.7	65.7	66.5	66.4	66.4	66.7	66.7
TiO2	0.000	0.000	0.018	0.000	0.007	0.015	0.023	0.000
Al2O3	19.1	19.3	19.3	19.3	19.3	19.4	19.1	19.3
FeO	0.243	0.228	0.243	0.220	0.246	0.207	0.220	0.208
MgO	0.006	0.000	0.000	0.000	0.000	0.000	0.000	0.005
CaO	0.435	0.455	0.391	0.437	0.425	0.381	0.315	0.381
Na2O	7.00	7.08	7.84	7.15	6.95	6.70	6.45	6.52
K2O	6.34	6.22	6.41	6.29	6.59	6.79	7.12	6.94
ppm:								
Ba	257	289	303	306	291	290	319	289
Sr	84.4	93.9	79.3	96.1	97.7	88.9	86.7	89.3
Rb	36.5	40.3	44.7	40.9	38.0	43.9	52.1	51.9

APPENDIX 2. Continued.

Tiva Canyon

ID	TC5BI-2 P1	TC5BI-2 P2	TC5BI-2 P3	TC5BI-2 P4	TC5BI-2 P5	TC5BI-2 P6	TC5BI-2 P7	TC5BI-2 P8
GROUP	HSR	HSR	HSR	HSR	HSR	HSR	HSR	HSR
distance to rim (µm)	1	50	100	150	200	250	300	350
wt%:								
SiO2	66.4	66.3	66.9	66.4	66.7	66.7	66.8	67.1
TiO2	0.015	0.024	0.014	0.008	0.008	0.003	0.004	0.011
Al2O3	19.0	19.4	19.0	19.4	19.4	19.5	19.4	19.1
FeO	0.215	0.230	0.216	0.262	0.256	0.246	0.260	0.167
MgO	0.001	0.000	0.000	0.000	0.000	0.000	0.000	0.009
CaO	0.298	0.365	0.420	0.471	0.532	0.574	0.561	0.501
Na2O	6.80	6.69	6.86	7.03	7.29	7.30	7.30	7.18
K2O	7.15	6.89	6.59	6.39	5.80	5.65	5.68	5.95
ppm:								
Ba	292	322	303	300	283	264	251	243
Sr	81.7	89.9	94.6	108	117	115	107	104
Rb	39.2	44.2	47.2	37.9	26.9	32.3	24.1	19.8

APPENDIX 2. Continued.

Tiva Canyon

ID	TC5BJ-2 P1	TC5BJ-2 P2	TC5BJ-2 P3	TC5BJ-2 P4	TC5BJ-2 P5	TC5BJ-2 P6	TC5BJ-2 P7	TC5BJ-2 P8
GROUP	HSR	HSR	HSR	HSR	HSR	HSR	HSR	HSR
distance to rim (μm)	1	50	100	150	200	250	300	350
wt%:								
SiO2	66.6	66.7	66.7	66.7	66.6	66.7	66.5	66.5
TiO2	0.000	0.000	0.009	0.014	0.017	0.016	0.005	0.014
Al2O3	19.3	19.1	19.2	19.2	19.3	19.2	19.3	19.2
FeO	0.202	0.257	0.201	0.246	0.218	0.241	0.192	0.244
MgO	0.002	0.009	0.002	0.004	0.000	0.000	0.006	0.006
CaO	0.388	0.282	0.355	0.354	0.440	0.404	0.412	0.354
Na2O	6.67	6.51	6.67	6.81	7.12	6.99	6.87	6.72
K2O	6.81	7.10	6.79	6.61	6.34	6.38	6.68	6.90
ppm:								
Ba	298	269	308	340	318	306	354	374
Sr	94.1	79.7	91.6	108	117	112	112	110
Rb	87.4	51.8	48.2	44.9	35.1	30.7	53.6	31.2

APPENDIX 2. Continued.

Tiva Canyon

ID	TC5BI-6 P1	TC5BI-6 P2	TC5BI-6 P3	TC5BI-6 P4	TC2EA-3 P1	TC2EA-3 P2	TC2EA-3 P3	TC2EA-3 P4
GROUP	HSR	HSR	HSR	HSR	HSR	HSR	HSR	HSR
distance to rim (μm)	1	50	100	150	1	50	100	150
wt%:								
SiO2	67.8	66.8	67.0	66.7	67.2	67.3	67.2	67.2
TiO2	0.013	0.003	0.005	0.018	0.013	0.016	0.007	0.026
Al2O3	19.5	19.3	19.0	19.2	19.4	19.5	19.1	19.0
FeO	0.228	0.259	0.256	0.233	0.227	0.247	0.265	0.224
MgO	0.000	0.006	0.000	0.003	0.000	0.000	0.000	0.000
CaO	0.411	0.418	0.410	0.397	0.456	0.549	0.407	0.410
Na2O	5.51	6.44	6.59	6.70	5.37	6.17	6.11	6.53
K2O	6.44	6.70	6.73	6.76	7.23	6.22	6.89	6.53
ppm:								
Ba	322	298	283	342	291	297	312	330
Sr	98.1	99.5	95.8	100	86.0	97.8	96.3	91.4
Rb	51.2	48.9	46.1	52.2	42.6	40.8	37.1	45.1

APPENDIX 2. Continued.

Tiva Canyon

ID	TC2EA-3 core	TC2EA-3 P6	TC2EA-3 P7	TC2EA-3 P8	TC2EA-2 P1	TC2EA-2 P2	TC2EA-2 P3	TC2EA-2 P4
GROUP	HSR	HSR	HSR	HSR	HSR	HSR	HSR	HSR
distance to rim (μm)	200	250	300	350	1	50	100	150
wt%:								
SiO2	66.4	66.6	67.0	66.8	66.8	67.4	67.3	67.0
TiO2	0.006	0.008	0.008	0.024	0.014	0.009	0.007	0.001
Al2O3	18.9	19.2	19.2	19.3	19.6	19.2	19.2	19.3
FeO	0.270	0.271	0.213	0.239	0.270	0.301	0.270	0.245
MgO	0.002	0.000	0.001	0.000	0.000	0.007	0.001	0.006
CaO	0.333	0.502	0.525	0.451	0.372	0.293	0.287	0.517
Na2O	6.91	7.36	6.66	6.21	5.52	5.55	5.88	7.12
K2O	6.98	6.05	6.31	6.92	7.33	7.23	7.04	5.79
ppm:								
Ba	351	277	296	269	316	333	311	258
Sr	85.7	95.6	85.0	78.9	109	101	95.4	124
Rb	59.8	36.9	42.3	43.8	44.8	52.1	43.8	40.3

APPENDIX 2. Continued.

Tiva Canyon

ID	TC5BN-3 P1	TC5BN-3 P2	TC5BN-3 P3	TC5BN-3 P4	TC5BN-3 P5	TC5BN-3 P6	TC-2ED-4 P1	TC-2ED-4 P2
GROUP	HSR	HSR	HSR	HSR	HSR	HSR	HSR	HSR
distance to rim (μm)	1	50	100	150	200	250	1	50
wt%:								
SiO2	66.1	66.6	66.6	66.2	66.6	66.7	66.4	66.2
TiO2	0.02	0.01	0.02	0.03	0.01	0.01	0.01	0.00
Al2O3	19.3	19.0	19.1	19.1	19.1	19.0	19.3	19.2
FeO	0.238	0.234	0.213	0.253	0.214	0.231	0.227	0.249
MgO	0.000	0.000	0.000	0.000	0.007	0.001	0.000	0.007
CaO	0.395	0.336	0.288	0.351	0.413	0.439	0.660	0.476
Na2O	7.67	6.89	6.78	7.11	7.10	7.02	7.93	7.42
K2O	6.19	6.90	6.95	6.92	6.57	6.59	5.39	6.40
ppm:								
Ba	263	389	330	325	284	301	404	569
Sr	86.0	79.5	76.1	82.5	84.3	81.5	120	125
Rb	30.9	36.8	37.7	42.8	38.6	32.6	28.6	24.8

APPENDIX 2. Continued.

Tiva Canyon

ID	TC2EA-1 P1	TC2EA-1 P2	TC2EA-1 P3	TC2EA-1 P4	TC5BM-9 P1	TC5BM-9 P2	TC5BM-9 P3	TC5BM-9 P4
GROUP	HSR	HSR	HSR	HSR	HSR	HSR	HSR	HSR
distance to rim (μm)	1	50	100	150	1	50	100	150
wt%:								
SiO2	66.9	66.6	66.4	66.5	66.0	65.9	66.7	66.2
TiO2	0.003	0.004	0.029	0.022	0.023	0.016	0.018	0.014
Al2O3	19.4	19.3	19.5	19.3	19.4	19.6	19.3	19.4
FeO	0.241	0.229	0.216	0.246	0.290	0.249	0.259	0.268
MgO	0.007	0.003	0.000	0.009	0.000	0.000	0.002	0.000
CaO	0.367	0.445	0.459	0.516	0.581	0.636	0.636	0.634
Na2O	6.71	7.21	7.09	7.38	8.11	7.82	7.62	7.77
K2O	6.39	6.16	6.22	6.04	5.48	5.68	5.40	5.52
ppm:								
Ba	334	292	305	291	794	767	776	801
Sr	98.7	98.3	111	110	167	178	159	146
Rb	50.7	36.2	42.9	33.9	33.7	36.3	27.7	50.5

APPENDIX 2. Continued.

Tiva Canyon

ID	TC5BM-8 P1	TC5BM-8 P2	TC5BM-8 P3	TC5BM-8 P4	TC5BM-8 P5	TC5BM-8 P6	TC5BM-3 P1	TC5BM-3 P2
GROUP	HSR	HSR	HSR	HSR	HSR	HSR	HSR	HSR
distance to rim (μm)	1	50	100	150	200	250	1	50
wt%:								
SiO2	66.7	67.1	66.3	67.0	66.2	66.7	65.9	66.6
TiO2	0.019	0.003	0.008	0.018	0.019	0.009	0.023	0.031
Al2O3	19.1	19.0	19.3	19.0	19.4	19.2	19.8	19.5
FeO	0.351	0.226	0.243	0.201	0.204	0.215	0.248	0.195
MgO	0.011	0.000	0.000	0.013	0.013	0.003	0.000	0.000
CaO	0.509	0.492	0.541	0.477	0.438	0.468	0.815	0.930
Na2O	7.36	7.51	7.43	7.24	7.31	7.68	8.48	8.28
K2O	5.90	5.55	5.84	6.03	6.30	5.72	4.71	4.37
ppm:								
Ba	286	288	257	304	311	365	352	304
Sr	92.6	102	103	138	133	148	117	140
Rb	38.8	30.5	32.2	29.1	49.2	37.0	18.1	16.7

APPENDIX 2. Continued.

Tiva Canyon

ID	TC5BM-3 P3	TC2ED-6 core	TC2ED-6 rim	TC2EA-5 rim	TC2EA-5 P2	TC2EA-5 P3	TC2EA-5 core	TC5BM-2 P1
GROUP	HSR	HSR	HSR	HSR	HSR	HSR	HSR	HSR
distance to rim (μm)	100	450	1	1	50	100	150	1
wt%:								
SiO2	66.5	65.8	66.3	66.8	67.0	66.7	66.7	67.1
TiO2	0.012	0.000	0.014	0.006	0.019	0.038	0.000	0.005
Al2O3	19.5	19.5	19.2	19.7	19.0	19.1	19.0	19.2
FeO	0.296	0.220	0.260	0.215	0.227	0.212	0.172	0.266
MgO	0.012	0.000	0.000	0.018	0.000	0.000	0.002	0.247
CaO	0.708	0.614	0.561	0.428	0.405	0.413	0.444	0.565
Na2O	7.86	8.10	7.82	6.56	6.64	6.94	6.94	6.88
K2O	5.12	5.76	5.80	6.28	6.61	6.56	6.62	5.76
ppm:								
Ba	375	270	285	561	337	309	321	284
Sr	135	83.6	113	101	93.2	91.5	88.7	108
Rb	27.0	41.6	47.2	61.4	59.3	38.2	34.3	35.8

APPENDIX 2. Continued.

Tiva Canyon

ID	TC5BM-2 P2	TC5BM-2 P3	TC5BM-2 P4	TC5BM-2 P5	TC2ED-3 P1	TC2ED-3 P2	TC2ED-3 P3	TC2ED-3 P4
GROUP	HSR	HSR	HSR	HSR	HSR	HSR	HSR	HSR
distance to rim (μm)	50	100	150	200	1	50	100	150
wt%:								
SiO2	66.8	66.4	66.6	66.0	67.4	67.3	67.3	67.0
TiO2	0.003	0.019	0.006	0.030	0.014	0.029	0.001	0.007
Al2O3	19.5	19.5	19.5	20.5	19.4	19.3	19.1	19.1
FeO	0.186	0.164	0.217	0.215	0.206	0.263	0.216	0.245
MgO	0.014	0.000	0.000	0.000	0.000	0.008	0.000	0.000
CaO	0.565	0.603	0.599	1.02	0.452	0.489	0.426	0.326
Na2O	7.20	7.66	7.87	7.78	6.08	6.19	6.48	6.40
K2O	5.65	5.68	5.15	4.35	6.45	6.40	6.47	6.91
ppm:								
Ba	263	246	265	361	266	261	273	305
Sr	113	122	122	151	98.1	89.0	101	91.3
Rb	32.0	35.4	23.3	21.2	44.4	38.0	34.2	44.0

APPENDIX 2. Continued.

Tiva Canyon

ID	TC2ED-3 P5	TC5BN-1 P1	TC5BN-1 P2	TC5BN-1 P3	TC5BN-1 P4	TC5BN-1 P5	TC5BN-1 P6	TC5BN-1 P7
GROUP	HSR	HSR	HSR	HSR	HSR	HSR	HSR	HSR
distance to rim (μm)	200	1	50	100	150	200	250	300
wt%:								
SiO2	66.8	66.9	66.4	66.4	66.3	66.5	66.3	66.6
TiO2	0.000	0.011	0.000	0.028	0.016	0.005	0.004	0.002
Al2O3	19.0	18.8	19.6	19.4	19.5	19.4	19.5	19.3
FeO	0.264	0.248	0.262	0.250	0.301	0.178	0.284	0.252
MgO	0.000	0.009	0.003	0.000	0.000	0.000	0.000	0.011
CaO	0.362	0.381	0.706	0.635	0.678	0.600	0.617	0.581
Na2O	6.41	7.07	7.78	7.67	7.75	7.61	7.76	7.65
K2O	7.05	6.62	5.27	5.66	5.39	5.63	5.39	5.63
ppm:								
Ba	318	237	239	233	239	254	239	232
Sr	102	105	132	123	127	123	122	114
Rb	57.8	33.2	30.3	30.5	30.8	31.5	29.1	36.5

APPENDIX 2. Continued.

Tiva Canyon

ID	TC5BN-1 P8	TC5BN-1 P9	TC5BI-7 P1	TC5BI-7 P2	TC5BI-7 P3	TC5BI-7 P4	TC5BI-7 P5	TC5BI-7 P6
GROUP	HSR	HSR	HSR	HSR	HSR	HSR	HSR	HSR
distance to rim (μm)	350	400	1	50	100	150	200	250
wt%:								
SiO2	66.5	66.5	66.7	66.6	66.9	66.4	66.7	66.5
TiO2	0.014	0.019	0.000	0.028	0.004	0.040	0.010	0.010
Al2O3	19.5	19.4	19.2	19.2	19.0	19.3	18.8	19.2
FeO	0.210	0.249	0.252	0.197	0.204	0.244	0.286	0.214
MgO	0.005	0.001	0.011	0.013	0.000	0.000	0.010	0.008
CaO	0.629	0.551	0.408	0.417	0.401	0.399	0.365	0.348
Na2O	7.63	7.62	7.09	7.15	7.10	7.10	6.83	6.98
K2O	5.50	5.60	6.30	6.41	6.35	6.45	7.01	6.75
ppm:								
Ba	226	237	251	268	272	327	324	302
Sr	118	103	93.3	98.8	96.9	99.1	95.8	89.9
Rb	27.3	32.5	50.1	41.6	41.6	44.5	47.7	37.5

APPENDIX 2. Continued.

Ammonia Tanks

ID	AT5-29-1-P1	AT5-29-1-P2	AT5-29-1-P3	AT5-29-1-P4	AT5-29-1-P5	AT5-29-1-P6	AT5-29-1-P7	AT5-8-1-P1
Group	HSR	HSR	HSR	HSR	HSR	HSR	HSR	HSR
distance to rim (μm)	1	50	100	150	200	250	300	1
wt%:								
SiO2	67.4	66.6	66.3	66.1	65.9	65.8	65.3	66.1
TiO2	0.009	0.000	0.022	0.036	0.030	0.021	0.036	0.000
Al2O3	19.5	19.6	19.0	19.0	19.0	19.2	19.3	19.0
FeO	0.18	0.20	0.16	0.18	0.22	0.14	0.17	0.18
MgO	0.006	0.000	0.000	0.007	0.003	0.008	0.000	0.005
CaO	0.33	0.44	0.39	0.27	0.25	0.27	0.34	0.32
Na2O	4.16	5.83	5.61	5.86	6.11	6.39	7.53	5.78
K2O	8.44	7.31	8.52	8.48	8.44	8.17	7.30	8.59
ppm:								
Ba	61.1	81.3	70.7	67.5	67.8	75.4		40.1
Sr	13.5	12.6	12.2	11.6	11.8	14.0		12.5
Rb	53.4	60.7	65.1	70.8	61.6	66.3		53.9

APPENDIX 2. Continued.

Ammonia Tanks

ID	AT5-8-1-P2	AT5-8-1-P3	AT5-8-1-P4	AT5-8-1-P5	AT5-8-1-P6	AT5-37-5-P1	AT5-37-5-P2	AT5-37-5-P3
Group	HSR	HSR	HSR	HSR	HSR	HSR	HSR	HSR
distance to rim (µm)	50	100	150	200	250	1	50	100
wt%:								
SiO2	66.2	66.2	66.4	66.4	66.5	67.0	66.4	66.5
TiO2	0.011	0.013	0.002	0.013	0.000	0.000	0.000	0.012
Al2O3	19.1	19.1	18.9	18.9	19.0	19.4	19.2	19.1
FeO	0.15	0.21	0.14	0.17	0.14	0.10	0.21	0.17
MgO	0.003	0.000	0.005	0.000	0.006	0.000	0.003	0.007
CaO	0.32	0.29	0.33	0.30	0.35	0.33	0.34	0.31
Na2O	5.68	5.76	5.91	5.86	5.79	4.80	5.43	5.48
K2O	8.54	8.40	8.33	8.35	8.16	8.36	8.29	8.46
ppm:								
Ba	49.3	50.7	60.9	69.0	59.7	54.9	54.4	58.8
Sr	14.3	15.2	13.3	15.2	16.1	14.0	15.7	19.0
Rb	64.4	61.5	55.7	79.8	65.1	71.8	60.7	64.8

APPENDIX 2. Continued.

Ammonia Tanks

ID	AT5-37-5-P4	AT5-37-5-P5	AT5-37-5-P6	AT5-37-5-P7	AT5-37-5-P8	AT5-37-5-P9	AT5-37-5-P10	AT5-37-9-1
Group	HSR	HSR	HSR	HSR	HSR	HSR	HSR	HSR
distance to rim (μm)	150	200	250	300	350	400	450	1
wt%:								
SiO2	66.3	66.2	66.4	66.4	66.3	66.2	66.3	66.8
TiO2	0.000	0.000	0.000	0.027	0.026	0.004	0.000	0.000
Al2O3	19.1	19.2	19.0	19.1	19.0	19.0	19.0	19.6
FeO	0.17	0.20	0.20	0.15	0.17	0.20	0.18	0.23
MgO	0.009	0.000	0.000	0.000	0.003	0.004	0.005	0.015
CaO	0.36	0.32	0.31	0.36	0.36	0.41	0.40	0.47
Na2O	5.76	5.68	5.77	5.90	5.82	5.91	6.01	5.37
K2O	8.34	8.47	8.23	8.05	8.36	8.23	8.12	7.56
ppm:								
Ba	84.4	125	169	141	127	133	143	75.7
Sr	20.7	22.4	31.8	29.8	30.7	34.6	38.4	22.0
Rb	69.5	66.2	96.4	64.2	81.5	61.8	65.1	74.0

APPENDIX 2. Continued.

Ammonia Tanks

ID	AT5-37-9-P2	AT5-37-9-P3	AT5-37-9-P4	AT5-37-9-P5	AT5-37-9-P6	AT5-37-9-P7	AT5-37-9-P8	AT5-37-9-P9
Group	HSR	HSR	HSR	HSR	HSR	HSR	HSR	HSR
distance to rim (μm)	50	100	150	200	250	300	350	400
wt%:								
SiO2	66.5	66.3	66.3	66.0	66.1	66.2	66.3	66.4
TiO2	0.006	0.026	0.019	0.000	0.010	0.000	0.004	0.011
Al2O3	20.1	19.8	19.1	19.1	19.3	19.3	19.2	19.1
FeO	0.18	0.19	0.18	0.15	0.15	0.12	0.23	0.17
MgO	0.000	0.000	0.000	0.002	0.000	0.000	0.002	0.000
CaO	1.03	0.94	0.38	0.38	0.39	0.36	0.37	0.35
Na2O	7.97	7.88	5.90	6.29	6.23	5.94	6.19	6.02
K2O	4.24	4.90	8.12	8.05	7.81	8.12	7.59	7.91
ppm:								
Ba	77.0	75.5	54.3	79.5	95.5	113	132	136
Sr	19.6	18.4	19.9	17.7	18.2	18.6	17.9	20.1
Rb	55.6	59.0	59.2	58.1	57.4	64.1	64.3	54.2

APPENDIX 2. Continued.

Ammonia Tanks

ID	AT5-37-9-P10	AT5-37-6-P1	AT5-37-6-P2	AT5-37-6-P3	AT5-37-6-P4	AT5-37-6-P5	AT5-37-6-P6	AT5-37-6-P7
Group	HSR	HSR	HSR	HSR	HSR	HSR	HSR	HSR
distance to rim (µm)	450	1	50	100	150	200	250	300
wt%:								
SiO2	66.1	65.1	65.3	65.8	66.2	66.1	66.0	66.0
TiO2	0.003	0.000	0.000	0.000	0.002	0.027	0.005	0.001
Al2O3	19.0	18.9	19.7	19.5	19.8	20.0	20.0	20.1
FeO	0.22	0.25	0.19	0.19	0.15	0.25	0.18	0.17
MgO	0.007	0.000	0.000	0.000	0.000	0.000	0.001	0.013
CaO	0.31	1.00	1.08	0.96	0.97	1.17	1.21	1.19
Na2O	6.10	9.79	9.14	7.84	8.21	8.17	8.31	8.25
K2O	8.19	4.89	4.47	5.61	4.65	4.25	4.24	4.27
ppm:								
Ba	121	27.6	31.3	32.4	23.5	29.0	33.0	38.0
Sr	18.4	18.7	23.6	25.2	23.7	24.5	26.9	26.2
Rb	56.5	41.4	49.6	71.7	29.3	43.3	0.00	18.3

APPENDIX 2. Continued.

Ammonia Tanks

ID	AT5-37-6-P8	AT5-29-3-P1	AT5-29-3-P2	AT5-29-3-P3	AT5-29-3-P4	AT5-37-4-P1	AT5-37-4-P2	AT5-37-4-P3
Group	HSR	HSR	HSR	HSR	HSR	HSR	HSR	HSR
distance to rim (μm)	350	1	50	100	150	1	50	100
wt%:								
SiO2	65.9	65.5	65.8	66.2	66.1	67.0	66.3	66.3
TiO2	0.008	0.005	0.000	0.000	0.045	0.017	0.021	0.016
Al2O3	20.1	19.8	20.0	20.0	19.6	19.2	18.9	19.0
FeO	0.20	0.20	0.21	0.14	0.18	0.18	0.11	0.17
MgO	0.007	0.005	0.000	0.000	0.002	0.000	0.007	0.000
CaO	1.18	1.11	1.31	0.98	0.85	0.26	0.28	0.28
Na2O	8.21	9.07	8.57	7.95	7.46	4.56	5.33	5.53
K2O	4.36	4.18	4.12	4.77	5.68	8.78	8.89	8.70
ppm:								
Ba	42.7	31.4	31.1	40.5	39.9	301	375	442
Sr	28.6	21.7	20.5	18.3	18.0	38.2	41.2	44.5
Rb	54.0	21.0	27.0	46.6	40.1	94.8	91.4	78.1

APPENDIX 2. Continued.

Ammonia Tanks

ID	AT5-37-4-P4	AT5-37-4-P5	AT5-37-4-P6	AT5-37-4-P7	AT5-37-4-P8	AT5-37-4-P9	AT5-37-10 P1	AT5-37-10 P2
Group	HSR	HSR	HSR	HSR	HSR	HSR	HSR	HSR
distance to rim (μm)	150	200	250	300	350	400	1	50
wt%:								
SiO2	66.3	66.1	66.1	66.1	66.1	66.0	62.7	66.3
TiO2	0.000	0.000	0.014	0.016	0.005	0.000	0.035	0.012
Al2O3	18.9	19.1	19.1	19.2	19.2	19.2	24.1	20.0
FeO	0.20	0.18	0.16	0.16	0.23	0.18	0.191	0.211
MgO	0.000	0.001	0.000	0.000	0.002	0.014	0.020	0.007
CaO	0.26	0.33	0.39	0.34	0.33	0.34	1.01	1.26
Na2O	5.54	5.76	5.90	5.89	5.82	5.89	7.80	8.33
K2O	8.83	8.36	8.18	8.34	8.23	8.25	4.15	3.80
ppm:								
Ba	525	669	704	708	709	655	32.6	61.0
Sr	46.1	54.6	54.8	44.0	43.7	45.2	25.7	19.5
Rb	60.5	61.4	56.0	71.1	72.0	58.9	24.9	39.5

APPENDIX 2. Continued.

Ammonia Tanks

ID	AT5-37-10 P3	AT5-37-10 P4	AT5-37-10 P5	AT5-37-10 P6	AT5-37-10 P7	AT5-37-10 P8	AT5-37-10 P9	AT5-37-1core
Group	HSR	HSR	HSR	HSR	HSR	HSR	HSR	HSR
distance to rim (µm)	100	150	200	250	300	350	400	500
wt%:								
SiO2	66.3	66.7	66.6	66.3	66.6	66.7	66.6	66.8
TiO2	0.000	0.001	0.000	0.037	0.000	0.000	0.008	0.027
Al2O3	19.0	18.7	18.6	19.2	19.1	19.0	19.0	19.6
FeO	0.138	0.189	0.193	0.181	0.137	0.154	0.206	0.179
MgO	0.000	0.007	0.000	0.000	0.006	0.005	0.000	0.000
CaO	0.426	0.397	0.294	0.421	0.380	0.326	0.305	1.048
Na2O	5.96	5.78	4.89	5.75	5.72	5.65	5.51	7.50
K2O	8.14	8.09	9.42	7.98	8.04	8.18	8.35	4.87
ppm:								
Ba	67.2	74.2	89.6	118	125	121	102	25.8
Sr	19.2	18.9	22.1	21.5	24.4	22.0	20.1	21.4
Rb	55.0	71.7	51.9	66.2	57.9	61.7	70.2	17.9

APPENDIX 2. Continued.

Ammonia Tanks

ID	AT5-8-3-P1	AT5-8-3-P2	AT5-8-3-P3	AT5-8-3-P4	AT5-8-3-P5	AT5-8-3-P6	AT5-8-3-P7	AT5-8-3-P8
Group	HSR	HSR	HSR	HSR	HSR	HSR	HSR	HSR
distance to rim (μm)	1	50	100	150	200	250	300	350
wt%:								
SiO2	66.2	66.4	66.3	66.4	66.5	66.4	66.4	66.4
TiO2	0.000	0.019	0.000	0.010	0.000	0.003	0.012	0.000
Al2O3	19.2	19.0	19.2	19.0	18.9	19.1	19.1	19.0
FeO	0.165	0.159	0.163	0.159	0.180	0.162	0.140	0.180
MgO	0.001	0.000	0.011	0.000	0.000	0.000	0.002	0.001
CaO	0.400	0.318	0.318	0.299	0.288	0.409	0.307	0.339
Na2O	5.53	5.51	5.49	5.43	5.51	5.56	5.54	5.68
K2O	8.55	8.56	8.55	8.68	8.58	8.33	8.51	8.41
ppm:								
Ba	61.5	55.4	53.1	49.4	47.2	55.4	57.8	53.4
Sr	18.6	14.8	20.0	17.3	16.1	19.0	20.8	18.3
Rb	81.6	77.2	81.2	68.3	81.3	78.5	77.4	76.5

APPENDIX 2. Continued.

Ammonia Tanks

ID	AT5-8-3-P9	AT5-8-3-P10	AT5-25-2-P1	AT5-25-2-P2	AT5-25-2-P3	AT5-25-2-P4	AT5-25-2-P5	AT5-25-2-P6	AT5-25-2-P7
Group	HSR	HSR	HSR	HSR	HSR	HSR	HSR	HSR	HSR
distance to rim (μm)	400	450	1	50	100	150	200	250	300
wt%:									
SiO2	66.2	66.3	66.5	66.2	66.3	66.3	66.0	66.2	65.7
TiO2	0.004	0.002	0.022	0.002	0.010	0.009	0.008	0.000	0.014
Al2O3	19.2	19.4	19.0	19.1	18.9	19.0	19.2	19.1	19.5
FeO	0.196	0.160	0.162	0.172	0.135	0.189	0.219	0.178	0.169
MgO	0.000	0.000	0.000	0.001	0.000	0.000	0.008	0.000	0.010
CaO	0.353	0.346	0.302	0.296	0.347	0.328	0.355	0.362	0.379
Na2O	5.67	5.70	5.58	5.80	5.73	5.71	5.72	5.76	5.81
K2O	8.39	8.08	8.42	8.39	8.62	8.42	8.40	8.48	8.42
ppm:									
Ba	70.1	72.8	49.9	46.0	47.3	51.0	53.5	60.0	68.1
Sr	21.0	17.9	19.4	15.6	16.8	16.3	18.6	17.1	18.0
Rb	80.4	71.1	76.6	70.7	66.4	60.0	63.7	63.4	75.7

APPENDIX 2. Continued.

Rainier Mesa

ID	99TM4-3-P1	99TM4-3-P2	99TM4-3-P3	99TM4-3-P4	99TM4-3-P5	99TM4-3-P6	99TM4-3-P7	99TM4-3-P8
GROUP	HSR-1	HSR-1	HSR-1	HSR-1	HSR-1	HSR-1	HSR-1	HSR-1
distance to rim (μm)	1	50	100	150	200	250	300	350
wt %:								
SiO2	65.9	66.0	65.9	65.8	65.94	66.0	65.8	66.2
TiO2	0	0	0.01	0.01	0.01	0	0.01	0.010
Al2O3	19.1	18.9	18.9	19.0	18.8	18.5	18.6	18.1
FeO	0.080	0.080	0.050	0.100	0.060	0.070	0.090	0.070
MgO	0	0	0	0	0.010	0	0.010	0
CaO	0.200	0.140	0.180	0.160	0.120	0.140	0.150	0.150
Na2O	5.47	4.71	4.56	4.52	4.50	4.60	4.53	4.45
K2O	9.19	10.2	10.4	10.4	10.5	10.7	10.8	11.0
ppm:								
Ba	67.8	59.0	57.2	34.2	28.8	30.4	31.9	28.1
Sr	36.0	25.9	26.0	25.4	25.9	20.8	35.8	33.4
Rb	152	125	124	125	119	113	105	102

APPENDIX 2. Continued.

Rainier Mesa

ID	99TM4-3-P9	99TM4-3-P10	RM18-5-3-P1	RM18-5-3-P2	RM18-5-3-P3	RM18-5-3-P4	RM18-5-3-P5	RM18-5-5 P1
GROUP	HSR-1	HSR-1	HSR-1	HSR-1	HSR-1	HSR-1	HSR-1	HSR-1
distance to rim (μm):	400	450	1	50	100	150	200	1
wt %:								
SiO2	66.1	66.0	66.0	66.2	66.1	66.2	65.9	65.3
TiO2	0	0.010	0.010	0	0	0.010	0.010	0
Al2O3	18.0	18.3	19.2	19.0	18.9	18.7	18.8	21.2
FeO	0.060	0.070	0.090	0.070	0.070	0.090	0.100	0.100
MgO	0.010	0	0	0.010	0	0	0	0
CaO	0.140	0.140	0.170	0.180	0.140	0.160	0.170	2.83
Na2O	4.29	4.04	4.33	3.98	4.03	3.98	3.95	8.98
K2O	11.4	11.4	10.17	10.53	10.77	10.8	11.04	1.53
ppm:								
Ba	27.3	33.8	77.0	75.7	71.1	62.8	70.1	12.1
Sr	29.9	29.8	33.4	30.3	24.9	23.6	26.7	23.6
Rb	107	97.6	128	122	111	114	124	17.5

APPENDIX 2. Continued.

Rainier Mesa

ID	RM18-5-5 P2	RM18-5-5 P3	RM18-6-7-P1	RM18-6-7-P2	RM18-6-7-P3	RM18-6-7-P4	RM18-6-7-P5	RM26-20-6-P1
GROUP	HSR-1	HSR-1	HSR-1	HSR-1	HSR-1	HSR-1	HSR-1	HSR-1
distance to rim (μm):	50	100	1	50	100	150	200	1
wt %:								
SiO2	65.1	65.4	64.9	65.7	65.8	66.2	66.0	66.0
TiO2	0.010	0	0.010	0	0.020	0	0	0.020
Al2O3	21.4	21.2	18.8	18.8	18.8	18.7	19.1	18.8
FeO	0.140	0.130	0.110	0.090	0.080	0.100	0.080	0.080
MgO	0	0	0	0	0.010	0	0	0
CaO	2.72	2.47	0.180	0.210	0.200	0.200	0.190	0.150
Na2O	9.18	9.26	4.53	4.36	4.18	4.05	4.13	5.25
K2O	1.46	1.54	11.5	10.9	10.9	10.7	10.5	9.67
ppm:								
Ba	12.9	22.5	80.5	76.9	75.9	69.3	65.5	99.8
Sr	27.0	21.8	21.9	25.37	24.4	27.5	23.7	30.5
Rb	11.1	10.0	99.3	114	126	129	123	103

APPENDIX 2. Continued.

Rainier Mesa

ID	RM26-20-6-P2	RM26-20-6-P3	RM26-20-6-P4	RM26-20-6-P5	R18-2-4-P1	R18-2-4-P2	R18-2-4-P3	R18-2-4-P4
GROUP	HSR-1	HSR-1	HSR-1	HSR-1	HSR-2	HSR-2	HSR-2	HSR-2
distance to rim (μm):	50	100	150	200	1	50	100	150
wt %:								
SiO2	65.8	65.8	65.9	66.2	65.7	65.7	65.9	65.5
TiO2	0.020	0	0	0.020	0.010	0.010	0.010	0.010
Al2O3	18.8	18.6	18.5	18.9	18.7	18.8	19.2	18.8
FeO	0.090	0.080	0.080	0.070	0.090	0.080	0.110	0.090
MgO	0.010	0.010	0	0	0	0.010	0	0.010
CaO	0.150	0.170	0.170	0.170	0.190	0.180	0.150	0.200
Na2O	4.64	4.54	4.24	3.68	3.78	3.75	3.63	3.77
K2O	10.4	10.8	11.2	11.0	11.5	11.5	11.0	11.6
ppm:								
Ba	73.8	58.4	53.6	67.0	57.2	52.3	71.8	59.7
Sr	28.1	26.6	24.2	25.7	18.6	19.3	24.2	20.8
Rb	113	108	112	112	146	151	159	128

APPENDIX 2. Continued.

Rainier Mesa

ID	R18-2-4-P5	R18-2-4-P6	R18-2-4-P7	R18-2-4-P8	R18-2-4-P9	R18-2-4-P10	R18-2-6-P1	R18-2-6-P2
GROUP	HSR-2	HSR-2	HSR-2	HSR-2	HSR-2	HSR-2	HSR-2	HSR-2
distance to rim (μm):	200	250	300	350	400	450	1	50
wt %:								
SiO2	65.7	65.6	65.6	65.5	65.3	65.6	65.3	65.3
TiO2	0.010	0.010	0.010	0	0.01	0.02	0	0.01
Al2O3	18.8	18.8	18.8	18.8	18.9	18.7	18.5	19.0
FeO	0.080	0.060	0.060	0.100	0.090	0.140	0.100	0.090
MgO	0.010	0	0	0	0	0	0	0
CaO	0.200	0.220	0.200	0.190	0.190	0.260	0.190	0.240
Na2O	3.3	3.77	3.76	3.75	3.61	2.86	3.33	3.8
K2O	11.9	11.6	11.5	11.6	11.9	12.5	12.6	11.5
ppm:								
Ba	53.8	69.4	71.6	72.1	65.2	243	224	217
Sr	19.1	22.6	24.6	30.6	37.469	50.7	75.3	74.0
Rb	123	134	127	121	164	97.5	109	112

APPENDIX 2. Continued.

Rainier Mesa

ID	R18-2-6-P3	R18-2-6-P4	R18-2-6-P5	R18-2-6-P6	R18-2-6-P7	R18-2-6-P8	R18-2-6-P9	R18-2-6-P10
GROUP	HSR-2	HSR-2	HSR-2	HSR-2	HSR-2	HSR-2	HSR-2	HSR-2
distance to rim (μm):	100	150	200	250	300	350	400	450
wt %:								
SiO2	65.4	65.3	65.4	65.5	65.4	65.5	65.4	65.2
TiO2	0.01	0	0.02	0	0.01	0.01	0.010	0
Al2O3	18.9	19.0	19.0	18.8	18.9	18.9	18.9	19.1
FeO	0.100	0.100	0.080	0.090	0.070	0.090	0.07	0.120
MgO	0	0	0	0.01	0		0	0
CaO	0.220	0.210	0.210	0.200	0.200	0.250	0.2	0.210
Na2O	3.82	3.88	3.82	3.79	3.78	3.85	3.86	3.85
K2O	11.5	11.5	11.4	11.6	11.6	11.4	11.6	11.4
ppm:								
Ba	117	228	95.2	77.4	75.8	76.8	72.815	70.7
Sr	65.6	60.2	64.8	44.8	45.0	42.7	45.51	39.3
Rb	118	111	106	130	130	118	145	116

APPENDIX 2. Continued.

Rainier Mesa

ID	R18-2-6-P11	R18-2-6-P12	R18-2-19-P1	R18-2-19-P2	R18-2-19-P3	R18-2-19-P4	R18-2-19-P5	R18-2-19-P6
GROUP	HSR-2	HSR-2	HSR-2	HSR-2	HSR-2	HSR-2	HSR-2	HSR-2
distance to rim (μm):	500	550	1	50	100	150	200	250
wt %:								
SiO2	65.3	65.4	52.3	65.4	65.6	65.5	65.7	65.7
TiO2	0.010	0.010	0	0.010	0	0	0	0.010
Al2O3	19.0	19.3	36.1	19.0	18.9	18.9	18.9	18.9
FeO	0.070	0.110	0.070	0.080	0.070	0.080	0.080	0.050
MgO	0.010	0	0.090	0.010	0	0	0	0
CaO	0.210	0.210	0.390	0.200	0.200	0.220	0.210	0.220
Na2O	3.98	4.77	2.91	3.89	3.90	3.94	3.93	3.84
K2O	11.4	10.2	8.12	11.4	11.3	11.4	11.2	11.3
ppm:								
Ba	78.9	73.8	990	318	80.4	56.0	76.3	63.4
Sr	39.9	43.2	162	83.0	29.4	26.5	29.0	27.0
Rb	127	132	238	134	152	170	162	171

APPENDIX 2. Continued.

Rainier Mesa

ID	R18-2-19-P7	R18-2-26-P1	R18-2-26-P2	R18-2-26-P3	R18-2-26-P4	R18-2-26-P5	R18-2-26-P6	R18-2-26-P7
GROUP	HSR-2	HSR-2	HSR-2	HSR-2	HSR-2	HSR-2	HSR-2	HSR-2
distance to rim (μm):	300	1	50	100	150	200	250	300
wt %:								
SiO2	65.2	65.8	65.5	65.5	65.6	65.48	65.4	65.5
TiO2	0	0	0.010	0	0.010	0	0	0.01
Al2O3	19.0	19.1	18.9	18.9	18.7	19.0	19.0	18.9
FeO	0.070	0.090	0.100	0.110	0.110	0.09	0.11	0.08
MgO	0.010	0.010		0	0	0	0.01	0
CaO	0.210	0.150	0.220	0.210	0.190	0.22	0.23	0.23
Na2O	3.89	4.83	3.86	3.78	3.73	3.84	3.79	3.85
K2O	11.6	9.98	11.3	11.5	11.6	11.3	11.4	11.5
ppm:								
Ba	58.0	527	528	556	441	296	190	135
Sr	23.4	82.7	75.6	74.9	75.9	62.0	58.3	61.4
Rb	169	90.7	106	104	123	97.6	104	112

APPENDIX 2. Continued.

Rainier Mesa

ID	R18-2-26-P8	R18-2-26-P9	R18-2-26-P10	R18-2-64-P1	R18-2-64-P2	R18-2-64-P3	R18-2-64-P4	R18-2-64-P5
GROUP	HSR-2	HSR-2	HSR-2	HSR-2	HSR-2	HSR-2	HSR-2	HSR-2
distance to rim (μm):	350	400	450	550	500	450	400	350
wt %:								
SiO2	65.4	65.9	65.7	65.3	65.6	65.5	65.4	65.4
TiO2	0.01	0	0	0.01	0.02	0.01	0.02	0.02
Al2O3	18.9	18.7	18.9	19.0	18.9	19.0	18.9	19.0
FeO	0.09	0.07	0.05	0.07	0.07	0.09	0.1	0.09
MgO	0	0.01	0		0.01	0.01	0	
CaO	0.23	0.25	0.26	0.24	0.21	0.21	0.23	0.19
Na2O	3.83	3.88	3.85	3.67	3.77	3.83	3.85	3.81
K2O	11.4	11.3	11.2	11.7	11.5	11.3	11.4	11.5
ppm:								
Ba	111	116	113	82.4	80.3	89.1	78.5	84.2
Sr	63.7	61.9	56.3	30.9	26.9	29.8	22.1	25.8
Rb	110	97.6	103	162	185	160	167	166

APPENDIX 2. Continued.

Rainier Mesa

ID	R18-2-64-P6	R18-2-64-P7	R18-2-64-P8	R18-2-64-P9	R18-2-64-P10	R18-2-64-P11	RM23-7-1-P1	RM23-7-1-P2
GROUP	HSR-2	HSR-2	HSR-2	HSR-2	HSR-2	HSR-2	HSR-2	HSR-2
distance to rim (μm):	300	250	200	150	100	50	1	50
wt %:								
SiO2	65.4	65.5	65.6	65.3	65.3	65.5	64.9	65.1
TiO2	0	0.01	0.01	0.01	0.01	0	0.02	0.02
Al2O3	18.9	19.0	19.0	19.0	19.1	19.1	19.3	18.9
FeO	0.08	0.1	0.07	0.12	0.07	0.07	0.19	0.17
MgO	0.01			0	0	0	0	0
CaO	0.22	0.18	0.20	0.20	0.19	0.20	0.48	0.46
Na2O	3.79	3.80	3.84	3.80	3.83	3.85	4.55	4.48
K2O	11.6	11.4	11.3	11.5	11.5	11.3	9.90	10.2
ppm:								
Ba	79.8	76.1	77.9	81.3	75.8		4368	4427
Sr	23.2	25.8	24.7	26.1	25.4		633	667
Rb	182	171	174	178	166		40.7	36.8

APPENDIX 2. Continued.

Rainier Mesa

ID	RM23-7-1-P3	RM23-7-1-P4	RM26-23-1-P1	RM26-23-1-P2	RM26-23-1-P3	RM26-23-1-P4	RM26-23-1-P5	RM26-23-1-P6
GROUP	HSR-2	HSR-2	HSR-2	HSR-2	HSR-2	HSR-2	HSR-2	HSR-2
distance to rim (μm):	100	150	1	50	100	150	200	250
wt %:								
SiO2	65.3	62.6	63.1	63.6	63.1	64.0	63.5	63.7
TiO2	0	0.04	0.02	0.01	0.01	0.01	0.01	0.03
Al2O3	19.1	23.5	22.4	22.0	22.7	22.2	22.7	22.8
FeO	0.18	0.29	0.18	0.18	0.18	0.21	0.2	0.2
MgO	0	0	0.01	0	0.01	0.02	0	0
CaO	0.51	4.87	3.92	3.99	4.11	3.67	3.97	4.06
Na2O	4.32	7.02	9.06	8.72	8.65	8.52	8.29	7.89
K2O	9.99	1.59	1.32	1.42	1.30	1.41	1.39	1.33
ppm:								
Ba	4099	615	26.0	27.5	32.7	29.1	31.0	35.6
Sr	700	878	121	126	133	138	135	141
Rb	39.5	4.71	4.39	3.96	3.67	4.09	2.79	5.31

APPENDIX 2. Continued.

Rainier Mesa

ID	RM18-16-2 P1	RM18-16-2 P2	RM18-16-2 P3	RM18-16-2 P4	RM18-16-2 P5	RM18-16-2 P6	RM18-16-2 P7	RM18-16-2 P8
GROUP	HSR-2	HSR-2	HSR-2	HSR-2	HSR-2	HSR-2	HSR-2	HSR-2
distance to rim (μm):	1	50	100	150	200	250	300	350
wt %:								
SiO2	65.7	65.8	65.3	65.8	65.9	65.8	65.9	66.1
TiO2	0.017	0	0.006	0.016	0	0.018	0.009	0.001
Al2O3	19.3	19.0	19.6	18.9	18.7	19.0	18.9	18.9
FeO	0.08	0.058	0.086	0.117	0.098	0.097	0.087	0.081
MgO	0	0.013	0.002	0	0	0.003	0	0
CaO	0.229	0.221	0.215	0.267	0.193	0.212	0.188	0.212
Na2O	3.29	3.67	3.75	3.89	3.69	3.69	3.72	3.74
K2O	11.4	11.3	11.1	11.0	11.3	11.2	11.2	11.0
ppm:								
Ba	166.3	152	164	198	153	135	120	116
Sr	79.8	77.3	77.9	69.0	67.1	72.1	67.9	66.6
Rb	134	110	112	110	114	129	110	103

APPENDIX 2. Continued.

Rainier Mesa

ID	RM18-16-2 P9	RM18-16-12 P1	RM18-16-12 P2	RM18-16-12 P3	RM18-16-12 P4	RM18-16-12 P5	RM18-16-12 P6	RM18-16-12 P7
GROUP	HSR-2	HSR-2	HSR-2	HSR-2	HSR-2	HSR-2	HSR-2	HSR-2
distance to rim (μm):	400	1	50	100	150	200	250	300
wt %:								
SiO2	65.6	66.0	65.7	65.9	66.1	66.0	65.8	65.9
TiO2	0.004	0	0.009	0.005	0.008	0	0.001	0.002
Al2O3	19.2	18.9	18.9	18.9	18.7	18.8	18.9	18.9
FeO	0.103	0.081	0.101	0.066	0.089	0.09	0.077	0.067
MgO	0.006	0.001	0.001	0.008	0.007	0	0	0.005
CaO	0.199	0.228	0.263	0.225	0.228	0.227	0.264	0.265
Na2O	3.74	3.54	3.74	3.80	3.76	3.72	3.82	3.85
K2O	11.2	11.1	11.1	11.1	11.1	11.1	11.1	11.0
ppm:								
Ba	111	385	344	261	148	74.9	64.9	72.0
Sr	64.2	99.8	93.6	78.2	66.6	58.0	49.4	43.8
Rb	97.6	73.4	84.8	94.4	99.3	84.9	80.0	99.9

APPENDIX 2. Continued.

Rainier Mesa

ID	RM18-16-11 P1	RM18-16-11 P2	RM18-16-11 P3	RM18-16-11 P4	RM18-16-11 P5	RM18-16-11 P6	RM18-16-11 P7	RM18-16-11 P8
GROUP	HSR-2	HSR-2	HSR-2	HSR-2	HSR-2	HSR-2	HSR-2	HSR-2
distance to rim (μm):	1	50	100	150	200	250	300	350
wt %:								
SiO2	65.8	65.8	65.6	65.7	65.7	65.7	65.6	65.7
TiO2	0.02	0	0	0	0.01	0.03	0	0
Al2O3	19.0	19.0	18.9	18.9	19.0	18.7	19.0	19.0
FeO	0.044	0.046	0.085	0.127	0.134	0.062	0.065	0.064
MgO	0.002	0	0	0.001	0.002	0.004	0.004	0.008
CaO	0.185	0.245	0.268	0.291	0.222	0.25	0.243	0.237
Na2O	3.77	3.82	3.91	3.96	3.90	3.88	3.95	3.99
K2O	11.2	11.1	11.2	11.0	11.1	11.3	11.1	11.0
ppm:								
Ba	76.2	73.8	72.2	77.3	77.5	83.9	79.0	80.4
Sr	94.4	58.6	59.6	73.0	77.4	89.0	85.6	90.1
Rb	84.6	89.6	86.6	85.6	104	71.7	73.4	78.1

APPENDIX 2. Continued.

Rainier Mesa

ID	RM18-16-11 P9	RM18-16-11 P10	RM8-42-3 P1	RM8-42-3 P2	RM8-42-3 P3	RM8-42-3 P4	RM8-42-3 P5	RM8-42-3 P6
GROUP	HSR-2	HSR-2	HSR-3	HSR-3	HSR-3	HSR-3	HSR-3	HSR-3
distance to rim (μm):	400	450	1	50	100	150	200	250
wt %:								
SiO2	65.9	65.6	66.1	65.8	65.6	65.7	65.5	65.8
TiO2	0.01	0.02	0.027	0.015	0.01	0	0.01	0.016
Al2O3	18.7	19.1	18.9	19.1	19.0	19.1	19.1	18.9
FeO	0.088	0.065	0.157	0.114	0.115	0.126	0.129	0.128
MgO	0.002	0.003	0	0	0.012	0	0.004	0.009
CaO	0.224	0.179	0.283	0.315	0.31	0.322	0.345	0.343
Na2O	3.87	3.93	3.94	4.11	4.22	4.24	4.28	4.29
K2O	11.1	11.2	10.5	10.3	10.2	10.1	10.2	10.4
ppm:								
Ba	81.3	104	761	2551	4103	2992	1668	635
Sr	74.3	83.7	276	316.74	365	324	221	176
Rb	70.2	79.6	54.5	47.6	54.3	50.6	54.8	50.4

APPENDIX 2. Continued.

Rainier Mesa

ID	RM8-42-3 P7	RM8-42-3 P8	RM8-42-1 P1	RM8-42-1 P2	RM8-42-1 P3	RM8-42-1 P4	RM8-42-1 P5	RM8-42-1 P6
GROUP	HSR-3	HSR-3	HSR-3	HSR-3	HSR-3	HSR-3	HSR-3	HSR-3
distance to rim (μm):	300	350	1	50	100	150	200	250
wt %:								
SiO2	65.6	65.6	65.5	65.8	65.9	66.1	65.8	65.8
TiO2	0.014	0.01	0.021	0.009	0.014	0.021	0	0.025
Al2O3	19.0	19.0	18.6	18.7	19.1	18.8	19.0	19.0
FeO	0.157	0.108	0.173	0.145	0.167	0.115	0.148	0.105
MgO	0.001	0.001	0.001	0	0.008	0	0.001	0.001
CaO	0.349	0.296	0.43	0.351	0.372	0.387	0.411	0.379
Na2O	4.26	4.18	4.40	4.37	4.33	4.30	4.27	4.30
K2O	10.5	10.7	10.8	10.4	9.99	10.1	10.2	10.3
ppm:								
Ba	463	536	1207	1217	1235	1160	1149	1219
Sr	167	178	188	190	198	196	204	196
Rb	50.9	45.6	51.7	49.4	51.5	57.3	55.3	55.6

APPENDIX 2. Continued.

Rainier Mesa

ID	RM8-42-1 P7	RM8-42-1 P8	RM8-42-1 P9	RM8-42-1 P10	RM8-42-1 P11	RM8-42-1 P12	RM8-42-1 P13	RM8-42-1 P14
GROUP	HSR-3	HSR-3	HSR-3	HSR-3	HSR-3	HSR-3	HSR-3	HSR-3
distance to rim (μm):	300	350	400	450	500	550	600	650
wt %:								
SiO2	65.5	65.8	66.0	65.7	65.9	66.1	65.9	65.9
TiO2	0.034	0.021	0	0	0.002	0.009	0.003	0.003
Al2O3	19.2	19.1	18.8	19.0	19.0	18.8	19.1	19.0
FeO	0.149	0.111	0.114	0.146	0.156	0.125	0.147	0.120
MgO	0.015	0.006	0	0	0	0	0.01	0.002
CaO	0.391	0.348	0.363	0.369	0.326	0.335	0.362	0.344
Na2O	4.24	4.28	4.36	4.27	4.22	4.23	4.24	4.27
K2O	10.3	10.2	10.3	10.3	10.2	10.2	10.0	10.2
ppm:								
Ba	1251	1195	1256	1221	1296	1272	1076	1060
Sr	182	183	194	181	181	179	183	185
Rb	55.1	45.6	46.3	50.3	55.0	48.8	52.8	52.1

APPENDIX 2. Continued.

Rainier Mesa

ID	RM8-42-1core	RM8-42-11 P1	RM8-42-11 P2	RM8-42-11 P3	RM8-42-11 P4	RM8-42-11 P5	RM8-42-11 P6	RM8-42-11 P7
GROUP	HSR-3	HSR-3	HSR-3	HSR-3	HSR-3	HSR-3	HSR-3	HSR-3
distance to rim (μm):	700	1	50	100	150	200	250	300
wt %:								
SiO2	65.9	65.5	65.7	65.6	66.0	65.9	65.5	65.9
TiO2	0.005	0	0.022	0.008	0	0.019	0.018	0
Al2O3	18.9	19.5	19.1	19.1	18.8	19.1	18.9	19.0
FeO	0.154	0.118	0.060	0.112	0.088	0.099	0.101	0.119
MgO	0.012	0	0.004	0	0	0	0.013	0
CaO	0.318	0.276	0.254	0.255	0.3	0.312	0.324	0.335
Na2O	4.20	3.79	3.99	4.24	4.12	4.28	4.35	4.23
K2O	10.3	10.7	10.7	10.6	10.7	10.26	10.8	10.3
ppm:								
Ba	1221	536	485	456	499	499	392	464
Sr	185	184	171	173	175	178	136	169
Rb	57.3	80.3	191	57.3	79.2	76.6	56.7	56.8

APPENDIX 2. Continued.

Rainier Mesa

ID	RM8-42-11 P8	RM8-42-11 P9	RM8-42-11 P10	RM8-42-5core	RM23-13-3-P1	RM23-13-3-P2	RM23-13-3-P3	RM23-13-3-P4
GROUP	HSR-3	HSR-3	HSR-3	HSR-3	LS	LS	LS	LS
distance to rim (μm):	350	400	450	500	1	50	100	150
wt %:								
SiO2	65.8	66.0	65.9	65.8	58.8	62.2	63.1	63.6
TiO2	0	0	0.004	0.013	0.035	0	0	0.025
Al2O3	19.0	18.8	18.9	19.1	19.7	19.4	19.7	19.7
FeO	0.069	0.109	0.105	0.022	0.32	0.22	0.18	0.19
MgO	0.009	0	0.001	0.003	0	0	0	0.007
CaO	0.302	0.297	0.31	0.306	0.690	0.640	0.620	0.600
Na2O	4.26	4.27	4.31	4.33	4.38	4.23	4.13	4.01
K2O	10.4	10.5	10.4	10.4	13.4	11.4	10.4	10.4
ppm:								
Ba	497	456	464	134	7631	9917	9303	10903
Sr	181	175	182	113	643	857	915	952
Rb	60.8	66.9	59.2	63.1	22.3	31.1	32.3	30.5

APPENDIX 2. Continued.

Rainier Mesa

ID	RM23-13-3-P5	RM23-13-3-P6	RM23-13-3-P7
GROUP	LS	LS	LS
distance to rim (μm):	200	250	300
wt %:			
SiO2	63.8	64.0	64.2
TiO2	0.023	0	0.051
Al2O3	19.6	19.6	19.5
FeO	0.19	0.18	0.16
MgO	0	0.001	0
CaO	0.620	0.470	0.540
Na2O	4.15	4.15	4.40
K2O	9.93	10.2	9.90
ppm:			
Ba	11308	7747	6927
Sr	1041	913	913
Rb	31.3	33.9	36.4

APPENDIX 3

APPENDIX 3. Major and trace element composition of melt inclusions. HSR = high-silica rhyolite; INT = intermediate (Tiva Canyon and Ammonia Tanks, only); LS = low silica (Ammonia Tanks and Rainier Mesa, only).Also listed are the Th, La, and Rb composition of the host pumice fragment. For Rainier Mesa, the melt inclusion group and host phase are listed.

Topopah Spring

Inclusion	BB815b-1-1	BB83A-1-1	BB83A-1-2	BB8-3A-9-1	CP3-1a-2-1	BB8-3a-10-1	BB8-3a-6-1	CP1-2e-3-1	BB8-15b-3-1
host magma	HSR	HSR	HSR	HSR	HSR	HSR	HSR	HSR	HSR
wt%									
SiO2	79.0	78.7	79.0	78.6	78.8	78.8	77.6	79.4	79.3
TiO2	0.093	0.138	0.06	0.028	0.093	0.061	0.109	0.073	0.039
Al2O3	12.8	12.5	12.6	13.1	12.6	12.9	12.9	12.8	13.0
FeO	0.609	0.771	0.921	0.697	0.367	0.672	0.731	0.474	0.235
MgO	0.022	0.064	0.038	0.054	0.026	0.055	0.016	0.04	0.03
MnO									
CaO	0.26	0.585	0.431	0.502	0.288	0.552	0.413	0.429	0.355
Na2O	2.01	1.86	1.73	1.81	2.70	2.11	2.43	2.32	2.08
K2O	5.15	5.30	5.25	5.18	5.13	4.90	5.85	4.45	4.88
ppm:									
Th	18.4	10.7	11.1	17.3	2.64	15.2	18.3	16.5	14.4
La	20.7	17.5	12.4	23.0	5.63	17.5	27.4	20.4	16.9
Nb	22.7	15.9	13.6	18.1	4.40	17.9	22.2	19.5	7.98
Rb	120	116	94.1	110	32.2	115	120	130	55.3
Th (pumice)	27.0	22.0	22.0	22.0	22.2	22.0	22.0	23.0	27.0
La (pumice)	36.0	31.0	31.0	31.0	35.0	31.0	31.0	31.0	36.0
Rb (pumice)	194	205	205	205	181	205	205	206	194

APPENDIX 3. Continued

Topopah Spring

Inclusion	BB8-15b-4-1	LW4-10a-3-1b	BB8-3a-5-1	BB8-3a-5-1b	BB8-3a-4-1b	LW4-1b-1-1	BB9-1C-2-1	CP3-1d-3-1
host magma	HSR	HSR	HSR	HSR	HSR	LS	LS	LS
wt%								
SiO2	77.7	88.1	78.8	78.6	76.4	76.1	75.3	73.0
TiO2	0.157	0.087	0.093	0.119	0.041	0.133	0.155	0.276
Al2O3	13.6	5.49	13.2	12.9	13.7	13.6	14.9	15.6
FeO	0.538	0.776	0.276	0.754	0.393	0.653	0.226	0.828
MgO	0.007	0.237	0.086	0.043	0.053	0.069	0.094	0.145
MnO						0.027	0	0.029
CaO	0.334	0.581	0.403	0.464	0.311	0.455	0.04	0.662
Na2O	2.52	1.60	1.93	1.98	6.47	3.12	2.98	3.51
K2O	5.17	3.16	5.23	5.23	2.55	5.72	6.25	5.86
ppm:								
Th	4.27	8.52	4.00	4.15	11.3	12.1	9.75	14.9
La	38.1	102	3.51	7.06	20.6	17.5	18.4	62.4
Nb	20.8	8.65	4.12	7.52	16.1	13.2	14.6	17.0
Rb	38.6	23.2	68.9	84.6	74.3	102	82.0	81.8
Th (pumice)	27.0	20.6	22.0	22.0	22.0	20.9	18.9	21.6
La (pumice)	36.0	43.0	31.0	31.0	31.0	93.0	185	163
Rb (pumice)	194	172	205	205	205	161	151	145

APPENDIX 3. Continued

Topopah Spring

Inclusion	CP3-1d-1-3	LW2-5-3A-1	LW2-5-3A-2
host magma	LS	LS	LS
wt%			
SiO2	67.1	72.3	70.9
TiO2	0.032	0.306	0.283
Al2O3	18.9	16.5	16.0
FeO	0.201	0.606	1.99
MgO	0.005	0.115	0.132
MnO	0.026	0	0.071
CaO	0.289	0.637	0.698
Na2O	6.09	2.58	3.52
K2O	7.41	6.87	6.34
ppm:			
Th	13.6	11.7	10.3
La	40.3	62.3	68.1
Nb	15.9	15.2	16.1
Rb	40.6	86.1	71.3
Th (pumice)	21.6	21.0	21.0
La (pumice)	163	111	111
Rb (pumice)	145	156	156

APPENDIX 3. Continued.

Tiva Canyon

Inclusion	TC5BI-5-1	TC5BI-4-1	TC5BJ-2-1	TC5BI-6-1	TC2EA-3-1	TC2EA-3-1b	TC2EA-1-1	TC5BM-3-1	TC2ED-6-1
host magma	HSR	HSR	HSR	HSR	HSR	HSR	HSR	HSR	HSR
wt%:									
SiO2	76.8	77.3	76.7	73.8	77.7	76.2	77.4	78.2	77.9
TiO2	0.069	0.129	0.111	0.152	0.081	0.134	0.098	0.15	0.086
Al2O3	13.0	12.7	13.1	13.8	12.1	12.3	12.5	12.4	12.0
FeO	0.814	0.877	0.791	0.906	0.304	0.868	0.834	0.804	0.724
MgO	0.044	0.032	0.032	0.034	0.042	0	0.056	0.079	0.021
MnO									
CaO	0.247	0.151	0.229	1.253	0.022	0.224	0.216	0.33	0.191
Na2O	3.23	3.69	2.78	4.04	4.06	3.61	2.51	2.12	3.23
K2O	5.77	5.19	6.27	5.99	5.71	6.63	6.40	5.90	5.85
ppm:									
Th	10.7	17.1	8.96	6.87		17.5	14.2	17.0	2.44
La	16.5	20.8	10.9	7.92		21.1	14.1	21.5	3.33
Nb	10.3	20.3	13.4	10.2		26.7	17.3	21.1	3.49
Rb	89.3	125	94.8	45.8		171	108	144	31.1
Th (pumice)	30.8	30.8	29.8	30.8	22.8	22.8	22.8	31.8	30.0
La (pumice)	31.1	31.1	30.8	31.1	28.8	28.8	28.8	32.1	27.9
Nb (pumice)	37.7	37.7	36.4	37.7				38.9	37.0
Rb (pumice)	195	195	206	195	214	214	214	184	220

APPENDIX 3. Continued.

Tiva Canyon

Inclusion host magma	TC2EA-5-1b HSR	TC5BM-2-2 HSR	TC2ED-3-1 HSR	TC5BN-1-1 HSR	TC5BI-7-1 HSR	TC5BN-3-1 HSR	TC5BN-3-2 HSR	TC-2ED-4-1 HSR
wt%:								
SiO2	77.5	77.8	77.6	78.3	78.4	77.1	78.1	77.8
TiO2	0.15	0.081	0.106	0.120	0.114	0.146	0.119	0.115
Al2O3	12.5	13.0	12.3	12.7	12.6	12.7	12.7	12.4
FeO	0.835	0.706	0.943	0.855	0.959	0.872	0.821	0.902
MgO	0.029	0.073	0.066	0.055	0.055	0.057	0.047	0.049
MnO								
CaO	0.068	0.236	0.290	0.239	0.295	0.229	0.301	0.186
Na2O	2.41	2.80	2.29	1.64	2.82	3.06	2.70	3.00
K2O	6.48	5.31	6.36	6.12	4.78	5.94	5.21	5.51
ppm:								
Th	17.1	4.34	18.3	11.9	13.7	6.98	12.9	5.57
La	17.4	7.04	19.3	13.7	15.3	8.97	12.8	6.20
Nb	23.2	8.53	26.8	16.8	17.9	9.41	14.5	8.49
Rb	144	45.1	127	132	108	57.0	79.8	46.0
Th (pumice)	22.8	31.8	30.0	31.7	30.8	31.7	31.7	30.0
La (pumice)	28.8	32.1	27.9	30.7	31.1	30.7	30.7	27.9
Nb (pumice)		38.9	37.0	38.3	37.7	38.3	38.3	37.0
Rb (pumice)	214	184	220	193	195	193	193	220

APPENDIX 3. Continued.

Ammonia Tanks

Inclusion	AT5-8-1-1	AT5-8-1-2	AT5-8-1-3	AT5-8-3-1	AT5-8-3-1b	AT5-8-4-1	AT5-25-2-1	AT5-29-1-1	AT5-29-1-1b
host magma	HSR	HSR	HSR	HSR	HSR	HSR	HSR	HSR	HSR
wt%:									
SiO2	77.0	77.6	77.7	76.7	74.9	77.4	78.3	77.4	77.8
TiO2	0.07	0.08	0.11	0.116	0.088	0.126	0.108	0.15	0.09
Al2O3	13.1	12.2	12.4	12.5	13.9	12.7	12.5	12.1	12.3
FeO	0.64	0.61	0.64	0.692	0.53	0.548	0.661	0.73	0.39
MgO	0.02	0.07	0.05	0.038	0.035	0.046	0.041	0.04	0.03
MnO						0.095			
CaO	0.23	0.28	0.22	0.236	0.245	0.262	0.243	0.25	0.28
Na2O	3.11	3.45	3.61	3.52	5.66	3.46	2.95	3.65	3.38
K2O	5.82	5.69	5.32	6.14	4.61	5.26	5.25	5.66	5.76
ppm:									
Th		18.0		25.2			25.2	23.3	
La		11.1		20.4			19.6	16.5	
Nb		20.6		32.5			38.1	25.6	
Rb		133.0		192.4			194	129	
Th (pumice)	33.9	33.9	33.9	33.9	33.9	33.9	32.1	32.1	32.1
La (pumice)	35.9	35.9	35.9	35.9	35.9	35.9	34.6	29.9	29.9
Nb (pumice)	38.5	38.5	38.5	38.5	38.5	38.5	30.5	34.4	34.4
Rb (pumice)	219	219	219	219	219	219	216	224	224

APPENDIX 3. Continued.

Ammonia Tanks

Inclusion host magma	AT5-29-3-1 HSR	AT5-29-3-2 HSR	AT5-37-1-1 HSR	AT5-37-1-1b HSR	AT5-37-4-1 HSR	AT5-37-4-2 HSR	AT5-37-5-1 HSR	AT5-37-5-2 HSR	AT5-37-6-2 HSR
wt%:									
SiO2	77.0	77.8	77.9	78.3	77.4	78.0	67.0	78.4	77.4
TiO2	0.12	0.048	0.164	0.113	0.17	0.146	0.04	0.161	0.153
Al2O3	12.9	12.2	11.8	11.8	12.28	11.9	19.7	12.1	12.6
FeO	0.61	0.722	0.651	0.689	0.68	0.664	0.18	0.591	0.596
MgO	0.02	0.053	0.051	0.055	0.05	0.053	0.01	0.055	0.066
MnO									
CaO	0.31	0.28	0.225	0.311	0.22	0.313	0.48	0.271	0.180
Na2O	3.34	3.43	3.09	2.53	3.41	3.1	8.07	2.66	3.68
K2O	5.65	5.51	6.06	6.25	5.81	5.85	4.58	5.78	5.29
ppm:									
Th	32.4	22.4	0		28.3	19.4	24.5	0	5.01
La	21.6	17.5	2.62		22.4	19.6	25.1	3.15	6.92
Nb	35.9	33.4	0		31.0	27.9	32.7	0	9.28
Rb	152	189	23.6		157	196	241	31.6	58.7
Th (pumice)	32.1	32.1	31.6	31.6	31.6	31.6	31.6	31.6	31.6
La (pumice)	29.9	29.9	31.9	31.9	31.9	31.9	31.9	31.9	31.9
Nb (pumice)	34.4	34.4	36.6	36.6	36.6	36.6	36.6	36.6	36.6
Rb (pumice)	224	224	223	223	223	223	223	223	223

APPENDIX 3. Continued.

Ammonia Tanks

Inclusion	AT5-37-7-1	AT5-37-9-1	AT5-37-9-2	AT5-37-10-1	AT5-37-10-2	AT5-79-6-1	AT4-70-3-1a	AT21-2-1A-1	AT5-30-3	AT5-30-1
host magma	HSR	HSR	HSR	HSR	HSR	HSR	INT	INT	LS	LS
wt%:										
SiO2	73.9	77.9	77.9	77.5	78.3	78.0	74.0	74.0	75.4	72.5
TiO2	0.12	0.11	0.1	0.068	0.102	0.068	0.152	0.184	0.28	0.4
Al2O3	14.5	12.39	12.3	12.5	12.2	12.8	15.0	14.8	14.0	16.2
FeO	0.56	0.57	0.65	0.554	0.573	0.61	0.957	1.03	1.14	1.41
MgO	0.04	0.04	0.07	0.054	0.002	0.04	0.189	0.163	0.15	0.18
MnO						0.083	0.058	0.078	0.18	0.04
CaO	0.58	0.22	0.33	0.307	0.289	0.28	0.634	0.651	0.5	0.72
Na2O	6.16	3.63	3.75	3.21	3.49	2.22	3.26	3.41	3.73	3.71
K2O	4.12	5.14	4.97	5.71	5.11	5.79	5.57	5.64	4.61	4.89
ppm:										
Th	32.2	26.0	27.1	27.3	29.0	14.5	18.5	25.3		
La	25.6	20.8	24.1	19.3	19.7	11.9	56.2	70.0		
Nb	36.8	41.0	40.0	41.7	39.5	20.9	31.0	20		
Rb	202	195	207	208	215	113	141.4	101		
Th (pumice)	31.6	31.6	31.6	31.6	31.6	30.5	18.2		17.4	17.4
La (pumice)	31.9	31.9	31.9	31.9	31.9	29.8	74.2		225	225
Nb (pumice)	36.6	36.6	36.6	36.6	36.6	28.0	27.0		16.9	16.9
Rb (pumice)	223	223	223	223	223	208	147		95.5	95.5

APPENDIX 3. Continued.

Rainier Mesa

Inclusion	RM6-16-1-1	RM6-16-4-1	RM6-16-5-1	RM6-16-6-1	RM18-5-1-1	RM18-5-3-1	RM18-10-1-1b	RM18-10-4-1	RM18-11-1-1b
host magma	HSR-1	HSR-1	HSR-1	HSR-1	HSR-1	HSR-1	HSR-2	HSR-2	HSR-1
host phase	qtz	qtz	qtz	qtz	plag	san	qtz	qtz	qtz
Incl.Group	Group A	Group A	Group A	Group A	Group A	Group A	Group A	Group A	Group A
wt%:									
SiO2	74.4	65.2	75.4	75.8	77.5	81.2	64.9	67.2	79.3
TiO2	0.070	0	0.022	0.191	0	0.010	0.004	0	0.140
Al2O3	15.3	18.5	18.7	19.0	19.6	11.3	18.4	18.9	12.7
FeO	0.470	0.180	0.090	0.180	0.400	0.220	0.31	0.210	0.450
MgO	0.009	0.002	0.007	0.009	0	0.009	0	0.010	0.040
MnO									
CaO	0.202	0.027	0.038	0.075	0.034	0.417	0.014	0.020	0.400
Na2O	6.87	0.960	4.41	3.17	1.64	5.41	0.654	9.26	2.23
K2O	2.70	15.1	1.33	1.60	0.826	1.42	15.7	4.25	4.77
ppm:									
Th	30.4	28.2	25.2	27.4	27.4	38.0	29.2	38.3	38.0
La	33.8	31.3	20.0	26.1	23.0	38.7	28.8	9.13	34.5
Nb	49.4	50.1	173	161	43.3	122		97.4	50.6
Rb	419	424	600	436	171	107	406	497	287
Th (pumice)	24.0	24.0	24.0	24.0	24.6	24.6	29.4	29.4	23.0
La (pumice)	19.0	19.0	19.0	19.0	22.6	22.6	36.4	36.4	22.0
Nb (pumice)	39.6	39.6	39.6	39.6	27.6	27.6	20.6	20.6	30.4
Rb (pumice)	259	259	259	259	245	245	195	195	252

APPENDIX 3. Continued.

Rainier Mesa

Inclusion	RM18-14-6-1	99TM14-1-1b	99TM14-3-2	RM18-16-5-2	RM18-16-7-1	RM6-16-8-1	RM6-16-9-1	RM6-16-9-2	RM18-2-4-1
host magma	HSR-1	HSR-1	HSR-1	HSR-2	HSR-2	HSR-1	HSR-1	HSR-1	HSR-2
host phase	qtz	qtz	san	qtz	qtz	qtz	qtz	qtz	san
Incl.Group	Group A	Group A	Group A	Group A	Group A	Group B	Group B	Group B	Group B
wt%:									
SiO2	65.1	66.2	65.5	68.0	64.7	70.7	65.3	72.6	76.5
TiO2	0	0	0	0.138	0.041	0.51	0.367	0.078	0.04
Al2O3	18.4	18.1	19.2	18.3	18.4	17.6	18.3	15.9	13.0
FeO	0.130	0.610	0.170	0.231	0.103	0.350	0.330	0.720	0.560
MgO	0.001	0.018	0	0.008	0.028	0	0.005	0.137	0.060
MnO									0.01
CaO	0	0.053	0.260	0.181	0.024	0.730	0.426	0.416	0.44
Na2O	2.11	2.04	4.72	4.65	0.661	8.63	0.841	9.52	3.87
K2O	14.3	12.9	10.1	8.55	16.1	1.51	14.4	0.560	5.46
ppm:									
Th	31.0	175	23.8	47.3	33.8	15.43			0
La	43.9	8.24	17.9	33.6	32.6	0		12.1	12.8
Nb	83.7	36.7	52.6	191	76.2	46.5			
Rb	289	368	210	453	164	148	105	121	247
Th (pumice)	21.0	33.0	33.0	31.5	31.5	24.0	24.0	24.0	33.7
La (pumice)	20.5	29.0	29.0	36.7	36.7	19.0	19.0	19.0	31.4
Nb (pumice)	33.6	29.8	29.8	11.1	11.1	39.6	39.6	39.6	20.4
Rb (pumice)	236	170	170	145	145	259	259	259	155

APPENDIX 3. Continued.

Rainier Mesa

Inclusion	RM18-2-6-1	RM18-2-19-1	RM18-2-24-1	RM18-2-24-1a	RM18-2-26-1	RM18-2-26-2	RM18-2-48-1	RM18-6-7-1	RM18-10-5-1
host magma	HSR-2	HSR-2	HSR-2	HSR-2	HSR-2	HSR-2	HSR-2	HSR-1	HSR-2
host phase	san	san	qtz	qtz	san	san	qtz	san	qtz
Incl.Group	Group B	Group B	Group B	Group B	Group B	Group B	Group B	Group B	Group B
wt%:									
SiO2	77.2	78.4	99.9	75.7	76.7	65.7	77.8	79.2	79.2
TiO2	0.08	0.04	0.032	0.127	0.054	0.007	0.07	0.087	0.092
Al2O3	12.6	13.1	0.04	14.2	14.0	18.9	12.5	12.7	12.5
FeO	0.61	0.11	0.018	0.6	0.443	0.121	0.45	0.44	0.56
MgO	0.06	0.05	0	0.069	0.084	0.001	0.04	0.064	0.045
MnO	0.01	0.01	0	0.007	0.055	0.045	0.01		
CaO	0.5	0.38	0.005	0.337	0.413	0.236	0.34	0.279	0.458
Na2O	3.42	2.52	0	3.26	2.45	3.80	3.85	2.41	2.70
K2O	5.51	5.34	0	5.58	5.74	11.2	4.97	4.85	4.46
ppm:									
Th	18.0	0	16.2	16.2	9.95	0	16.2		
La	18.3	0	16.2	16.2	12.9	0	11.9	2.33	37.7
Nb									
Rb	218	294	0	0	120	92.0	316	70.9	99.6
Th (pumice)	33.7	33.7	33.7	33.7	33.7	33.7	33.7	22.6	29.4
La (pumice)	31.4	31.4	31.4	31.4	31.4	31.4	31.4	21.2	36.4
Nb (pumice)	20.4	20.4	20.4	20.4	20.4	20.4	20.4	28.8	20.6
Rb (pumice)	155	155	155	155	155	155	155	252	195

APPENDIX 3. Continued.

Rainier Mesa

Inclusion	RM26-20-6-1	RM26-23-1-1	99TM14-3-1	RM8-42-3-2	RM8-42-4-1	RM8-42-5-1	RM8-42-5-2	RM8-42-5-3	RM8-42-5-4
host magma	HSR-1	HSR-2	HSR-1	HSR-3	HSR-3	HSR-3	HSR-3	HSR-3	HSR-3
host phase	san	plag	san	san	qtz	san	san	san	san
Incl.Group	Group B	Group B	Group B	Group B	Group B	Group B	Group B	Group B	Group B
wt%:									
SiO2	78.6	78.6	78.6	77.5	66.3	77.8	77.7	79.7	77.9
TiO2	0.096	0.131	0.066	0.175	0	0.077	0.075	0.079	0.014
Al2O3	12.5	12.7	12.8	11.9	17.8	12.8	12.8	13.3	12.5
FeO	0.500	0.640	0.480	0.875	0.625	0.407	0.527	0.332	0.393
MgO	0.080	0.084	0.052	0.094	0.026	0.103	0.096	0.01	0.10
MnO									
CaO	0.347	0.472	0.458	0.454	0	0.488	0.431	0.381	0.375
Na2O	2.73	2.30	2.76	3.34	2.74	2.62	2.45	1.20	2.86
K2O	5.12	5.10	4.83	5.67	12.5	5.73	5.87	4.99	5.83
ppm:									
Th	15.2	9.39	24.8	10.1	11.1	5.35	12.4	13.7	15.5
La	11.3	15.4	14.3	20.8	4.96	7.26	10.8	14.9	17.3
Nb	32.2	21.0		8.27	26.8	14.9	23.7	32.3	34.3
Rb	253	156	121	64.2	288	110	148	157	143
Th (pumice)	23.4	30.5	33.0	37.6	37.6	37.6	37.6	37.6	37.6
La (pumice)	25.5	49.6	29.0	86.5	86.5	86.5	86.5	86.5	86.5
Nb (pumice)	29.9	19.8	29.8	16.4	16.4	16.4	16.4	16.4	16.4
Rb (pumice)	216	150	170	121	121	121	121	121	121

APPENDIX 3. Continued.

Rainier Mesa

Inclusion	RM8-42-6-2	RM8-42-6-3	RM8-42-7-2	RM18-16-1-1	RM18-16-2-1	RM18-16-5-1	RM18-16-8-1	RM18-16-9-1	RM18-16-11-1
host magma	HSR-3	HSR-3	HSR-3	HSR-2	HSR-2	HSR-2	HSR-2	HSR-2	HSR-2
host phase	qtz	qtz	san	san	san	qtz	san	qtz	san
Incl.Group	Group B	Group B	Group B	Group B	Group B	Group B	Group B	Group B	Group B
wt%:									
SiO2	69.1	67.8	77.9	76.1	77.2	69.5	77.0	90.5	77.9
TiO2	0.023	0.014	0.195	0.113	0.049	0	0.08	0.043	0.087
Al2O3	17.5	19.6	12.0	13.1	12.7	18.3	12.8	5.59	12.9
FeO	0.318	0.269	0.67	0.658	0.46	0.402	0.622	0.1	0.588
MgO	0	0.005	0.007	0.08	0.086	0.05	0.077	0.005	0.075
MnO									
CaO	2.12	0.049	0.384	0.468	0.483	0.086	0.53	0.091	0.366
Na2O	10.1	9.65	3.08	3.31	3.54	10.5	3.51	2.03	2.53
K2O	0.753	2.52	5.80	6.16	5.47	1.14	5.42	1.56	5.53
ppm:									
Th	7.73	8.61	3.97	13.6	11.4	19.7	15.4	13.7	11.1
La	4.45	4.52	7.21	12.0	9.51	14.1	16.5	21.3	10.4
Nb	42.6	59.8	3.98	31.5	27.8	41.3	24.4	14.0	28.1
Rb	307	235	39.8	198	133	178	203	29.3	123
Th (pumice)	37.6	37.6	37.6	31.5	31.5	31.5	31.5	31.5	31.5
La (pumice)	86.5	86.5	86.5	36.7	36.7	36.7	36.7	36.7	36.7
Nb (pumice)	16.4	16.4	16.4	11.1	11.1	11.1	11.1	11.1	11.1
Rb (pumice)	121	121	121	145	145	145	145	145	145

APPENDIX 3. Continued.

Rainier Mesa

Inclusion	RM18-16-12-1	RM6-16-2-3	RM8-42-1-1	RM8-42-3-1	RM8-42-6-4	RM8-42-8-1	RM18-16-9-1b	RM8-44-3-1	RM8-45-1-1
host magma	HSR-2	HSR-1	HSR-3	HSR-3	HSR-3	HSR-3	HSR-2	LS	LS
host phase	san	qtz	san	san	qtz	qtz	qtz	qtz	qtz
Incl.Group	Group B	Group C	Group C	Group C	Group C	Group C	Group C	LS	LS
wt%:									
SiO2	81.9	72.0	77.1	77.0	65.8	74.8	85.2	77.6	73.4
TiO2	0.141	0.066	0.14	0.125	0.024	0.133	0.014	0.097	0.22
Al2O3	10.1	18.4	12.6	13.0	18.0	13.9	9.39	12.6	16.5
FeO	0.301	0.462	0.69	0.640	0.633	0.694	0.09	0.591	0.720
MgO	0.031	0.002	0.088	0.101	0.024	0.101	0.187	0.051	0.140
MnO								0.063	0.11
CaO	0.374	0.167	0.407	0.44	0.081	0.162	1.15	0.465	1.15
Na2O	2.91	8.90	3.53	2.94	2.92	5.28	3.69	3.82	3.97
K2O	4.31	0.050	5.45	5.78	12.4	4.93	0.330	4.65	3.69
ppm:									
Th	16	29	25	27.3	41.6	24.8	26.4	0	21.1
La	27	38	39	29.2	44.7	30.0	43.6	0	64.2
Nb	63	26	16	19.1	17.8	21.1	26.5		
Rb	109	15.6	106	116	159	121	73.1	16.5	57.1
Th (pumice)	31.5	24.0	37.6	37.6	37.6	37.6	31.5	29.4	22.2
La (pumice)	36.7	19.0	86.5	86.5	86.5	86.5	36.7	136	112
Nb (pumice)	11.1	39.6	16.4	16.4	16.4	16.4	11.1	14.8	12.8
Rb (pumice)	145	259	121	121	121	121	145	146	90.2

APPENDIX 3. Continued.

Rainier Mesa

Inclusion	RM11-5-4-6	RM23-13-2-1a	RM23-13-2-2a	RM23-13-2-3	RM23-13-Q-1	RM23-13-3-1	RM23-13-6-1	RM23-24-5-2	R23-24-7-1
host magma	LS	LS	LS	LS	LS	LS	LS	LS	LS
host phase	plag	qtz	qtz	qtz	qtz	san	san	san	plag
Incl.Group	LS	LS	LS	LS	LS	LS	LS	LS	LS
wt%:									
SiO2	72.1	74.4	69.1	76.3	77.7	72.3	77.0	71.2	71.1
TiO2	0.307	0.107	0.035	0.007	0.082	0.32	0.23	0.35	0.33
Al2O3	15.5	14.8	19.1	13.5	12.4	14.5	12.6	15.5	15.8
FeO	1.332	0.612	0.551	0.366	0.569	1.21	0.74	1.745	1.66
MgO	0.329	0.087	0.039	0.006	0.052	0.24	0.07	0.285	0.38
MnO		0.086	0	0.043	0.022		0.02	0.066	
CaO	0.814	0.39	0.053	0.05	0.319	0.77	0.38	1.65	1.2
Na2O	3.93	2.98	2.44	6.01	3.27	4.23	3.41	3.91	4.44
K2O	5.69	6.42	8.66	3.65	5.46	6.41	5.62	5.28	4.99
ppm:									
Th	1.61	0	80.0	13.4	12.1	4.61	20.4	12.4	12.8
La	19.6	0	52.9	11.1	9.55	17.9	33.4	92.3	42.7
Nb	2.93					5.78			9.83
Rb	23.6	378	544	152	303	50.6	130	123	54.5
Th (pumice)	18.8	25.2	25.2	25.2	25.2	25.2	25.2	14.9	14.9
La (pumice)	96.0	80.7	80.7	80.7	80.7	80.7	80.7	80.4	80.4
Nb (pumice)	13.1	13.4	13.4	13.4	13.4	13.4	13.4	12.7	12.7
Rb (pumice)	123	113	113	113	113	113	113	72.7	72.7

APPENDIX 3. Continued.

Rainier Mesa

Inclusion	R23-24-11-1	RM23-26-1-2	RM23-26-6-1
host magma	LS	LS	LS
host phase	plag	san	san
Incl.Group	LS	LS	LS
wt%:			
SiO2	71.1	71.6	72.8
TiO2	0.36	0.305	0.29
Al2O3	16.9	15.5	15.7
FeO	0.34	1.65	1.18
MgO	0.03	0.241	0.19
MnO		0.062	0.09
CaO	1.94	0.871	0.80
Na2O	6.51	3.20	4.58
K2O	2.82	6.44	4.26
ppm:			
Th	9.93	21.5	32.0
La	58.1	115	117
Nb	8.27		
Rb	55.7	107	115
Th (pumice)	14.9	21.8	21.8
La (pumice)	80.4	101	101
Nb (pumice)	12.7	12.0	12.0
Rb (pumice)	72.7	76.7	76.7

REFERENCES

REFERENCES

Anderson, A.T., 1974, Evidence for a picritic, volatile-rich magma beneath Mt. Shasta, California. Journal of Petrology, v. 15, p. 243-267.

Bacon, C.R., 1989, Crystallization of accessory phases in magmas by local saturation adjacent to phenocrysts. Geochimica et Cosmochimia Acta, v. 53, p. 1055-1066.

Bindeman, I.N., and Valley, J.W., 2003, Rapid generation of both high- and low-$\delta^{18}O$, large-volume silicic magmas at the Timber Mountain/Oasis Valley caldera complex, Nevada. Geological Society of America Bulletin 115, no. 5, p. 581-595.

Byers, F.M. Jr, Carr, W.J., and Orkild, P.P., 1989, Volcanic centers of southwestern Nevada: Evolution of understanding, 1960-1988. Journal of Geophysical Research, v. 94, p. 5908-5924.

Cambray, F.W., Vogel, T.A., and Mills, J.G., Jr., 1995, Origin of compositional heterogeneities in tuffs of the Timber Mountain Group: The relationship between magma batches and magma transfer and emplacement in an extensional environment. Journal of Geophysical Research, v. 100, no. B8, p. 15793-15805.

Christiansen, R.L., Lipman, P.W., Carr, W.J., Byers, F.M. Jr, Orkild, P.P. and Sargent, K.A., 1977, Timber Mountain – Oasis Valley caldera complex of southern Nevada. Geological Society of America Bulletin, v. 88, p. 943-959.

Eaton, G.P., 1984, The Miocene Great Basin of western North America as an extending back-arc region, *in* Carlson, R.L., and Kobayashi, K., eds., Geodynamics of back-arc regions. Tectonophysics, v. 102, p. 275-295.

Ehrlich, R., and Full, W.E., 1987, Sorting out Geology, Unmixing Mixtures. *In*: Use and Abuse of Statistical Methods in Earth Sciences, Size W., ed., Oxford University Press, p. 34-46.

Farmer, G.L., Perry, F.V., Semken, S., Crowe, B., Curtis, D., and DePaolo, D.J., 1989, Isotopic evidence on the structure and origin of subcontinental lithospheric mantle in southern Nevada, v. 94, p. 7885-7898.

Farmer, G.L., Broxton, D.E., Warren, R.G., and Pickthorn, W., 1991, Nd, Sr, and O isotopic variations in metaluminous ash-flow tuffs and related volcanic rocks at the Timber Mountain/Oasis Valley Caldera, SW Nevada: Implications for the origin and evolution of large-volume silicic magma bodies. Contributions to Mineralogy and Petrology, v. 109, p. 53-68.

Fedele, L., Bodnar, R.J., DeVivo, B., and Tracy, R., 2003, Melt inclusion geochemistry and computer modeling of trachyte petrogenesis at Ponza, Italy. Chemical Geology, v. 194, p. 81-104.

Flood, T.P., Vogel, T.A., and Schuraytz, B.C., 1989a, Chemical Evolution of a magmatic system: the Paintbrush Tuff, southwest Nevada volcanic field. Journal of Geophysical Research, v. 94, no. B5, p. 5943-5960.

Flood, T.P., Schuraytz, B.C., and Vogel, T.A., 1989b, Magma mixing due to disruption of a layered magma body. Journal of Volcanology and Geothermal Research, v. 36, p. 241-255.

Frezzoti, M.-L., 2001, Silicate-melt inclusions in magmatic rocks: applications to petrology. Lithos, v. 55, p. 273-299.

Full, W.E., Ehrlich, R., and Klovan, J.E., 1981, Extended QModel – objective definition of external end members in the analysis of mixtures, Journal of Mathematical Geology, v. 13, p. 331-344.

Full, W.E., Ehrlich, R., and Bezdek, J.C., 1982, Fuzzy QModel – A new approach for linear unmixing. Journal of Mathematical Geology, v. 14, p. 259-270.

Ginibre, C., Wörner, G., and Kronz, A., 2002, Minor- and trace-element zoning in plagioclase: implications for magma chamber processes at Parinacota volcano, northern Chile. Contributions to Mineralogy and Petrology, v. 143, p. 300-315.

Grove, T.L., Baker, M.B., and Kinzler, R.J., 1981, Coupled CaAl-NaSi diffusion in plagioclase feldspar: experiments and application to cooling rate speedometry. Geochimica et Cosmochimica Acta, v. 58, p. 2113-2121.

Halter, W.E., Pettke, T., Heinrich, C.A., and Rothen-Rutishauser, B., 2002, Major to trace element analysis of melt inclusions by laser-ablation ICP-MS: methods of quantification. Chemical Geology, v. 183, p. 63-86.

Huysken, K.T., Vogel, T.A., and Layer, P.W., 2001, Tephra sequences as indicators of magma evolution: 40Ar/39Ar ages and geochemistry of tephra sequences in the southwest Nevada volcanic field. Journal of Volcanology and Geothermal Research, v. 106, p. 85-110.

Imbrie, J., 1963, Factor and vector analysis programs for analyzing geologic data. Office of Naval Research Tech Report, no. 6, 83 pp.

Imbrie, J., and Kipp, N., 1971, A new micropaleoontological method for quantitative paleoclimatology: Application to a late Pleistocene Caribbean core. *In*: Turekian, K.K., ed., The Late Cenozoic Glacial Ages. New Haven, Yale University Press, p. 71-181.

Johnson, G.W., 1997, Application of Polytopic Vector Analysis to Environmental Geochemistry Problems. Ph.D. Dissertation, University of South Carolina, Columbia, S.C.

Johnson, G.W., Jarman, W.J., Bacon, C.E., Davis, J.A., Ehrlich, R., and Risebrough, R.W., 2000, Resolving polychlorinated biphenyl source fingerprints in suspended particulate matter in San Francisco Bay. Environmental Science Technology, v. 34, p. 552-559.

Johnson, G.W., Ehrlich, R., and Full, W., 2002, Principle component analysis and receptor models in environmental forensics, *In*: An Introduction to Environmental Forensics, Murphy, B., and Morrison, R., eds., Academic Press, San Diego, CA, p. 461-515.

Klovan, J.E., 1968, Q-mode factor analysis program in FORTRAN-IV for small computers. Kansas Geological Survey Computer Contribution, v. 20, p. 39-51.

Klovan, J.E., and Imbrie, J., 1971, An algorithm and FORTRAN-IV program for large-scale Q-mode factor analysis and calculation of factor scores. Mathematical Geology, v. 3, p. 61-77.

Klovan, J.E., and Miesch, A.T., 1976, EXTENDED CABFAC and QMODEL, computer programs for Q-mode factor analysis of compositional data. Computers and Geosciences, v. 1, p. 161-178.

Lipman, P.W., Christiansen, R.L, and O'Conner, J.T., 1966, A compositionally zoned ash-flow sheet in southern Nevada. U.S. Geological Survey Professional Paper 524-F, 47p.

Lipman, P.W., Protska, H.J., and Christiansen, R.L., 1972, Cenozoic volcanism and plate tectonic evolution of the western United States; I. Early and middle Cenozoic. Royal Society of London Philosophical Transactions, A 271, p. 217-248.

Lu, F., Anderson, A.T., and Davis, A.M., 1995, Diffusional gradients at the crystal/melt interface and their effect on the composition of melt inclusions. Journal of Geology, v. 103, p. 591-597.

Lyakhovich, V.V., 1967, Distribution of rare-earths among the accessory minerals of granites. Geochemistry, v. 7, p. 691-696.

Mackie, W., 1928, The heavier accessory minerals in the granites of Scotland. Edinburgh Geological Society Transactions, v. 12, p. 22-40.

Mahood, G., and Hildreth, W., 1983, Large partition coefficients for trace elements in high-silica rhyolites. Geochemica et Cosmochimica Acta, v. 47, p.11-30.

McAdams, R.E., 1936, The accessory minerals of the Wolf Mountain granite, Llano County, Texas. American Mineralogist, v. 21, p. 128-135.

Miesch, A.T., 1976a, Q-mode factor analysis of geochemical and petrologic data matrices with constant row sums. Geological Survey Professional Paper, v. 574-g, p. 1-47.

Miesch, A.T., 1976b, Interactive computer programs for petrologic modeling with Extended Q-mode factor analysis. Computers and Geosciences, v. 2, p. 439-492.

Mills, J.G., Jr., 1991, The Timber Mountain tuff, southwest Nevada volcanic field: geochemistry, mineralogy and Petrogenesis, Ph.D. dissertation, Michigan State University, East Lansing, Michigan

Mills, J.G., Jr., Saltoun, B.W., and Vogel, T.A., 1997, Magma batches in the Timber Mountain magmatic system, Southwestern Nevada Volcanic Field, Nevada, USA. Journal of Volcanology and Geothermal Research, v. 78, p. 185-208.

Nielsen, R.L., Michael, P.J., and Sours-Page, R., 1998, Chemical and physical indicators of compromised melt inclusions. Geochimica et Cosmochimica Acta, v. 62, no. 5, p. 831-839.

Noble, D.C., and Hedge, C.E., 1969, $^{87}Sr/^{86}Sr$ variations within individual ash-flow sheets. U.S. Geological Survey Professional Paper, no. 650-C., p. C133-C139.

Qin, Z., Lu, F., and Anderson, A.T., Jr., 1992, Diffusive reequilibration of melt and fluid inclusions. American Mineralogist, v. 77, p. 565-576.

Rapp, R.P., and Watson, E.B., 1986, Monazite solubility and dissolution kinetics: implications for the thorium and light rare earth chemistry of felsic magmas. Contributions to Mineralogy and Petrology, v. 94, p. 304-316.

Roedder, E., and Weibblen, P.W., 1970, Lunar petrology of silicate melt inclusions, Apollo 11 rocks. Proceedings of Apollo 11 Lunar Science Conference, Geochimica et Cosmochimica Acta, v. 1, p. 801-837.

Sawyer, D.A., Fleck, R.J., Lanphere, M.A., Warren, R.G., Broxton, D.E., and Hudson, M.R., 1994, Episodic caldera volcanism in the Miocene southwestern Nevada volcanic field: revised stratigraphic framework, $^{40}Ar/^{39}Ar$ geochronology, and implications for magmatism and extension. Geological Society of America Bulletin, v. 106, p. 1304-1318.

Schuraytz, B.C., Vogel, T.A., and Younker, L.W., 1989, Evidence for dynamic withdrawal from a layered magma body: the Topopah Spring tuff, southwestern Nevada. Journal of Geophysical Research, v. 94, no. B5, p. 5925-5942.

Singer, B.S., Dungan, M.A., and Layne, G.D., 1995, Textures and Sr, Ba, Mg, Fe, K, and Ti compositional profiles in volcanic plagioclase: clues to the dynamics of calc-alkaline magma chambers. American Mineralogist, v. 80, p. 776-798.

Taylor, R.P., Jackson, S.E., Longerich, H.P., and Webster, J.D., 1997, In situ trace-element analysis of individual silicate melt inclusions by laser ablation microprobe-inductively coupled plasma-mass spectrometry (LAM-ICP-MS). Geochimica et Cosmochimica Acta, v. 61, no. 13, p. 2559-2567.

Thomas, J.B., Bodnar, J.B., Shimizu, N., and Chesner, C., 2001, The role of boundary layers during entrapment of melt inclusions: evidence from the Toba Tuffs, Sumatra, Indonesia. EOS Transactions, AGU 82 (47) (Fall Meeting Suppl. Abs. V32D-1014).

Urusov, V.S., and Dudnikova, V.B., 1998, The trace-component trapping effect: experimental evidence, theoretical interpretation, and geochemical applications. Geochimica et Cosmochimica Acta, v. 62, no.7, p. 1233-1240.

Vogel, T.A., and Aines, R., 1996, Melt inclusions from chemically zoned ash flow sheets from the southwest Nevada volcanic field. Journal of Geophysical Research, v. 101, no. B3, p. 5591-5610.

Warren, R.G., Byers, F.M. Jr., Broxton, D.E., Freeman, S.H., and Hagan, R.C., 1989, Phenocryst abundances and glass and phenocrysts compositions as indicators of magmatic environments of large-volume ash flow sheets in southwestern Nevada. Journal of Geophysical Research, v. 94, no. B5, p. 5987-6020.